(2)

WL-TR-92-2033

A HEAT PIPE COUPLED PLANAR THERMIONIC CONVERTER Performance Characterization, Nondestructive Testing, and Evaluation

T.J. Young and T.R. Lamp
Power Components Branch
Aerospace Power Division
Wright-Patterson AFB, OH 45433-6563

B.H. Tsao and M.L. Ramalingam
UES, Inc.
4401 Dayton-Xenia Road
Dayton, OH 45432-1894

15 March 1992

Final Report for Period August 1990 - November 1991

AERO PROPULSION AND POWER DIRECTORATE
WRIGHT LABORATORY
AIR FORCE SYSTEMS COMMAND
WRIGHT-PATTERSON AIR FORCE BASE, OHIO 45433-6563

NOTICE

When Government drawings, specifications, or other data are used for any purpose other than in connection with a definitely Government-related procurement, the United States Government incurs no responsibilty or any obligation whatsoever. The fact that the government may have formulated or in any way supplied the said drawings, specifications, or other data, is not to be regarded by implication, or otherwise in any manner construed, as licensing the holder, or any other person or corporation; or as conveying any rights or permission to manufacture, use, or sell any patented invention that may in any way be related thereto.

This report is releasable to the National Technical Information Service (NTIS). At NTIS, it will be available to the general public, including foreign nations.

This technical report has been reviewed and is approved for publication.

Timothy J. Young
Timothy J. Young
Project Engineer

Lowell D. Massie
Chief, Power Components Branch
Aero Propulsion and Power Directorate

FOR THE COMMANDER

WILLIAM U. BORGER
Chief, Aerospace Power Division
Aero Propulsion & Power Directorate

If your address has changed, if you wish to be removed from our mailing list, or if the addressee is no longer employed by your organization please notify WL/POOC, Wright-Patterson AFB, OH 45433-6563 to help us maintain a current mailing list.

Copies of this report should not be returned unless return is required by security considerations, contractual obligations, or notice on a specific document.

REPORT DOCUMENTATION PAGE

Form Approved
OMB No. 0704-0183

1a. REPORT SECURITY CLASSIFICATION UNCLASSIFIED	1b. RESTRICTIVE MARKINGS
2a. SECURITY CLASSIFICATION AUTHORITY	3. DISTRIBUTION / AVAILABILITY OF REPORT Approved for public release; distribution is unlimited.
2b. DECLASSIFICATION / DOWNGRADING SCHEDULE	
4. PERFORMING ORGANIZATION REPORT NUMBER(S) WL-TR-92-2033	5. MONITORING ORGANIZATION REPORT NUMBER(S) WL-TR-92-2033
6a. NAME OF PERFORMING ORGANIZATION Aero Propulsion and Power Directorate, Wright Laboratory 6b. OFFICE SYMBOL (If applicable) WL/POOC-2	7a. NAME OF MONITORING ORGANIZATION Aero Propulsion and Power Directorate Wright Laboratory
6c. ADDRESS (City, State, and ZIP Code) Wright-Patterson Air Force Base, OH 45433-6563	7b. ADDRESS (City, State, and ZIP Code) WL/POOC-2 Wright-Patterson Air Force Base, OH 45433-6563
8a. NAME OF FUNDING / SPONSORING ORGANIZATION 8b. OFFICE SYMBOL (If applicable)	9. PROCUREMENT INSTRUMENT IDENTIFICATION NUMBER N/A
8c. ADDRESS (City, State, and ZIP Code)	10. SOURCE OF FUNDING NUMBERS

PROGRAM ELEMENT NO.	PROJECT NO.	TASK NO.	WORK UNIT ACCESSION NO.
63218C	D812	00	01

11. TITLE (Include Security Classification)
A Heat Pipe Coupled Planar Thermionic Converter
Performance Characterization, Nondestructive Testing, and Evaluation

12. PERSONAL AUTHOR(S)
Young, Timothy J., Lamp, Thomas R., Tsao, Bang-Hung, Ramalingam, Mysore L.

13a. TYPE OF REPORT	13b. TIME COVERED	14. DATE OF REPORT (Year, Month, Day)	15. PAGE COUNT
Final	FROM 8-1-90 TO 11-30-91	1992, March 15	118

16. SUPPLEMENTARY NOTATION
N/A

17. COSATI CODES		
FIELD	GROUP	SUB-GROUP

18. SUBJECT TERMS (Continue on reverse if necessary and identify by block number)
Thermionics, Heat Pipes, Computer Modelling, Nondestructive Testing, Tomography, Planar Converter, Cesium Reservoir

19. ABSTRACT (Continue on reverse if necessary and identify by block number)

This report provides the technical details on the research activities conducted by Wright Laboratory and UES, Inc. personnel during the period of August 1990 to November 1991. The performance of two heat pipe coupled, planar thermionic energy converters was characterized using experimental and analytical methods. Nondestructive failure analysis was performed to evaluate the causes for the failure of a molybdenum-rhenium converter. The experimentation was carried out at the thermionic facilities at the USAF Wright Laboratory while the computer simulations were performed at Wright Laboratory and the University of Central Florida. A maximum current density of 10.1 amps/cm^2 and a peak power density of 7.7 watts/cm^2 were obtained from the rhenium-rhenium diode operating in the ignited mode.

20. DISTRIBUTION / AVAILABILITY OF ABSTRACT	21. ABSTRACT SECURITY CLASSIFICATION
☒ UNCLASSIFIED/UNLIMITED ☐ SAME AS RPT. ☐ DTIC USERS	UNCLASSIFIED

22a. NAME OF RESPONSIBLE INDIVIDUAL	22b. TELEPHONE (Include Area Code)	22c. OFFICE SYMBOL
Mr. Timothy J. Young	(513) 476-4780	WL/POOC

TABLE OF CONTENTS

SECTION	TITLE	PAGE
	LIST OF FIGURES	v
	LIST OF TABLES	ix
	FOREWORD	x
	ACKNOWLEDGEMENTS	xi
	NOMENCLATURE	xii
I	INTRODUCTION	1
	1.1 Thermionic Background	4
	1.2 Thermionic Research	6
	1.3 Computer Modelling of TEC	7
II	THERMIONIC ENERGY CONVERSION	9
	2.1 Electron Emission	9
	2.2 Vacuum Ideal Thermionic Converter	10
	2.3 Real Thermionic Converters	14
III	EXPERIMENTAL CHARACTERIZATION OF A MO-RE CONVERTER	20
	3.1 Experimental Procedure	22
	3.2 Output Characteristics	24
IV	FAILURE ANALYSIS OF MO-RE CONVERTER BY NONDESTRUCTIVE EVALUATION	29
	4.1 Electrode Evaporation and Expansion	29
	4.2 Interelectrode Cesium Investigation	32
	4.3 Computed Tomography	33
	4.4 X-Ray Radiography	38
V	TESTING AND CHARACTERIZATION OF A RE-RE CONVERTER	40
	5.1 Experimentation	40
	5.2 Characterization of Output Data	42

TABLE OF CONTENTS (Cont'd)

SECTION	TITLE	PAGE
VI	COMPARISON OF THERMIONIC CONVERSION COMPUTER SIMULATIONS	52
	6.1 First Principles TEC Analyses	52
	6.2 Phenomenological TEC Analyses	54
	6.3 TEC Simulation Comparison	56
VII	CONCLUSIONS AND RECOMMENDATIONS	64
VIII	REFERENCES	66
	APPENDIX A - EXPERIMENTAL DATA FROM THE MO-RE CONVERTER	71
	APPENDIX B - EXPERIMENTAL DATA FROM THE RE-RE CONVERTER (HEAT PIPE NOT SHIELDED)	76
	APPENDIX C - DERIVATION OF RADIANT ENERGY EXCHANGE RELATION	81
	APPENDIX D - EXPERIMENTAL DATA FROM THE RE-RE CONVERTER (HEAT PIPE SHIELDED)	87
	APPENDIX E - ASM AEROMAT '91 CONFERENCE AND FLOWERS '92 CONFERENCE ABSTRACTS	95
	APPENDIX F - EXPERIMENTAL DATA FROM THE RE-RE CONVERTER (EMITTER TEMPERATURE PERFORMANCE MAPPING)	98
	APPENDIX G - COMPARISONS OF EXPERIMENTAL DATA WITH THERMIONIC COMPUTER SIMULATION PROGRAMS GT-TEC AND TECMDL	103

LIST OF FIGURES

FIGURE	TITLE	PAGE
1.1	Schematic of a thermionic energy converter	2
1.2	LEOS planar thermionic converter for Romashka-type nuclear reactor. Note the heat pipe used to transfer waste heat to the radiator	3
1.3	LEOS thermionic converter life-test station in operation at the Thermionics Lab, Wright-Patterson AFB	5
2.1	Work function, ϕ, for (A) a pure surface, (B) reduced by $\Delta\phi$, and (C) increased by $\Delta\phi$	11
2.2	Electron motive diagram for an ideal thermionic converter	13
2.3	Vacuum ideal thermionic J-V and P-V output characteristics	15
2.4	High pressure, cesium vapor thermionic converter output characteristics	18
2.5	Motive diagrams for ignited and unignited modes. Source: Rasor, N.S. "Thermionic Energy Conversion." Chap.5 in *Applied Atomic Collision Physics.*	19
3.1	Thermionic Romashka reactor system schematic	21
3.2	Test station load circuit	25
3.3	Experimental output from the Mo-Re converter. T_C = 717°C and T_R = 377°C	25
3.4	LEOS generated output data for Mo-Re converter	26
4.1	Distance along converter imaged by the computed tomography method	35
4.2	X-ray count data from CT slices of Mo-Re converter	36
5.1	Re-Re converter output without a heat shield. T_E = 1600°C, T_C = 562°C, T_R = 324°C	41
5.2	Effect of radiation shielding upon heat pipe temperature drop	43
5.3	Re-Re diode temperature calibration curves with and without heat pipe shielding	43
5.4	Experimentally measured work function of a cesiated molybdenum collector. Source: Hatsopoulos, G.N. and E.P. Gyftopoulos. *Thermionic Energy Conversion Vol II.*	45
5.5	Cross plot from J-V output showing the dependence of output voltage on collector temperature at J = 8 A/cm^2	45
5.6	Maximum current and power densities versus emitter temperature	47
5.7	Ignition current densities and voltages for the Re-Re diode versus emitter temperature	48

LIST OF FIGURES (Cont'd)

FIGURE	TITLE	PAGE
5.8	Linear nature of output characteristics in the ignited mode. The numbers refer to figures in Appendix D where T_E ranged from 1450 to 1750°C.	50
6.1	Diagram of a hypothetical cycle relating the various emission and transition energies. Source: Rasor, N.S. and C. Warner. "Correlation of Emission Processes for Adsorbed Alkali Films on Metal Surfaces."	57
6.2	Comparison of TECMDL, GT-TEC, and experimental data for T_E = 1500°C, ϕ_O = 5.16 eV and 5.28 eV	59
6.3	The revised TECMDL simulations compared to experimental results. (A) 1450 ≤ T_E ≤ 1550°C, (B) 1600 ≤ T_E ≤ 1750°C	60
6.4	Voltage change, at J = 8 A/cm^2, for Re-Re diode experimental data and revised TECMDL simulations	62
Appendix A		
A1	Mo-Re converter output. T_C = 717°C, T_R = 227°C	72
A2	Mo-Re converter output. T_C = 717°C, T_R = 252°C	72
A3	Mo-Re converter output. T_C = 717°C, T_R = 277°C	73
A4	Mo-Re converter output. T_C = 717°C, T_R = 302°C	73
A5	Mo-Re converter output. T_C = 717°C, T_R = 327°C	74
A6	Mo-Re converter output. T_C = 717°C, T_R = 352°C	74
A7	Mo-Re converter output. T_C = 717°C, T_R = 377°C	75
Appendix B		
B1	Re-Re converter output without heat pipe shielding. T_E = 1450°C, T_C = 495°C, T_R = 316°C	77
B2	Re-Re converter output without heat pipe shielding. T_E = 1500°C, T_C = 517°C, T_R = 323°C	77

LIST OF FIGURES (Cont'd)

FIGURE	TITLE	PAGE
B3	Re-Re converter output without heat pipe shielding. T_E = 1550°C, T_C = 538°C, T_R = 323°C	78
B4	Re-Re converter output without heat pipe shielding. T_E = 1600°C, T_C = 562°C, T_R = 323°C	78
B5	Re-Re converter output without heat pipe shielding. T_E = 1650°C, T_C = 582°C, T_R = 323°C	79
B6	Re-Re converter output without heat pipe shielding. T_E = 1700°C, T_C = 602°C, T_R = 323°C	79
B7	Re-Re converter output without heat pipe shielding. T_E = 1750°C, T_C = 626°C, T_R = 323°C	80
Appendix C		
C1	Control volume for radiant energy analysis	83
Appendix D		
D1	Re-Re converter output with heat pipe shielding. T_E = 1450°C, T_C = 560°C, T_R = 301°C	88
D2	Re-Re converter output with heat pipe shielding. T_E = 1475°C, T_C = 572°C, T_R = 303°C	88
D3	Re-Re converter output with heat pipe shielding. T_E = 1500°C, T_C = 585°C, T_R = 305°C	89
D4	Re-Re converter output with heat pipe shielding. T_E = 1525°C, T_C = 599°C, T_R = 310°C	89
D5	Re-Re converter output with heat pipe shielding. T_E = 1550°C, T_C = 611°C, T_R = 312°C	90
D6	Re-Re converter output with heat pipe shielding. T_E = 1575°C, T_C = 624°C, T_R = 315°C	90
D7	Re-Re converter output with heat pipe shielding. T_E = 1600°C, T_C = 637°C, T_R = 318°C	91
D8	Re-Re converter output with heat pipe shielding. T_E = 1625°C, T_C = 650°C, T_R = 323°C	91
D9	Re-Re converter output with heat pipe shielding. T_E = 1650°C, T_C = 662°C, T_R = 322°C	92

LIST OF FIGURES (Cont'd)

FIGURE	TITLE	PAGE
D10	Re-Re converter output with heat pipe shielding. T_E = 1675°C, T_C = 674°C, T_R = 323°C	92
D11	Re-Re converter output with heat pipe shielding. T_E = 1700°C, T_C = 686°C, T_R = 323°C	93
D12	Re-Re converter output with heat pipe shielding. T_E = 1725°C, T_C = 697°C, T_R = 323°C	93
D13	Re-Re converter output with heat pipe shielding. T_E = 1750°C, T_C = 709°C, T_R = 323°C	94
Appendix F		
F1	Re-Re converter output, emitter temperature optimization. T_E = 1450°C, T_C = 556°C, T_R = 327°C	99
F2	Re-Re converter output, emitter temperature optimization. T_E = 1500°C, T_C = 582°C, T_R = 327°C	99
F3	Re-Re converter output, emitter temperature optimization. T_E = 1550°C, T_C = 609°C, T_R = 327°C	100
F4	Re-Re converter output, emitter temperature optimization. T_E = 1600°C, T_C = 634°C, T_R = 327°C	100
F5	Re-Re converter output, emitter temperature optimization. T_E = 1650°C, T_C = 659°C, T_R = 327°C	101
F6	Re-Re converter output, emitter temperature optimization. T_E = 1700°C, T_C = 684°C, T_R = 329°C	101
F7	Re-Re converter output, emitter temperature optimization. T_E = 1750°C, T_C = 709°C, T_R = 338°C	102
Appendix G		
G1	Comparison between GT-TEC, TECMDL, and experiment. T_E = 1450°C	104
G2	Comparison between GT-TEC, TECMDL, and experiment. T_E = 1500°C	104
G3	Comparison between GT-TEC, TECMDL, and experiment. T_E = 1550°C	104
G4	Comparison between GT-TEC, TECMDL, and experiment. T_E = 1600°C	104

LIST OF FIGURES (Cont'd)

FIGURE	TITLE	PAGE
G5	Comparison between GT-TEC, TECMDL, and experiment. T_E = 1650°C	105
G6	Comparison between GT-TEC, TECMDL, and experiment. T_E = 1700°C	105
G7	Comparison between GT-TEC, TECMDL, and experiment. T_E = 1750°C	105

LIST OF TABLES

TABLE	TITLE	PAGE
2.1	Types of Thermionic Converters	16
3.1	Conceptual Thermionic Power System Parameters	22
4.1	Vapor Pressures of Molybdenum and Rhenium at Elevated Temperatures	30
C4	Parameters to Estimate Heat Transfer Change	86

FOREWORD

This report provides the details of the experimental testing and evaluation of a planar electrode thermionic converter employing liquid sodium heat pipe to radiator cooling. This activity was conducted at the University of Central Florida, Orlando, Florida, and at the Thermionics Lab of Wright Laboratory, Wright-Patterson AFB, Ohio. This investigation also helped Mr. T.J. Young partially satisfy the requirements for the degree of Master of Science in Mechanical Engineering. The USAF Palace Knight program provided the funding for the education and experimental work of Mr. Young. The remainder of the funding was provided by the Strategic Defense Initiative Office / Innovative Science and Technology (SDIO/IST) through Wright Laboratory with UES, Inc. as the prime contractor under the Program Management of Dr. M.L. Ramalingam. The AF contract number was F33615-89-C-2950 and it was entitled, "The Advanced Thermionic Technology Initiative Program."

ACKNOWLEDGEMENTS

The authors would like to thank Mr. P. Jalichandra and his group at Loral Electro-Optical Systems for the design and fabrication of the converters. Thanks are also due to Professors Loren Anderson, Austin Grogan, and Ramon Hosler of the University of Central Florida for their contributions towards the thesis and education of Timothy J. Young. The guidance and encouragement of Dr. Thomas Mahefkey and Mr. Steve Cloyd of Wright Laboratory is greatly appreciated as is the experimental assistance of Mr. Chris Tunstall of UES, Inc.

NOMENCLATURE

A . . . . . Richardson-Dushmann constant, $A = 120$ amp/(cm^2•K^2)
A_i . . . . . Surface area of radiating body, (m^2)
d . . . . . Interelectrode gap, (mm)
e . . . . . Electron charge, $e = 1.60209 \cdot 10^{-19}$ coulombs
F_{ij} . . . . . Radiation shape factor
$\hbar$ . . . . . Planck's constant, $\hbar = 6.6254 \cdot 10^{-34}$ joule•sec
I . . . . . Electron current, (amperes)
J . . . . . Output electron current density, (amp/cm^2)
k . . . . . Boltzmann's constant, $k = 8.6168 \cdot 10^{-5}$ eV/K
KE . . . . . Kinetic energy, (eV)
L . . . . . Length, (m)
m . . . . . Mass, (kg)
$\dot{N}$ . . . . . Molecular arrival rate, (m^{-2}sec^{-1})
n . . . . . Charged particle number density, (m^{-3})
p . . . . . Cesium pressure, (torr)
P . . . . . Output power density, (W/cm^2)
q . . . . . Heat transfer, (W)
r . . . . . Mean electron reflection coefficient
T . . . . . Absolute temperature, (K)
u_{av} . . . . . Average electron velocity, (m/s)
V . . . . . Voltage, (V)
V_i . . . . . First ionization energy of cesium, $V_i = 3.89$ eV
V_o . . . . . Contact potential, (V)
x . . . . . Distance, (m)

Greek Characters

β . . . . . Coefficient of thermal expansion, (°C^{-1})
Δ . . . . . Change
ε . . . . . Permittivity, (F/m); Total, hemispherical emissivity
η . . . . . Carnot efficiency, (%)
λ . . . . . Electron mean free path, (m)
π . . . . . Pi = 3.1415927...
σ . . . . . Stefan-Boltzmann constant, $\sigma = 5.67 \cdot 10^{-8}$ W/(m^2•K^4); Surface charge density, (V/m)
ϕ . . . . . Work function, (eV)
ψ . . . . . Electron motive, (eV)

Subscripts/Superscripts

C . . . . . Collector
CS . . . . . Cesium
d . . . . . Arc drop
e . . . . . Electron
E . . . . . Emitter
ES . . . . . Emitter saturation
f . . . . . Fermi level
i . . . . . Radiating body; Ion
j . . . . . Receiving body
max . . . . . Maximum
pd . . . . . Plasma drop
R . . . . . Cesium reservoir
rad . . . . . Radiation
sat . . . . . Saturation level
vapor . . . . . Vapor pressure
′ . . . . . Ignited region transition
~ . . . . . Ion current

Acronyms

CT . . . . . Computed Tomography
CVD . . . . . Chemical Vapor Deposition
HfC . . . . . Hafnium Carbide
J-V . . . . . Current density versus Voltage
LEOS . . . . . Loral Electro-Optical Systems
Mo . . . . . Molybdenum
NASA . . . . . National Aeronautics and Space Administration
NDE . . . . . NonDestructive Evaluation
P-V . . . . . Power density versus Voltage
Re . . . . . Rhenium
TEC . . . . . Thermionic Energy Conversion
TFE . . . . . Thermionic Fuel Element
USAF . . . . . United States Air Force
W . . . . . Tungsten
Z . . . . . Atomic number

SECTION I
INTRODUCTION

Thermionic Energy Conversion (TEC) is a method for the direct conversion of heat into electrical energy through thermionic electron emission. Terrestrial and future military and civilian space power applications require reliable and efficient electrical power generation systems. Thermionic converters are simple, modular, have small volume, light weight, and no moving parts. A schematic of a thermionic converter is shown in Figure 1.1. The high temperature operation and high output power density of TEC can be applied to nuclear electric propulsion [1,2], cycle topping [3,4,5], and combined cycle power systems [4,6] in addition to solar and radioisotopic power generation.

The Thermionics Lab of the Wright Laboratory at Wright-Patterson Air Force Base, Ohio, is concerned with many areas of thermionics, including the experimental and computer simulated characterization of TEC. Effective materials and operating conditions are essential for optimum emission and high performance thermionic devices. The development of improved vapor converters means extensive testing of promising electrode materials operating in various ranges of temperatures and interelectrode spacings. In the performance mapping of thermionic converters, computerized data acquisition has been used to record current density versus voltage (J-V) data [7,8]. Yet as converter conditions change and electrodes yield better performance, the range of operating conditions for thermionic systems becomes broader.

Under USAF contract, Loral Electro-Optical Systems (LEOS) fabricated two thermionic diodes for use in studies of the Romashka-type nuclear reactor system. The details of the Romashka-type reactor are available in earlier documents [9,10,11]. In this design the TEC diodes are coupled to the nuclear reactor through radiant heat transfer, allowing each planar diode to be tested and evaluated by heat from an electrical source, unlike in-core or Thermionic Fuel Element (TFE) [12,13,14] converters. The radiative heat source supplies thermal energy to the emitter shoe. A heat pipe transfers the waste heat from the collector to a radiator with heat dissipating fins. Figure 1.2 shows the LEOS thermionic converter design for the Romashka reactor.

At the Thermionics Lab, both a molybdenum emitter-rhenium collector (Mo-Re) and a rhenium emitter-rhenium collector (Re-Re) converter were experimentally evaluated. The testing was performed under ultrahigh vacuum, 10^{-8} torr, within a water-cooled, stainless-steel bell jar

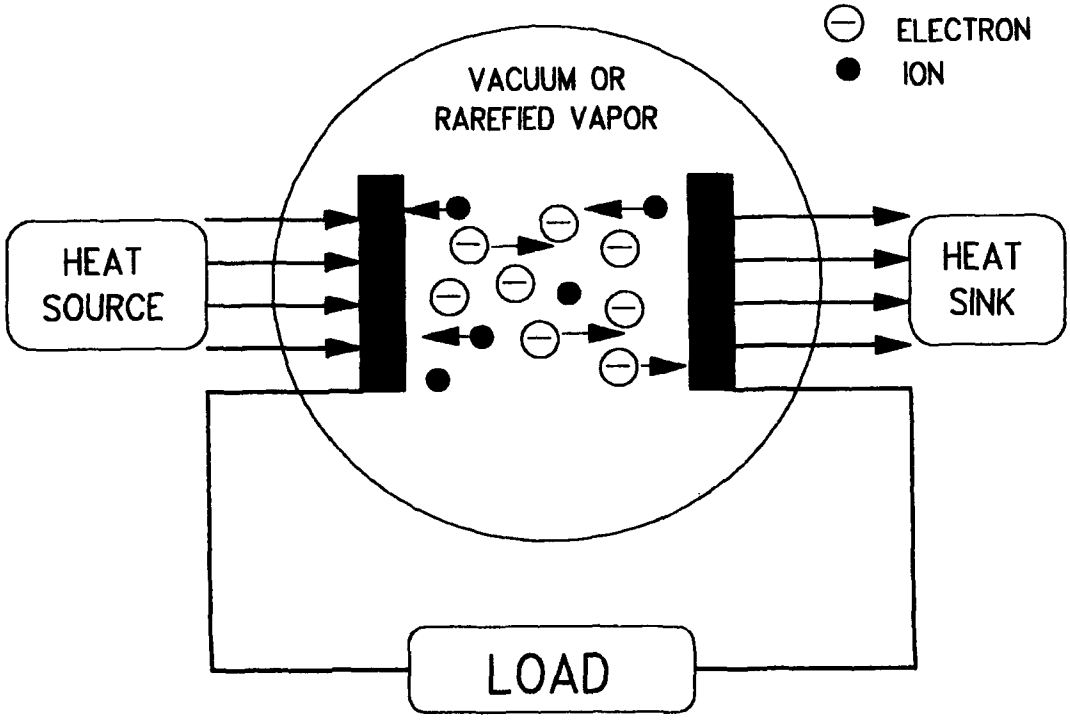

Figure 1.1. Schematic of a thermionic energy converter.

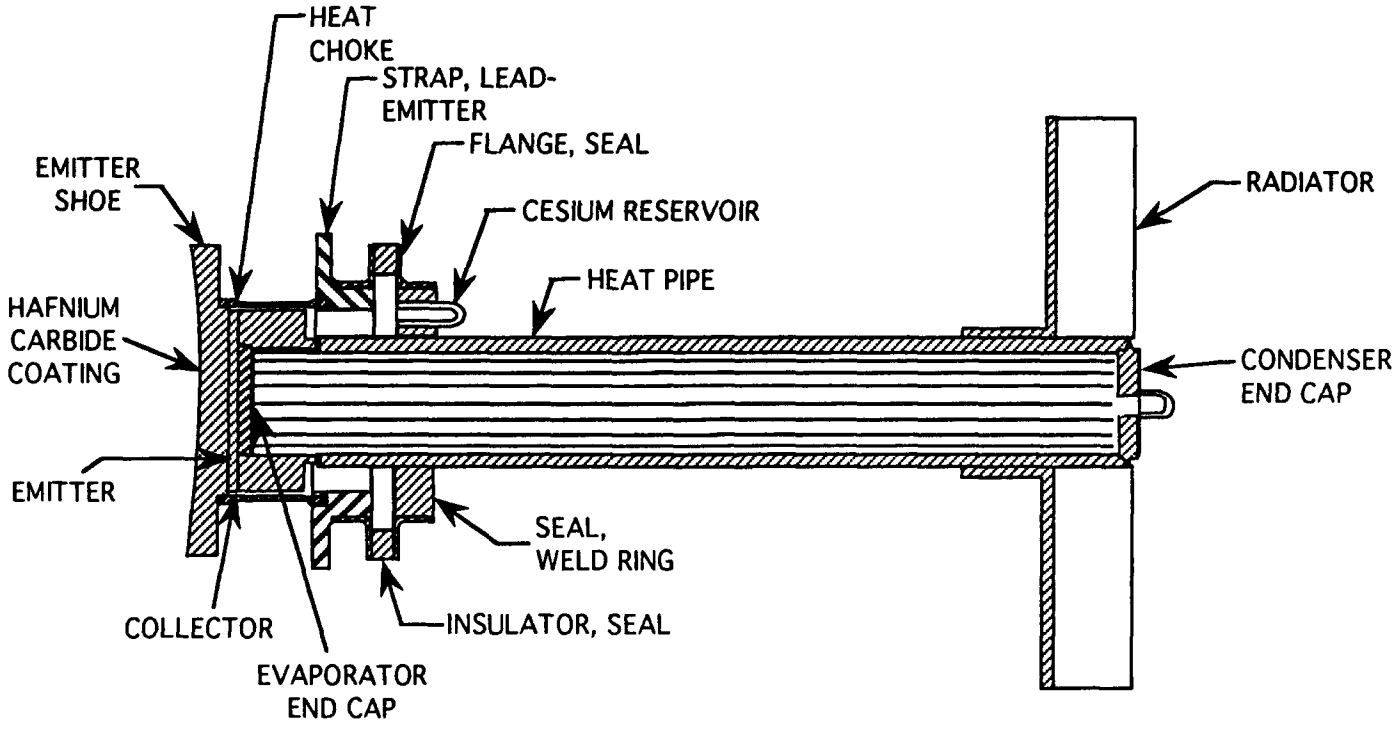

Figure 1.2. LEOS planar thermionic converter for Romashka-type nuclear reactor. Note the heat pipe used to transfer waste heat to the radiator.

mounted on a fully instrumented life-test station. A picture of the life-test station is shown in Figure 1.3. The output J-V and power density versus voltage (P-V) characteristics were successfully obtained from both diodes. Testing of the Mo-Re diode was terminated when the emitter heating system malfunctioned. A short circuit between the emitter and collector electrodes of the diode was found while fixing the emitter heater. To determine the cause of the short circuit, nondestructive evaluation (NDE) was chosen for the preliminary mode of failure analysis instead of cutting the diode casing open.

To allow further characterization of the LEOS diodes, computer TEC simulations were performed. These simulations used the operating and material parameters of the Re-Re converter. A comparison is made between the TECMDL program from Rasor Associates, Inc. and the GT-TEC model from the Georgia Institute of Technology. The simulations performed by TECMDL were able to follow the experimental trends much better than those predicted by GT-TEC.

The hardware developed and fabricated for use in this work was sponsored by the Strategic Defense Initiative Office. The work was performed at the Wright Laboratory, Aero Propulsion and Power Directorate, Aerospace Systems Division, Wright-Patterson AFB, in compliance with USAF Palace Knight Program requirements.

1.1 Thermionic Background

The discovery that the space near a red-hot body conducted electricity was made by Charles DuFay in the mid 1700's. The phenomenon of thermionic electron emission was first described by Thomas Edison in an 1884 patent [15]. The Edison effect was shown by the deflection of a galvanometer connecting a plate to the positive end of a battery heated filament. A vacuum was maintained between the filament and plate. It was not until 1879 that J.J. Thomson found that the charge to mass ratio of the Edison effect negative charge carriers agreed, within experimental uncertainty, with the value he found for electrons.

In 1905, Fleming described an electrical signal rectifier using a thermionic diode [16]. In his 1915 dissertation, Schlichter alluded to using the Edison effect to convert heat directly into electricity [17]. Much research regarding plasmas and electron emission was performed in the 1920's and 30's by Langmuir and others. It was not until the 1950's, however, that the thermionic energy converter was adequately described theoretically and experimentally. The virtual simultaneous engineering of thermionic energy conversion in the USSR by Morgulis [18], in

Figure 1.3. LEOS thermionic converter life-test station in operation at the Thermionics Lab, Wright-Patterson AFB.

France by Champeix [19], and in the USA by Hatsopoulos [20], among others, ushered in the age of rapid thermionic development.

1.2 Thermionic Research

By the late 1950's, much thermionic conversion research was being performed. Due to its youth, many different methods of analysis were being performed. At Los Alamos Scientific Laboratory, the plasma diode was regarded as a thermocouple with the plasma and metal electrodes as branches. Using this definition, expressions for both the Seebeck EMF and thermoelectric conversion efficiency were obtained as functions of the emitter and collector temperatures [21]. Later investigations derived the open circuit voltage [22] and efficiency of the plasma thermocouple [23]. Overall efficiencies up to 32% were predicted. This is about twice the value found experimentally.

By the early 1960's thermionic research had targeted the physics occurring at the electrode surfaces and within the interelectrode gap. One of the primary reasons for the failure of thermionic converters to attain performance near theoretical limits was electron transport effects in the gap. Two major transport effects were the electron space-charge and the scattering of electrons in transit between the electrodes [24]. The space-charge effect, determined to be the most detrimental, could be neutralized by volume or surface ionization. The former consumes a large portion of the output power while the latter is not effective. Emission processes were found to establish the upper limit of the obtainable performance of a TEC device [25]. Adsorbed cesium layers were found to enhance electron emission and reduce electrode vaporization. Cesium ions reduce the space-charge through both types of ionization, though volume ionization dominates.

Much experimental work was being documented by the late 1960's and early 1970's. At the NASA Lewis Research Center, several diode stations were being tested. It was determined that, within experimental error, no measurable temperature gradients existed on the emitter surface of a thermionic diode [26]. The diminiode, a miniature thermionic diode employing two small electrodes, was used to screen and develop high efficiency thermionic converters using several electrode combinations [27]. Single crystal (110) tungsten, when used as the emitter due to its high bare work function, was found to produce peak power densities of nearly 8 W/cm^2 and short circuit current densities from 20 to 40 A/cm^2 [28]. Many other electrode materials, rarefied

vapors, pressures, and temperatures were investigated until funding for thermionic activities was terminated in 1973.

Thermionics research was revived in the mid 1980's. The NASA Lewis diminiode stations were sent to Arizona State University, where W(110) and Re(0001) diodes were found to have peak power densities of 9 W/cm^2 and 7 W/cm^2, respectively [29]. These diminiode stations then found their way to the Thermionics Lab at Wright-Patterson AFB where updated instrumentation systems were installed [30]. It was found that peak power was observed for collector temperatures between 850 and 1000 K.

European thermionics research has continued to develop since the early 1970's. The Soviets have used thermionic diodes, called tacitrons, for switching systems and power commutation [31,32,33]. The Soviets have already placed, into Earth orbit, two nuclear powered thermionic converters. In early 1991, the Soviet Kurchatov Institute of Atomic Energy sold a Topaz 2 nuclear thermionic space power system to a U.S. company [34]. This converter is being tested at the USAF Phillips Laboratory. In the Netherlands, thermionic converters utilizing combustion heat have been explored for the cogeneration of heat and electricity for domestic use in remote locations [35,36].

1.3 Computer Modelling of TEC

In the U.S., computer modelling of thermionic conversion has been used to enhance thermionic investigations and to compensate for the lack of research funding and hardware. Effective materials and operating conditions are essential for long life, high output power, and high efficiencies. The development of improved vapor converters means extensive testing of promising electrode materials operating in various ranges of temperatures and spacings. Effective TEC computer simulations would allow the performance characteristics of various diode models to be evaluated before costly and time consuming fabrication and testing.

Two systematic views of the processes involved in thermionic conversion have emerged in the design of thermionic models. The first is phenomenological and the second is based upon first principles. These theories have been used to model TEC devices alone or in system studies involving configurations and heat sources.

Thermionic conversion systems models must couple thermionic performance to an appropriate heat source and sink, cooling/heating system, control system, and configuration. Reference [37] describes an overall systems design code to model an in-core, TEC-based nuclear

reactor system for space applications at power levels of 10 to 50 kWe. The code modules are used to determine specific system parameters, including neutronics and core criticality, TFE performance, radiation shielding, power conditioning, and control. A general purpose reactor system simulation code capable of modelling coupled heat transfer, fluid flow, neutronics, and control in an arbitrary reactor system configuration is described in [38]. Calculated steady-state results for a model of the Soviet Topaz 2 are in excellent agreement with design parameters reported for that system.

SECTION II
THERMIONIC ENERGY CONVERSION

2.1 Electron Emission

Thermionic electron emission is the process that occurs at all metal surfaces above absolute zero temperature. At zero Kelvin, the quantum energy states of the electrons are at or below the Fermi level, ε_f. The Fermi level is defined by the Fermi distribution function, which gives the average number of fermions of a system in equilibrium, at temperature, T, to be found in a quantum state of energy, ε. A fermion is a particle described by antisymmetric eigenfunctions, such as electrons, protons, neutrons, positrons, and muons. The Fermi distribution function is

$$n_{Fermi}(\epsilon) = \frac{1}{e^{\left(\frac{\epsilon-\epsilon_f}{kT}\right)}+1} \quad . \tag{2.1}$$

At an energy equal to the Fermi level, the probability of a quantum state being occupied is one-half. The electrons in the outer shells of the metal atoms are allowed to move freely between the positive ion cores of the metal lattice. Although the electrons can move freely throughout the bulk of the metal, the region near the metal surface is a discontinuity.

The energies of the electrons are distributed over an unlimited range described by the Fermi distribution. The energy of a few electrons will far exceed the average energy of the bulk. These high energy electrons will leave the surface of the metal if they acquire an energy greater than the work function, ϕ, of the metal surface. The work function is defined as the energy required to remove an electron from the metal surface. The forces opposing the removal of an electron are Coulombic, electrostatic forces and the change in potential due to passing through a nonzero surface charge density σ. The work function is given by

$$\phi = \int_{x=x_1}^{\infty} \frac{e^2}{4\pi\epsilon x^2}\, dx - 4\pi e \sigma x_2 \, . \tag{2.2}$$

x_1 is the distance outside the metal surface, on the order of an atomic radius, where Coulomb's law is invalid. x_2 is the distance from the electrode surface to the surface charges. The work function, a surface property, is strongly affected by impurities on the metal surface, such as adsorbed ions or atoms. Figure 2.1 shows an energy level diagram for a pure surface and surfaces with adsorbed ions causing an increase or decrease in ϕ. The magnitude and sign of the change in work function depends upon the substrate and whether the adsorbate deposits upon the grains or on grain boundaries.

2.2 Vacuum Ideal Thermionic Converter

The vacuum ideal model of a thermionic energy converter provides a basis for the comparison of real thermionic converters. In this ideal model, the space between the hot emitter and cold collector is a high vacuum. The interelectrode gap is considered collisionless. The space-charge induced by previously emitted electrons traversing the gap upon the electrons near the electrode surface is assumed nullified. The back electron emission from the collector to the emitter is also neglected, as is any current of ions or neutral particles.

The electrons must overcome the work function of the emitter, ϕ_E, to leave the surface of the emitter. A similar barrier to electron flow, the collector work function, ϕ_C, exists at the collector. The contact potential, V_o, between the two metallic electrodes is defined to be

$$V_o = \frac{\phi_E - \phi_C}{e} \quad . \tag{2.3}$$

A potential difference is established between the electrodes when they are connected electrically. If the two surfaces are in thermodynamic equilibrium, the total current flowing between them is zero. The most energetic electrons in the collector will flow into the emitter, filling the energy levels of the emitter just above its Fermi level and depleting the upper levels in the collector. This process continues until the electrodes are at the same energy and equilibrium is reached. The total energy of the system is minimized by this arrangement. The result is that the collector becomes positively charged and the emitter negatively charged. The contact potential maintains the zero current condition.

Two different conventions are used when defining the signs of current and potential energy. In the electrical viewpoint, positive charge carriers flow from a high electrical potential to a lower potential. The potential energy of an electron in the bulk of a metal is negative from

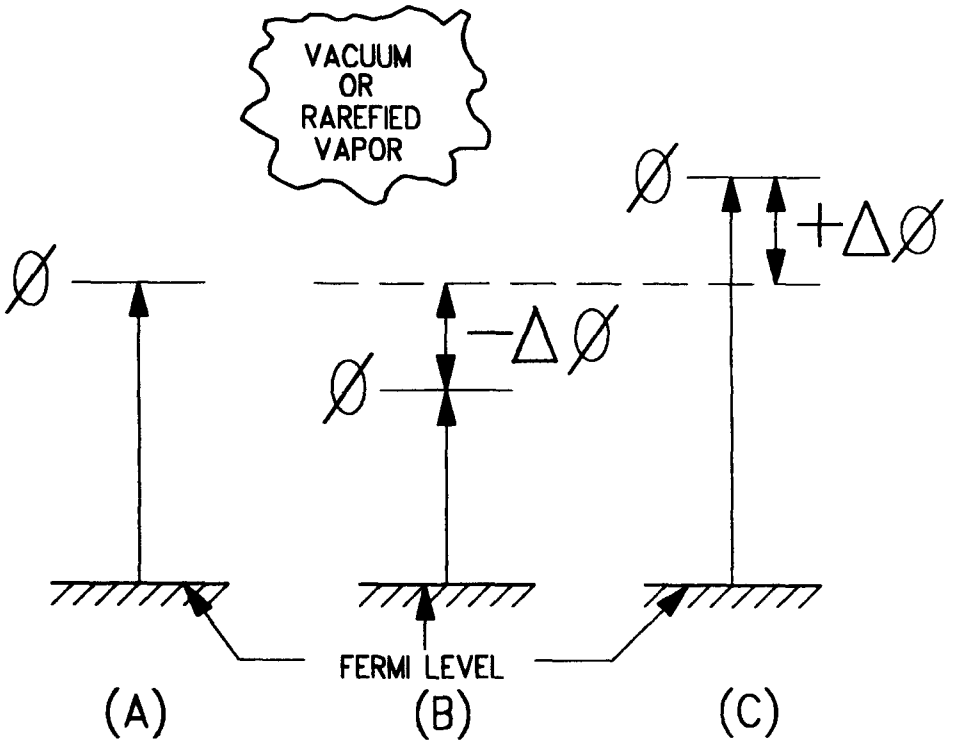

Figure 2.1. Work function, ϕ, for (A) a pure surface, (B) reduced by $\Delta\phi$, and (C) increased by $\Delta\phi$.

an electrical point of view. The perspective commonly used in thermionic studies is the electron viewpoint. Electrons travel the gap from the hot emitter to the cold collector and return to the emitter after passing through the load. The charge carriers (electrons) travel from low to high electrical potential. The electron motive, defined to be the energy of the electron, is positive. The electrical and electron viewpoints differ by their signs (±). The electron viewpoint will be used in this work.

A net electron current will flow from the emitter to the collector if the emitter is at a higher temperature, $T_E > T_C$, and the emitter Fermi level is lower, $\varepsilon_{fE} < \varepsilon_{fC}$, than the corresponding collector value. The thermionic converter is a heat engine operating between the electrode temperatures and is limited by Carnot efficiency, $\eta = 1-(T_C/T_E)$. Figure 2.2 shows the electron motive for the vacuum ideal thermionic converter. When an electron in the emitter electrode has gained sufficient energy from a high temperature source to raise its energy past the Fermi level to some energy $\varepsilon_{fE}+\phi_E+KE$, it may leave the emitter surface. After crossing the collisionless interelectrode gap, the electron must overcome the barrier imposed by the collector work function and release any additional kinetic energy to penetrate the collector surface. This energy must be rejected to a heat sink. The electron then reaches the Fermi level of the collector. The potential difference, $\varepsilon_{fC}-\varepsilon_{fE}$, can then be used to drive electrons through a load.

When the output voltage, $eV = \varepsilon_{fC} - \varepsilon_{fE}$, is less than the contact potential, the emitted electrons must surmount a barrier imposed by the work function of the emitter. When the output voltage is greater than V_o, the energy barrier is the sum of the output voltage and the collector work function. The net current density in the ideal thermionic converter is given by the Richardson-Dushmann equation,

$$J = A(1-r)T_E^2 \exp\left(-\frac{\phi_E}{kT_E}\right) - A(1-r)T_C^2 \exp\left(-\frac{\phi_E - eV}{kT_C}\right) \quad \text{for } V \le \frac{\phi_E - \phi_C}{e} \qquad (2.4)$$

and

$$J = A(1-r)T_E^2 \exp\left(-\frac{\phi_C + eV}{kT_E}\right) - A(1-r)T_C^2 \exp\left(-\frac{\phi_C}{kT_C}\right) \quad \text{for } V \ge \frac{\phi_E - \phi_C}{e} \qquad (2.5)$$

where

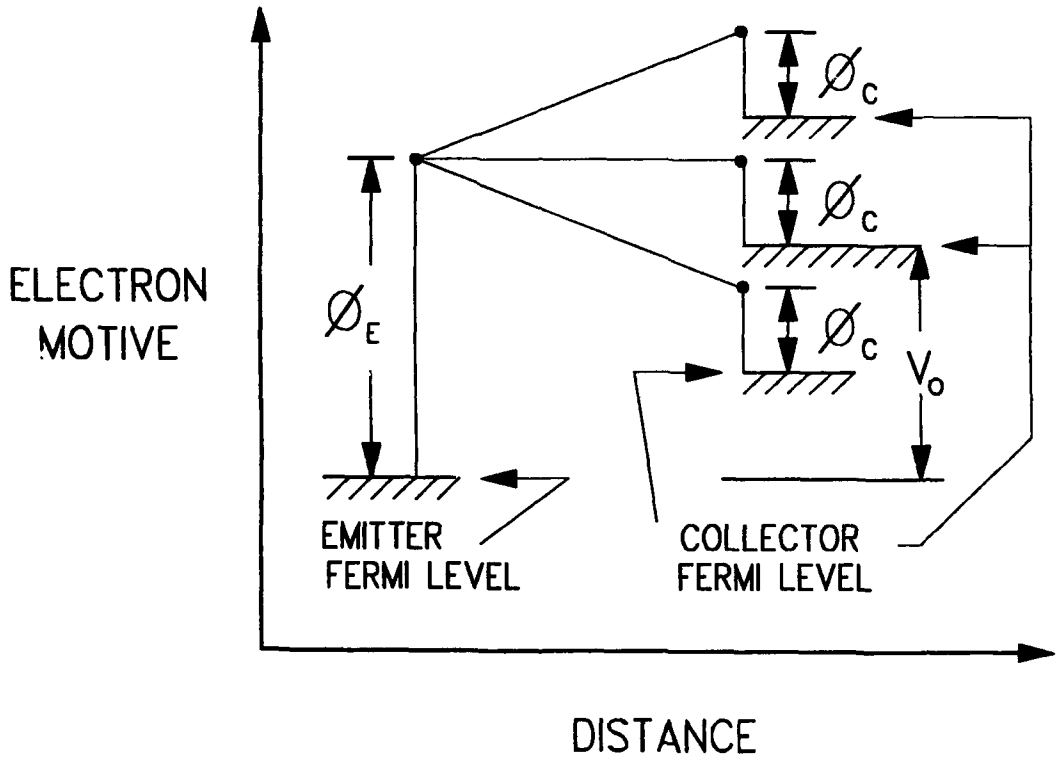

Figure 2.2. Electron motive diagram for an ideal thermionic converter.

$$A \equiv \frac{4\pi m_e k^2}{h^3} = 120 \frac{amp}{cm^2 K^2} \quad . \tag{2.6}$$

The mean electron reflection coefficient is usually much smaller than one ($r \ll 1$) and can be neglected or assumed incorporated into *A*. The derivation of the Richardson-Dushmann equation can proceed from thermodynamic considerations [39] or from the Fermi-Dirac statistics of quantum physics [4]. The ideal J-V relationships, which include collector electron emission, are exact only from a uniform surface in the absence of strong, externally applied electric fields. When space-charge, transport and plasma effects, back emission, ion flows, surface properties, and other real phenomena are considered, the fundamental equations become much more complex. An output J-V characteristic for the vacuum ideal thermionic converter is given in Figure 2.3. The ideal P-V characteristic is also shown where the power density is the product of the current density and output voltage, P = J•V.

2.3 Real Thermionic Converters

In real thermionic converters, space-charge effects in the interelectrode gap lead to large deviations from the ideal. The close-spaced, high-vacuum diode employs a very small interelectrode gap, d, to reduce the space charge. The length of the gap is on the order of 10^{-6} m such that $d \ll \lambda$. The electron mean free path, λ, is defined to be the average distance an electron travels between collisions. This type of converter can produce curves near the ideal only when the gaps are very small. Manufacturing and maintaining the extremely small interelectrode gap is problematic. Excessive electrode evaporation will change the electrode work functions or cause a short circuit if a whisker connects the electrodes. These effects limit the useful life of a vacuum converter.

The introduction of positive ions into the interelectrode gap reduces the space-charge effects. The plasma generated between the hot electrodes transports the electron and ion currents. Though many varied methods have been employed, as shown in Table 2.1, the introduction of cesium vapor into the gap has shown the most promise for ion production and the elimination of electrode evaporation.

Several major phenomena occur when cesium vapor is introduced into a converter with refractory metal electrodes. The work functions of the electrodes are reduced when cesium is

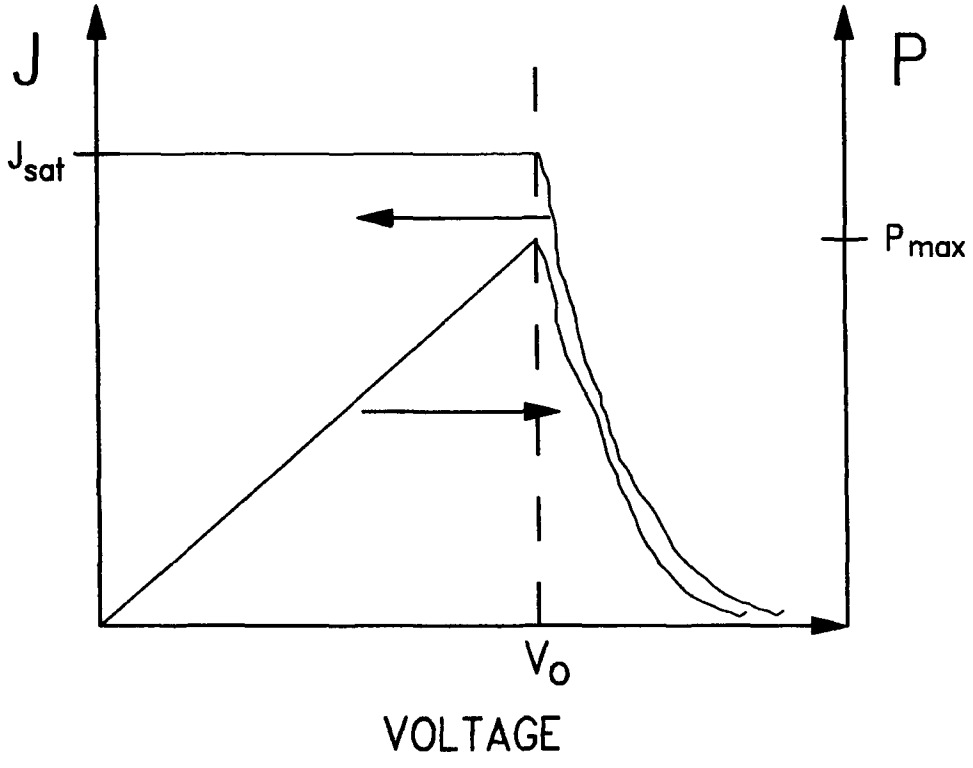

Figure 2.3. Vacuum ideal thermionic J-V and P-V output characteristics.

adsorbed on the electrodes. Some of the adsorbed atoms are thermionically emitted as ions, reducing the space-charge effect. Cesium has the lowest ionization potential of any stable element. This allows cesium to have the highest thermionic ion emission of any metal adsorbed in a thermionic converter. Collisions between the electrons and cesium in the plasma produce additional ions and may return some electrons to the emitter. The return of electrons to the emitter reduces the net current from the emitter, but the beneficial reduction of work functions and increased ion production allows a net gain to be realized.

Table 2.1
Types of Thermionic Converters

FAMILY	TYPE	VARIATIONS
High Vacuum		
	Close Spaced Diode	
	Vacuum Triode	Magnetic Triode
		Electrostatic Triode
Vapor Filled		
	Cesium Diode	
	Supplemented Diodes	Pulsed Diode
		Radiation Diode
	Ion Emission Triodes	Surface Ionization Triode
		Ion Dispenser Triode
	Arc Triode	Dual Emitter Arc Triode
		Dual Collector Arc Triode

Source: Hatsopoulos, G.N. and E.P. Gyftopoulos. *Thermionic Energy Conversion Vol. I: Processes and Devices.*

An electropositive additive, such as barium, can be used to directly reduce the electrode work functions more than possible with cesium alone. The net effect of an electronegative additive, such as oxygen, is to further reduce the cesiated work functions. The potential of cesium converters with gaseous additives will be realized only when their advantages outweigh the disadvantages. Increased pressures, higher collector temperatures, and complex systems and controls are some of the drawbacks.

The product of cesium pressure, p, and the gap length distinguishes the vapor diodes. A low pressure diode has a p•d product less than about one mil•torr, where for a high pressure

diode p•d ≈> 1 mil•torr. One mil equals 10^{-3} inches or 0.0254 mm. One torr equals 1/760 atmospheres or 1mm-Hg. The number of collisions in the gap is proportional to the ratio of the interelectrode gap to the mean free path, d/λ. The mean free path is inversely proportional to the vapor pressure. Therefore, the p•d product is a measure of the number of collisions that occur in a plasma. A qualitative graph of the J-V and P-V output of a real, high pressure cesium diode is shown in Figure 2.4.

In the ignited mode of operation, power is dissipated internally in the interelectrode gap by collisions. This energy is used to heat the plasma to ionize the cesium vapor and maintain a macroscopically neutral plasma. On a microscopic scale, an imbalance of electrons creates a negative electric field on the order of a Debye length. The Debye length is a measure of the extent of deviation from electrical neutrality in a plasma. This negative field will attract positive ions to reduce the imbalance. The overall effect is to stabilize the plasma by maintaining a neutral charge across the bulk of the plasma. An arc drop voltage, V_d, is established to sustain the ignited plasma. In the obstructed region, there is an insufficient potential drop to maintain the ignited plasma. A negative space-charge sheath, formed between the emitter and plasma, limits the electron current flowing from the emitter to a level that can be sustained by the reduced arc drop. In the unignited mode, the plasma is maintained entirely by thermionic ion emission from the emitter surface. The space-charge that can be neutralized by ion emission is much smaller than can be offset by volume ionization.

Figure 2.5 shows the electron motive diagrams for a plasma diode. In the ignited mode obstructed region (A), a double-valued sheath has formed outside the emitter to maintain a neutral plasma. The current and voltage are both at intermediate levels. When the converter operates in the saturation region (B), the emitter sheath becomes single valued and the current is high while the voltage is low. In the unignited retarding region (C), the plasma erects a collector barrier that limits the current flow. In the plasma saturation mode (D), additional current is neutralized by ions reflected back into the plasma by the collector sheath.

For a given output current, the output voltage of a cesium diode is higher than a vacuum diode. The electron number density in the gap is also larger with cesium, as is the difference in electron motives $\psi_C - \psi_E$. The electron motive is equal to the sum of the Fermi energy and work function, $\psi = \varepsilon_f + \phi$. The larger $\psi_C - \psi_E$ yields the greater output voltage of the cesium diode.

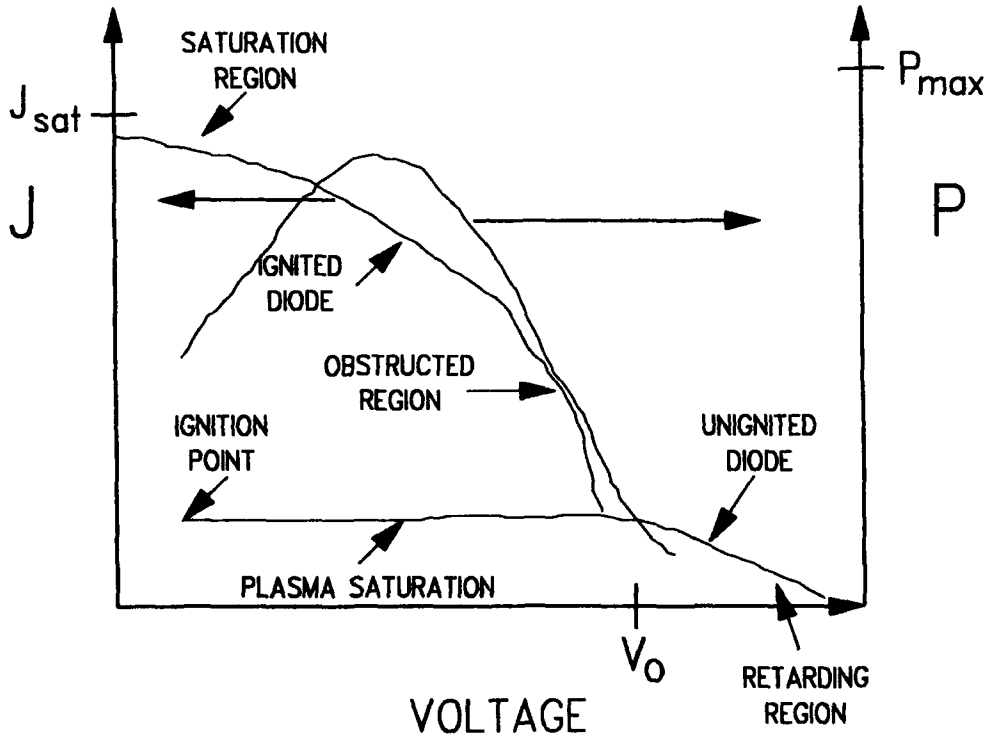

Figure 2.4. High pressure, cesium vapor thermionic converter output characteristics.

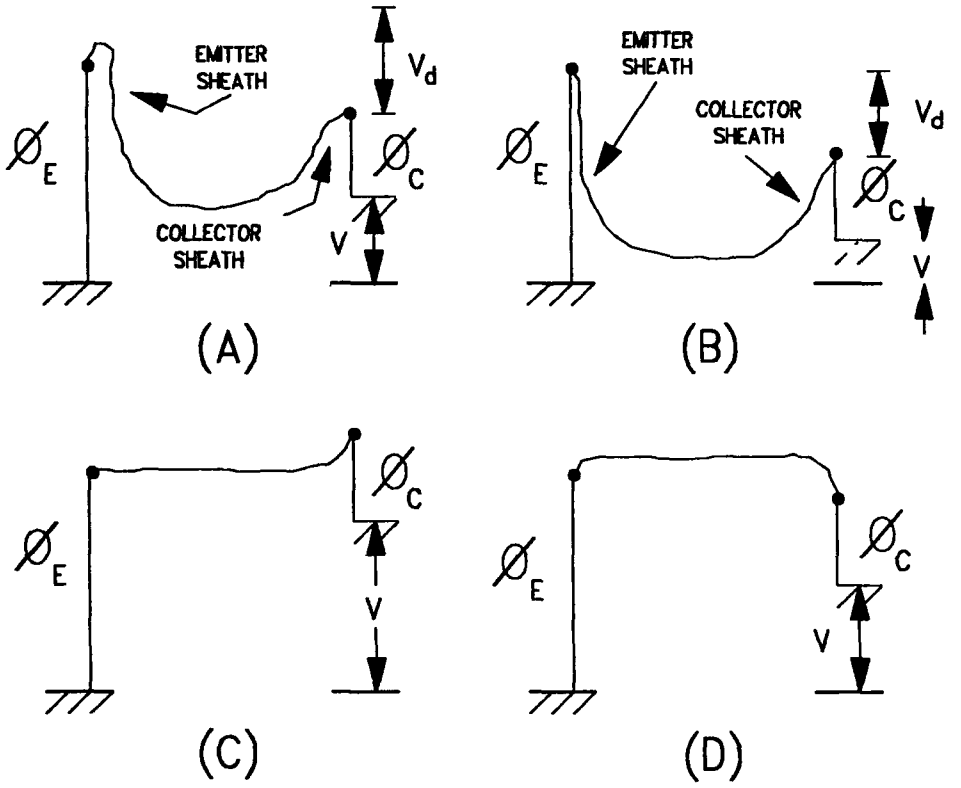

Figure 2.5. Motive diagrams for ignited and unignited modes.
Source: Rasor, N.S. "Thermionic Energy Conversion." Chap. 5 in *Applied Atomic Collision Physics.*

SECTION III
EXPERIMENTAL CHARACTERIZATION OF A MO-RE CONVERTER

The LEOS Mo-Re TEC diode was experimentally tested to provide its output characteristics. This diode was designed to work with the Romashka-type reactor system to provide power for space platforms. This reactor-thermionic converter power system has been optimized for size, weight, reliability, and survivability criteria.

The Romashka reactor system uses uranium carbide fuel in graphite trays. To obtain optimum power and a convenient area for radiation heat transfer, the trays are a cylindrical geometry. The heat generated by the reactor is radiated radially towards the emitter shoes of the thermionic array. Within the diodes, heat is converted into electricity and the waste heat is carried away from the collector by a heat pipe.

The thermionic converter-Romashka reactor system, moderated by graphite, does not require the complex cooling system of a liquid metal cooled reactor. The fuel is separated from the converters by a small gap. This allows for fuel swelling without affecting the interelectrode gap, unlike the TFE. The lack of integral nuclear fuel also means that this converter can be fabricated more readily and does not require expensive in-core testing. Figure 3.1 shows schematic details of the thermionic Romashka reactor system. The conceptual parameters of this power system are given in Table 3.1.

The materials used for the construction of the thermionic converters must be evaluated on several criteria. These major factors include

- Stable high temperature properties
- Creep strength at high temperatures
- Chemical compatibility (dissimilar metals and alkali metals)
- High strength to density ratio
- Thermal cycling capability (recrystallization)
- Space launch survival.

Based upon the above standards, refractory metals, their carbides, and ceramics can be successfully used in thermionic converters. CVD rhenium on molybdenum was chosen by LEOS for the electrode surfaces because of its low cesiated work function. The Mo-Re converter was built because the original attempt to CVD rhenium onto a molybdenum substrate, using LEOS proprietary technology, failed. The interelectrode gap of 0.1016 mm (4.0 mils) and a cesium

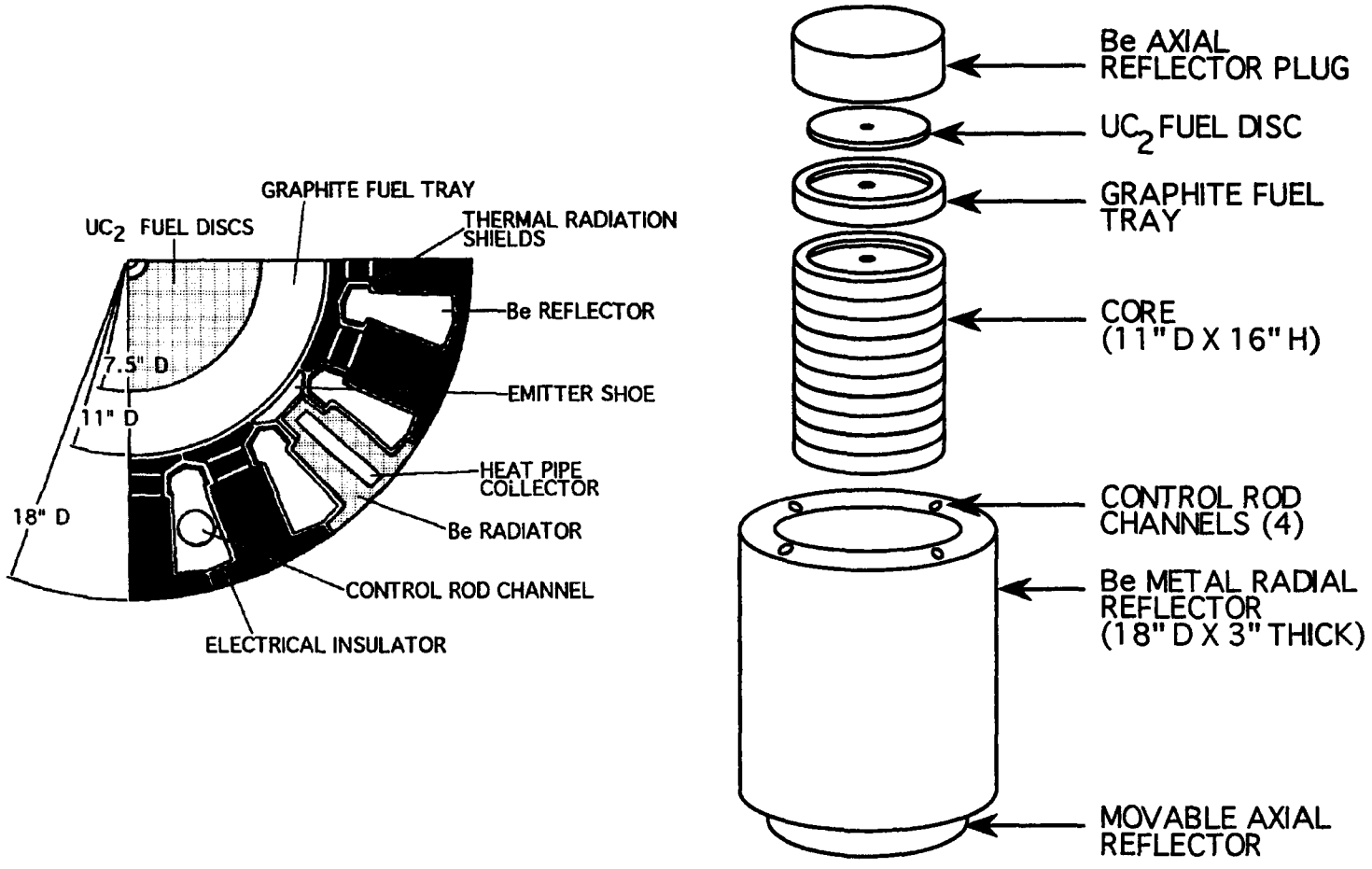

Figure 3.1. Thermionic Romashka reactor system schematic.

pressure of 4.0 torr correspond well to the general p•d bench mark of ≈15 to 20 mil•torr for TEC devices.

Table 3.1
Conceptual Thermionic Power System Parameters

Reactor Power	69.2 kW
Electrical Output	9.6 kWe
System Efficiency	13.9 %
Core C/L Temperature	2270 K
Core Dimensions	
• Diameter	25.5 cm
• Length	50.0 cm
Emitter Temperature	1850 K
Collector Temperature	990 K
Carnot Efficiency	46.5 %
Cesium Reservoir Temperature	600 K
Cesium Pressure	4 torr
Electrode Spacing	0.1016 mm

Source: Anderson, E.A., P. Jalichandra, and R.W. Hamerdinger. "Thermionic Critical Technology Investigation: Report-Task 1."

The emitter heat source is a tungsten wire filament. The wire, coated with hafnium carbide (HfC), is shaped like a potato masher (parallel lines with semicircular connections). The HfC coating is used because of its high emissivity values at high temperatures. An integral sodium-charged, niobium heat pipe transfers heat away from the collector. An HfC coated radiator fin is brazed to the condenser end of the heat pipe. Heat pipes convey more heat than a metal conductor since energy is conveyed by the latent heat of vaporization of the working fluid [40]. The collector temperature is very important to the efficient operation of a thermionic converter. The back emission of electrons and the cesium coverage of the electrodes is controlled by the collector temperature. The use of the boiling/condensing transition of the heat pipe working fluid dampens fluctuations in thermal load so the collector temperature is stabilized.

3.1 Experimental Procedure

The test station for the LEOS thermionic diode provides the ultrahigh vacuum in the bell jar and the emitter and cesium reservoir temperature controls. The load circuit and output screening and data collection systems are also located within the test station.

The bell jar, housing the thermionic converter, must be maintained at ultrahigh vacuum to increase the radiant heating efficiency of the emitter shoe. Rough pumping of the system down to $\approx 10^{-4}$ torr, from atmospheric, is accomplished using a turbomolecular pump. Once this level is attained, an ion pump is used to produce a vacuum of $\approx 10^{-7}$ torr. An ionization gauge measures the pressure in the bell jar. Degassing of the diode, at increasing temperature, is performed to remove molecules and ions remaining in the bell jar interior until $\approx 10^{-8}$ torr is obtained. The ion pump is run continuously to maintain high vacuum during testing.

Once degassing has been accomplished the temperatures of the cesium reservoir and emitter are set to testing levels. Each system has its own independent controller. The temperatures are measured using thermocouples placed along the reservoir and in a cavity in the emitter shoe. The reservoir uses a proportional control system while the emitter uses a proportional-integral-derivative (PID) controller. The reservoir is heated by its own resistance heater and cooled by a compressed air system. The PID controller is used for the emitter because of its ability to reduce oscillations in emitter temperature. The emitter heating element requires ≈60 amperes to generate 733 watts of thermal power. Excess current adjustments or on/off switching would damage the tungsten filament at these high current levels. Electron cooling and radiation to the collector cool the emitter. The collector, radiatively coupled to the emitter, does not have a temperature control system. A calibration curve allows the collector temperature to be determined from the emitter temperature. A thermocouple attached to the heat pipe evaporator provides the measurement for collector temperature. The inability of the collector temperature to be controlled is a major disadvantage of this design. Performance mapping of the TEC diode is limited to the emitter and reservoir temperatures because of the T_E - T_C interdependence.

After degassing, and emitter and cesium reservoir temperature stabilization, the experiment is performed. A scanning thermocouple reader displays the temperatures of the cesium reservoir, the top and bottom of the heat pipe, the radiator fin, cooling water inlet and outlet, and cesium cooling inlet and outlet. The load circuit, a shunt resistance and voltage sweep generator, is connected to the diode as shown in Figure 3.2.

The sweep controller uses an AC waveform to bias the collector across a variable range (usually ±2 volts) in ≈15 milliseconds. This allows a full J-V output curve to be obtained in much less time than the time constant of the electrode-plasma system so there is virtually no change in temperatures. A digital oscilloscope is used to screen the data obtained at every sweep. The

output voltage is read across the electrodes. The current is determined from the voltage across a precision 0.1Ω shunt resistance. The output is captured and saved on floppy disks using the oscilloscope. The data files, after conversion, can be processed on Macintosh or PC for analysis and presentation.

3.2 Output Characteristics

The Mo-Re converter output characteristics were obtained for collector and cesium reservoir temperatures from 652 to 717°C and 227 to 377°C, respectively. The thermocouple within the emitter shoe was not properly positioned and its readings were incorrect. Collector temperature was used as the characteristic temperature. A maximum current density of 340 mA/cm^2 was obtained at T_C = 717°C and T_R = 377°C. The peak power density of 33 mW/cm^2 occurred at T_C = 652°C and T_R = 327°C.

Figure 3.3 shows typical output from the Mo-Re converter. A set of output from this diode is contained in Appendix A. The maximum current density was obtained at large negative voltages, leading to large power usage. The P-V curves show power input on the order of 2 watts and power generation in the 0.1-watt range. The output does show plasma ignition where large currents are generated as the voltage is decreased. In the ignited mode of operation, positive ions are primarily produced in the gap by means of inelastic collisions. Thermionically emitted ions from the electrodes have a negligible effect upon the output characteristics in the ignited region.

Before the emitter thermocouple could be repaired or further testing performed to generate higher output, a short circuit was suspected to have developed between the emitter and collector. The short was found after the diode was removed from the testing chamber for heater repairs. Further performance characterization could not be performed, but the determination of the cause of the short would, in itself, provide valuable information.

LEOS has provided output characteristics for the Mo-Re diode gathered at their facility. These characteristics were gathered for emitter temperatures of 1550 to 1700°C. The temperatures of the collector and cesium reservoir were not provided. The data, though limited, show a peak current density of over 18 A/cm^2 and a maximum power density of nearly 8.6 W/cm^2 at T_E = 1700 °C. Both the J-V and P-V curves increase with increasing emitter temperature. These output curves are shown in Figure 3.4.

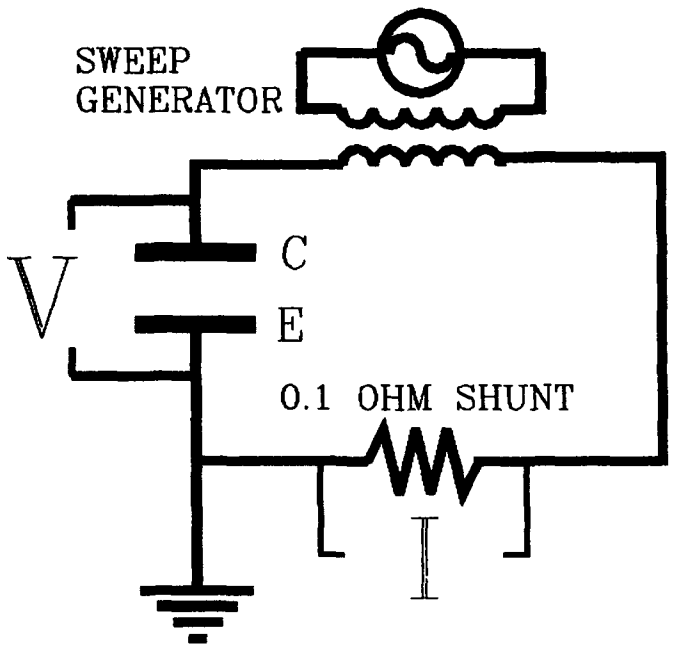

Figure 3.2. Test station load circuit.

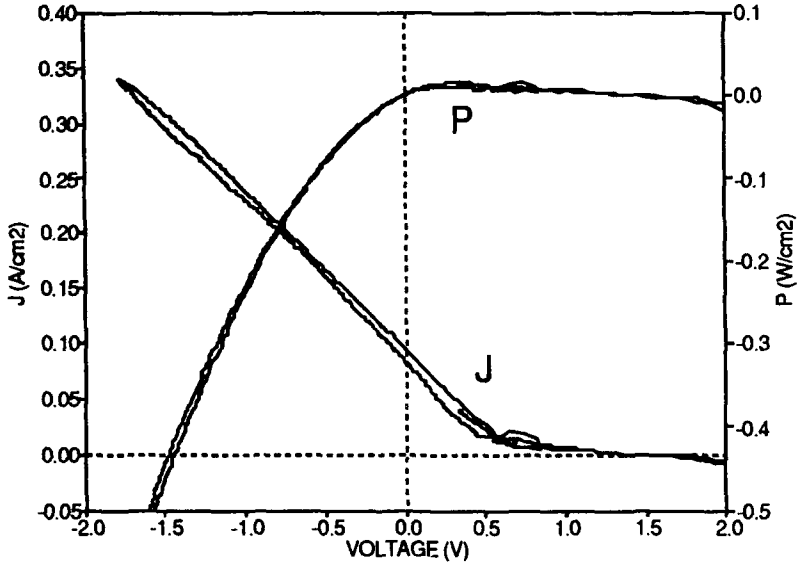

Figure 3.3. Experimental output from the Mo-Re converter. T_C = 717°C and T_R = 377°C.

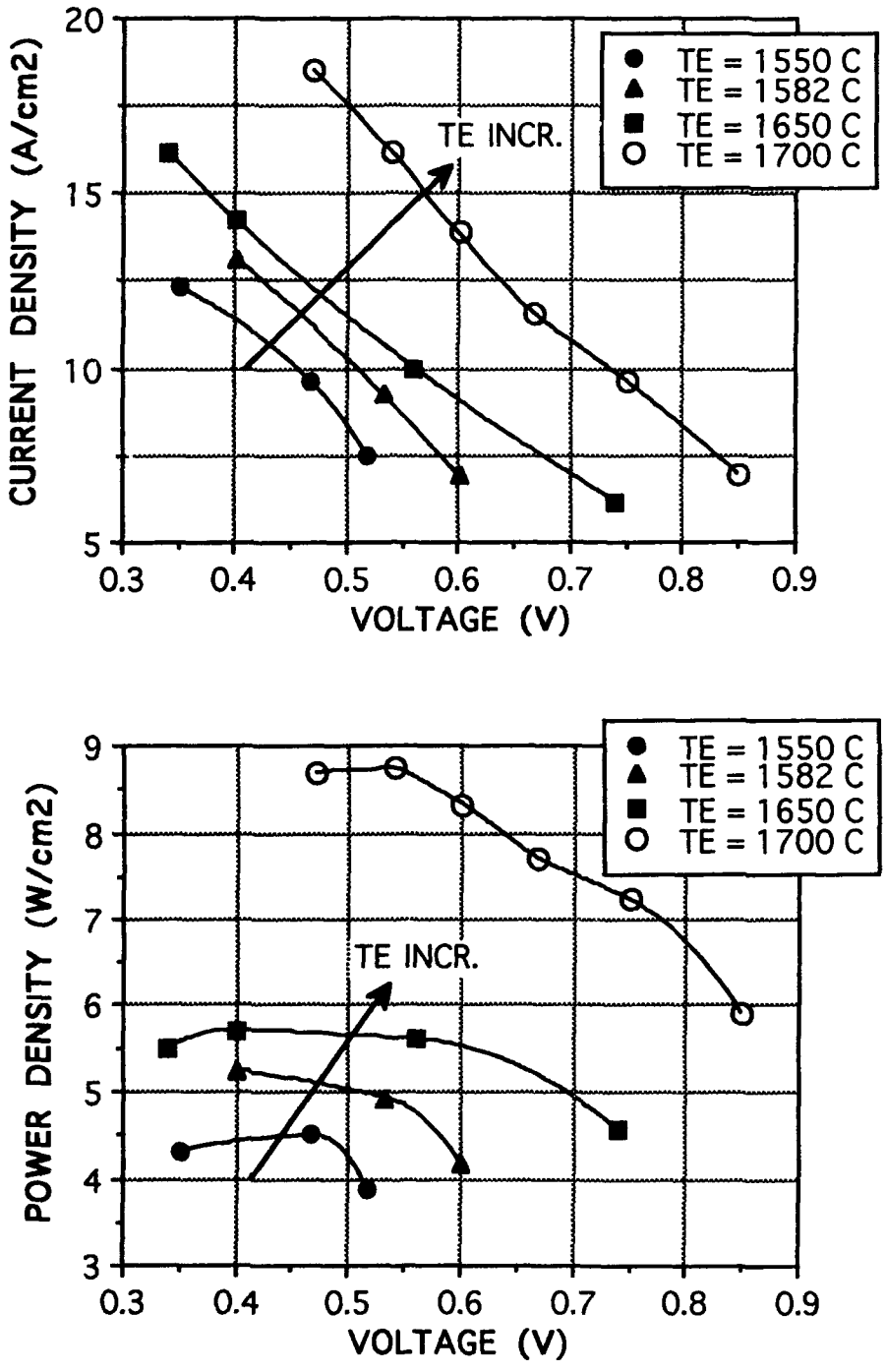

Figure 3.4. LEOS generated output data for Mo-Re converter.

Even without the temperature data necessary for an accurate comparison, it can be seen that the LEOS output is much greater than that obtained at Wright Laboratory using the same diode. The experimental output has the characteristics of a plasma diode, but the maximum current is two orders of magnitude below expected values. The output J-V curves begin with the reverse current region at high voltages, then progress to the retarding and pseudosaturation regions. Ignition of the plasma occurs near V ≈0.5 volts and J ≈25 mA/cm^2. The rapidly rising ignition region approaches its maximum as the voltage becomes increasingly negative. Large power input is required to keep the diode producing current.

The J-V characteristics of the Mo-Re converter deviate considerably from the ideal. Many elastic and inelastic collisions occur within the cesium plasma as a result of the low mean free path for electrons. The magnitude and direction of the original electron velocities are altered by particle interactions. Elastic collisions reduce the average momentum by reversing the direction of a fraction of the electrons. Inelastic collisions result in the ionization and excitation of atoms. The total translational kinetic energy of the particles involved in inelastic collisions is not conserved.

The effects of inelastic collisions and the ion-richness ratio, β, can be seen in the Mo-Re output curves. The ion-richness ratio expresses the effectiveness of positive ions to reduce the negative space-charge near the electrodes, and is given by

$$\beta = \sqrt{\frac{m_I}{m_e}}\,\frac{\tilde{J}_{ES}}{J_{ES}} = 492\,\frac{\tilde{J}_{ES}}{J_{ES}} \quad . \tag{3.1}$$

The ion and electron emitter saturation currents, given by the Saha-Langmuir and Richardson-Dushmann equations, respectively, are

$$\tilde{J}_{ES} = \frac{e\,p_{CS}}{\sqrt{2\pi\, m_{CS}\, kT_{CS}}\left[1 + 2\exp\left(\frac{V_I - \phi_E}{kT_E}\right)\right]} \tag{3.2}$$

and

$$J_{ES} = AT_E^2 \exp\left(-\frac{\phi_E}{kT_E}\right) . \qquad (3.3)$$

When $\beta < 0.8$ the operation of the converter is in the electron-rich regime. As β decreases, the ions cannot neutralize the space-charge. The result is an output current reduced below ideal.

It appears that the Mo-Re converter was operating in the electron-rich regime as shown by the low current density values. The output does show ignition, however. Generally, ignition signifies high current values on the order of tens of amps per cm^2. The ignition of these data suggests that inelastic collisions in the plasma must have ignited electron and ion production in the gap. The ions produced were unable to compensate for the increase in space-charge due to an increase in electron density.

The performance of a planar thermionic diode employing molybdenum and CVD-Re electrodes was investigated. The maximum output current density and power density obtained was 340 mA/cm^2 and 33 mW/cm^2, respectively. A short circuit within the converter prevented the cause of the low output from being ascertained. A short circuit terminated efforts for the performance evaluation of the Mo-Re diode but provided the motivation for further investigations.

SECTION IV
FAILURE ANALYSIS OF MO-RE CONVERTER BY NONDESTRUCTIVE EVALUATION

After obtaining several sets of experimental data from the Mo-Re diode, a spark inside the chamber was observed and the filament power input fuse was blown. The emitter heating filament was found broken at a ceramic standoff. The diode was removed from the test station for repairs. During the repair it was found that the electrodes were short circuited. The electrodes of a properly working converter should be open with respect to ground. The emitter heater was not repaired and LEOS recommended separating the converter components to investigate the electrode area. This method would destroy the converter and release the highly reactive cesium.

Nondestructive evaluation (NDE) of the converter was chosen to determine the cause of the short circuit. NDE employs advanced methods to detect, characterize, and evaluate the significance of defects. This technique will allow valuable information to be gathered without destroying the converter. Several tests can be performed and their results examined. A destructive evaluation, correlated with the NDE, can be resorted to if the NDE fails to ascertain the cause of the short. Possible causes of the short circuit could be whisker growth, contact due to electrode warping, or solidified cesium in the interelectrode gap.

4.1 Electrode Evaporation and Expansion

High electron emission is accompanied by high evaporation from the electrode surfaces. An electrode area not covered by adsorbed cesium would allow evaporation of the electrode. This material would condense on a cooler surface, such as the emitter support. The deposition of material could create a connection between the electrodes.

The vapor pressure of the electrode material governs the rate of material evaporation. From the Clausius-Clapeyron relation of classical thermodynamics, which relates pressure to temperature in a two-phase system in equilibrium, it is found that the logarithm of the vapor pressure varies with the inverse of temperature. More accurate analytical expressions have been developed which introduce additional terms. Reference [41] has compiled and reviewed vapor pressure data from many sources. Table 4.1 lists the vapor pressures of molybdenum and

rhenium calculated near emitter temperatures. The equation used to determine the vapor pressures has the following form:

$$\log P_{vapor} = A - \frac{B}{T} + CT + D\log T \qquad (4.1)$$

where A, B, C, and D are the constants determined from empirical fits to the experimental data in [41].

Table 4.1
Vapor Pressures of Molybdenum and Rhenium at Elevated Temperatures

TEMPERATURE (°C)	Mo VAPOR PRESSURE (torr)	Re VAPOR PRESSURE (torr)
1450	$3.464 \cdot 10^{-10}$	$8.597 \cdot 10^{-14}$
1500	$1.241 \cdot 10^{-9}$	$4.003 \cdot 10^{-13}$
1550	$4.157 \cdot 10^{-9}$	$1.702 \cdot 10^{-12}$
1600	$1.307 \cdot 10^{-8}$	$6.658 \cdot 10^{-12}$
1650	$3.874 \cdot 10^{-8}$	$2.413 \cdot 10^{-11}$
1700	$1.087 \cdot 10^{-7}$	$8.153 \cdot 10^{-11}$
1750	$2.898 \cdot 10^{-7}$	$2.583 \cdot 10^{-10}$
1800	$7.361 \cdot 10^{-7}$	$7.708 \cdot 10^{-10}$

The pressure inside the diode is governed by the temperature of the cesium reservoir. The cesium pressure, at temperatures near 300 to 330°C, is 2.0 to 4.0 torr. The vapor pressure of the electrode materials is 7 to 14 orders of magnitude lower than the pressure inside the converter. The number of molecules evaporating from the electrodes can be estimated from knowledge of the vapor pressure. From kinetic theory, the rate at which particles cross a unit surface in unit time is

$$\dot{N} = \frac{1}{4} n u_{av} \quad . \qquad (4.2)$$

If the number of particles is expressed by the ideal gas law as $n = p/(kT)$ and the arithmetic mean speed, found from a Maxwellian distribution, is

$$u_{av} = \sqrt{\frac{8kT}{\pi m}} \tag{4.3}$$

than the number of particles crossing a unit area per unit time is

$$\dot{N} = \frac{p}{\sqrt{2\pi mkT}} \quad . \tag{4.4}$$

The least conservative estimate of material evaporation would assume the electrode is held at emitter temperature in a vacuum. At a temperature of 1800°C, the vapor pressure of molybdenum is found from Table 4.1. The evaporation rate, calculated using equation 4.4, is $5.8 \cdot 10^{17}$ atoms/(cm^2•sec). The amount of material evaporated from the molybdenum emitter is only $2.83 \cdot 10^{-5}$ cm/year. The number of molecules evaporating from the electrodes can, therefore, be neglected. It is improbable that a connection has formed between the electrodes composed of evaporated electrode material.

The high temperature of thermionic converter operation will cause an increase in the volume of the electrodes and reduce the interelectrode gap from its room temperature value. A short circuit may occur if the total expansion of the electrodes into the gap is comparable to the gap length. An estimate of electrode expansion can be made using the linear coefficient of thermal expansion for molybdenum. The following equation was used to estimate the change in gap length as a function of temperature:

$$-\Delta d = \beta_{Mo} L_E \Delta T_E + \beta_{Mo} L_C \Delta T_C \quad . \tag{4.5}$$

The value of the linear coefficient of thermal expansion for molybdenum was found in [42]. The emitter and collector thicknesses are 1.27 and 1.65 mm, and their temperature changes are 1700 and 700°C, respectively. The gap length change was found to be $1.65 \cdot 10^{-3}$ mm. This change in gap length is small compared to the interelectrode distance. The temperature reduced gap is well within the manufacturing limits of 0.076 to 0.127 mm. Warping of the electrodes due to temperature induced expansion is an unlikely cause of the Mo-Re converter short circuit.

4.2 Interelectrode Cesium Investigation

The cesium within the converter will condense on cooler surfaces as the converter cools. Some cesium will also condense upon the hot electrode surfaces. Alkali metals, such as cesium, are used in heat pipes because of their high surface tension and ability to wick. This wicking action will tend to draw cesium into the gap. When the diode finally cools to room temperature, the cesium could fill the interelectrode gap. Since cesium is a conductive metal, the electrodes would be at the same electrical potential.

The objective of this NDE investigation was to heat the cesium reservoir without heating the diode. As the temperature of the cesium increases, cesium between the electrodes will melt and vaporize. At room temperature and atmospheric pressure, cesium is semiliquid with its melting point at 28.5°C. The boiling point is 670°C. As the pressure is reduced to 9.0 and 4.2 torr, the boiling point decreases to 365 and 330°C, respectively [43]. The low pressure inside the diode allows the cesium to boil near the reservoir temperature. The hot cesium vapor particles will have to transfer their energy to the cesium within the gap. The small edge area of the thin gap will slow this heat transfer. The goal of this investigation was to measure the change in resistance across the electrodes as a function of the cesium reservoir temperature. If cesium is not the cause of the short, then no change in resistance will be measured. Insufficient heating and evaporation of the interelectrode cesium may result in a small change in resistance.

This experiment was performed in a high vacuum test station used for the characterization of high temperature insulators, such as diamond films. This station has the instrumentation and equipment for evacuating the test chamber, supplying power to the cesium heater, and measuring the cesium reservoir temperature. The station is also equipped with a programmable electrometer to measure the resistance across the electrodes. This device can accurately measure resistances up to 200 GΩ.

The test station was evacuated to 10^{-6} torr before the test was conducted. The temperature of the diode was 25°C. The electrometer measured 0.6-0.7Ω across the electrodes. The cesium reservoir temperature was set, in steps of ≈100°C, to a maximum of 327°C on the PID temperature controller. The resistance was monitored as the temperature increased.

The diode was allowed several hours to equilibrate at a reservoir temperature of 317°C. The resistance of the diode, monitored during the temperature increase and after sufficient time for the interelectrode cesium to evaporate, did not change. After maintaining high temperature for several more hours the resistance still did not change. The heater was turned off and the

diode was allowed to return to room temperature. The resistance had not changed through an entire thermal cycle.

A resistance change was also not registered during second and third tests with the reservoir maintained at 330 and 350°C. The conclusion from this investigation is that solidified cesium between the electrodes cannot be the cause of the short circuit. The cesium, contained within the diode at low pressure, was given sufficient heat energy and time to vaporize away from the interelectrode region.

If a very small leak had developed between the interelectrode space/cesium reservoir and the atmosphere, a small amount of cesium may have leaked out or air leaked in. This gas leakage out or in may cause the very low currents observed in the experimental testing. If excess oxygen had entered the interelectrode space, cesium oxides, CsO_x, would have formed. These oxides would corrode the internal surfaces and, in effect, reduce the cesium pressure. The pressure would also reduce in cesium had leaked out. With a low cesium pressure, the plasma would still ionize, but the output would be extremely low, as shown in Appendix A. Tests are currently being planned to determine if a leak exists in the converter and, using a computer TEC simulation, what the effects on the output would be.

4.3 Computed Tomography

The first NDE technique used to investigate the interior of the shorted diode is an X-ray imaging system. Computed tomography (CT) produces two-dimensional, interior cross sections of a sample. The CT system inspects objects on a through body plane, called a slice, that removes the superposition of information in the material. The original CT systems were derivatives of the medical CAT scan. The CT slices are imaged at different heights along the sample enabling a three-dimensional image to be reconstructed by a computer. The reconstructed images can be queried to provide the number of X-ray counts as a function of position on the image. The number of counts projected onto the slice is related to the average material density in the thickness of the slice. The change in material density across (x- and y-axes) and along (z-axis) a sample can be determined nonintrusively.

The X-ray computed tomography system employed can image objects as large as 50 by 85 cm weighing 45 kg. There are 72 detector paths for the X-rays. The X-ray source produces a 420-kV continuous beam from a tungsten filament.

The anticipated result of using the CT system on the Mo-Re diode was a set of slices clearly showing a gap between two metallic electrodes. High X-ray counts within the gap would mean cesium has collected within the gap whereas low counts would mean the gap is properly evacuated. The slices would also verify the internal construction of the converter and the materials used in its construction.

The Mo-Re diode was imaged from the emitter shoe to the heat pipe, as shown in Figure 4.1, in 0.5-mm increments. The slice thickness was 2 millimeters. Twenty scans were performed for a total scan length of 1 centimeter. The scans were overlapped to assist the detection of the interelectrode gap and the change in materials near the electrode region.

The CT system can penetrate and image several centimeters of steel with its high power source. The high Z materials used in the construction of the converter were easily penetrated and CT images successfully collected. The 16-bit digital images were reconstructed by a VAX computer and imaged by digital-image-processing software on a Macintosh computer. This software allows the number of X-ray counts along a cut line to be plotted versus position along the line.

The CT system produced eight slices starting at the emitter shoe and ending within the heat pipe. The slices outside this range provided no additional information. The plots of counts versus diametrical position of these slices is shown in Figure 4.2. The materials used in the diode construction are shown in the position of their approximate number of counts. The number of counts is the material density in mg/cm^3. The detectors have only been calibrated up to molybdenum, reducing the confidence in extrapolating to rhenium.

Slice five begins the CT account of the Mo-Re diode. In this slice the edge count is higher than the count in the center. The edge count corresponds to the rhenium emitter support while the center count corresponds to a mix of molybdenum and rhenium. Because the counts shown across the slice face is, in actuality, the average count in the thickness of the slice, the count data comprises several materials. Knowing the height of the slice and its thickness, it is likely that the interelectrode gap is contained within this slice or the next. Slice six is similar to slice five, except that low counts are registered just within the boundaries of the slice. This is the start of the annular gap between the collector/heat pipe and the emitter support. This gap allows cesium vapor to flow from its reservoir into the electrode region.

Slices seven through nine show the higher count emitter support, the annular gap, and the center region. The diameter of the center region corresponds to the diameter of the collector

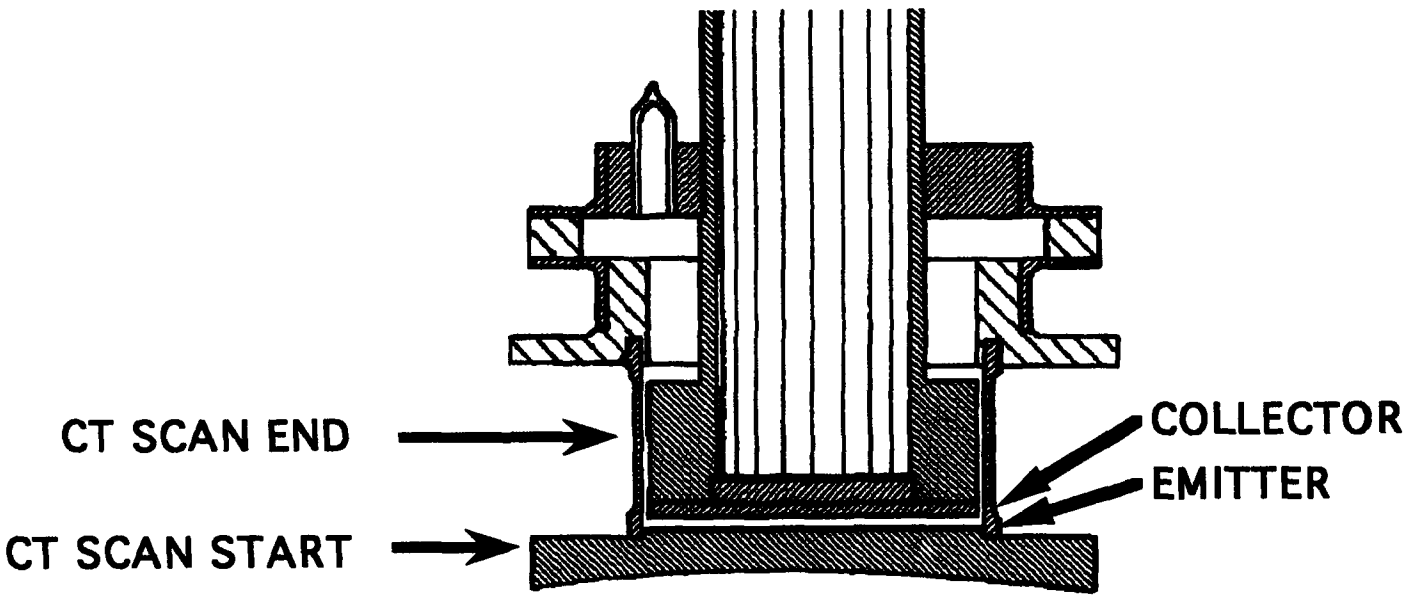

Figure 4.1. Distance along converter imaged by the computed tomography method.

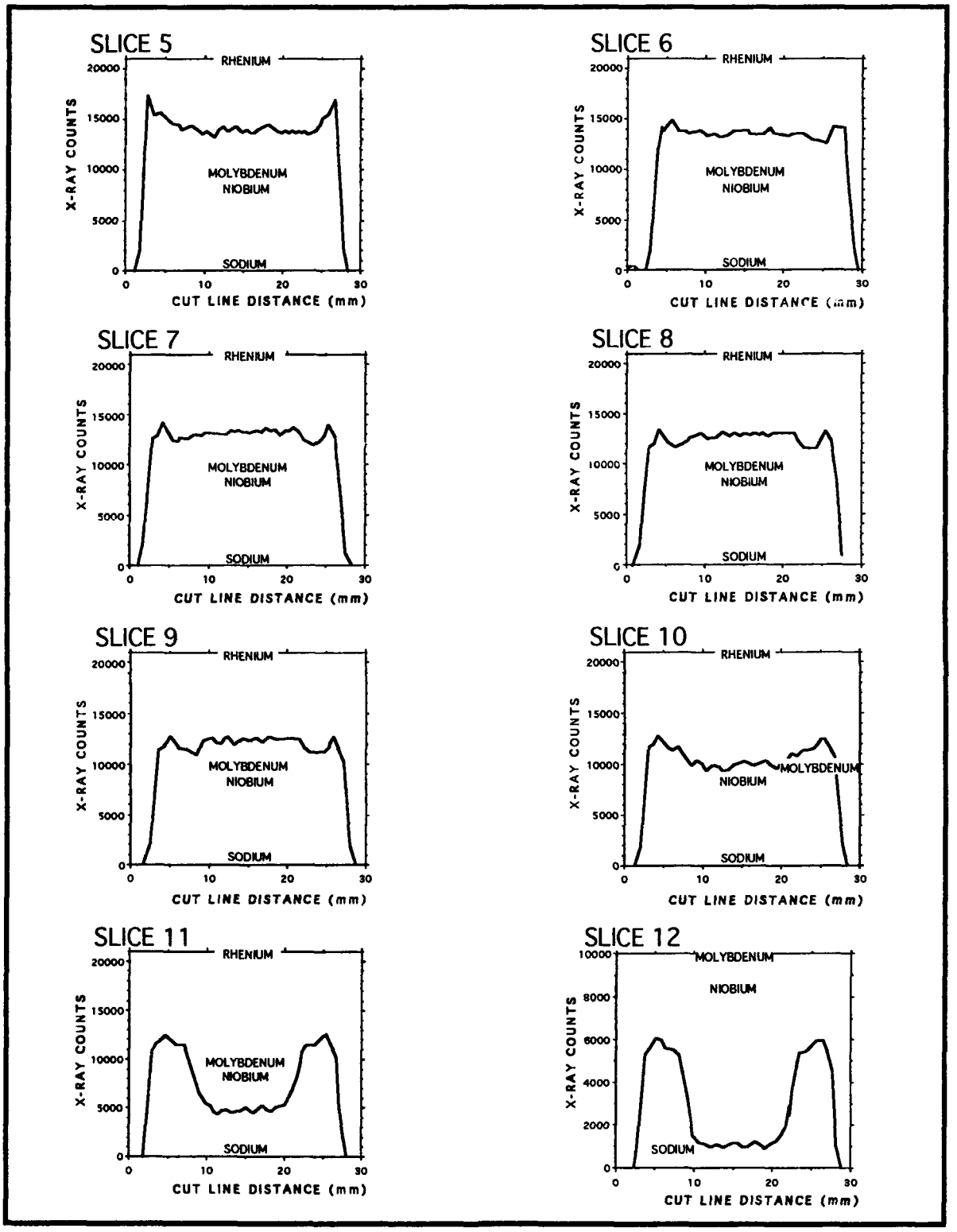

Figure 4.2. X-ray count data from CT slices of Mo-Re converter.

face. The edge peaks in slice nine are slightly lower and can be attributed to the influence of the niobium heat pipe.

The center region of slice ten shows reduced counts near or below that of the molybdenum cap. The sodium used as the heat pipe working fluid is influencing these counts. The diameter of the center is also reduced. Slice ten has imaged that portion of the collector/end cap that fits into the heat pipe. Slice eleven is similar to ten with the center counts reduced even further. In slice twelve the center counts correspond to the density of sodium. The sodium within the heat pipe solidified at the evaporator due to the vertical orientation of the converter in the test station.

The energy of the CT system allowed its X-rays to penetrate and image the converter. The system configuration allows for an optimum spatial resolution of 0.25 mm. This resolution is, however, not enough to clearly image the gap. By averaging the X-ray count of the 2-millimeter slice, the 0.1016-mm gap was lost within the metal bulk. Thinner slices decrease the signal-to-noise ratio and reduce resolution. The CT did allow the material changes within the diode to be qualitatively investigated. The rhenium emitter support, molybdenum electrodes, niobium heat pipe, and sodium working fluid were all detected using the CT system. What is needed is a high energy system combined with high resolution.

A microtomograph CT system is also available. This system generates CT images with an ultimate resolution of 0.025 mm. The microtomograph uses a 175-kV X-ray source and can only rotate the sample. The X-ray energy and intensity of this system is low. Imaging through several millimeters of metal is possible, but resolution suffers. This system is primarily for very thin samples constructed from low Z materials, such as microcircuit boards.

Improved X-ray CT systems are being developed that can, theoretically, combine high energy with high resolution. The most promising configuration will utilize a high energy source, such as a synchrotron or a linear accelerator, placed far from the detector. The sample would be placed as close as possible to the detector. The source must be capable of the high energy flux necessary to produce an image from long distances. The close proximity of the sample to the detector reduces detector-dependent resolution distortions. The high energy and flux of the source would compensate for resolution reduction due to the extreme distance between the source and sample. It is speculated that a system of this type, using 500-kV X-rays, should be able to image several centimeters of steel at 0.025-mm resolution. High energy-high resolution CT imaging is currently in the planning stages awaiting funding.

4.4 X-Ray Radiography

A second X-ray imaging, NDE technique was also employed for examining the diode. X-ray radiography uses X-rays to penetrate a sample and produce a shadow image. The image is the superposition of density data from all material located between the source and detector. The attenuation of the X-ray signal is determined by the atomic number of the material penetrated. The final sample image is collected upon a radiographic plate similar to a medical X-ray.

A real-time, microfocus X-ray radiograph was used to image the diode. The X-rays, generated from a cylindrical tungsten target, had an energy of 160 kV. Microfocus refers to an X-ray point source produced by focusing the electron beam. A point source reduces geometric intolerance and produces crisp edges. The sample table has translational and rotational capabilities. This radiograph has previously been used to image 0.127-mm diameter holes in copper plates. The magnification factor was high with that small sample, enabling the hole to be easily found. The size of the plate and the relative positioning of the source, detector, and sample dictate the magnification factor. The resolution of the microfocus X-ray system is on the order of 0.025 mm.

It was expected that the microfocus X-ray system would produce an image showing the interelectrode gap. The gap would appear as a region of little or no X-ray attenuation between the metallic, high Z electrodes. If cesium was present within the gap, it would be difficult to distinguish the electrodes. A physical connection between the electrodes would also be apparent if its size was within the detectable limits.

Imaging a 0.1016 mm gap is within the resolution of this equipment, but the large size of the converter limits the obtainable magnification factor. This makes finding the gap on the radiographic plate more difficult. The high atomic number of the elements used in the construction of the diode also reduces the ability of the system. The gap is shielded by a rhenium emitter support ($Z_{Re} = 75$). Other materials used in the construction of the diode are molybdenum ($Z_{Mo} = 42$) and niobium ($Z_{Nb} = 41$).

The image of the Mo-Re converter, obtained from the microfocus X-ray system, has a magnification factor of 5. The image has excellent resolution through the niobium heat pipe. The capillary channels on the inside heat pipe wall are clearly shown. The channels are 0.203 mm wide and 0.406 mm deep. Their clear resolution implies that 0.1016 mm is within the resolution

of this equipment. The gap region, however, was not imaged using this equipment. Zero intensity was registered by the detector in this region. The X-rays had neither the energy nor intensity to penetrate the converter and be registered.

The X-ray source is the limiting factor of this system. The microfocus unit had enough energy and intensity to penetrate and image the thin-walled niobium heat pipe but not enough to penetrate and image the much thicker and higher Z area near the electrodes. This system works best imaging integrated circuit boards or other small, thin samples that can be directly attached to the X-ray source and placed at a maximum distance from the detector.

Commercial microfocus X-ray systems are available that employ higher energy X-rays than used in this investigation. These units have the resolution to detect the gap if the diode can be fully penetrated. A standard radiographic system using energetic X-rays could also be used to image the diode. The major problem associated with this type of system would be positioning the gap exactly parallel with the incoming X-rays. Only then would the radiographic plate image a gap between electrodes.

Several NDE investigations were performed on the nonfunctioning Mo-Re converter. Electrode evaporation and swelling were found to be negligible. By heating the cesium reservoir and measuring no change in the resistance across the electrodes, it was determined that solidified cesium had not shorted the converter. A very small leak may have developed, though, between the interelectrode space and the environment. This would cause only extremely low currents to be produced by the converter. X-ray radiography was performed using both a real-time, microfocus system and a computed tomography method. The microfocus unit produced a shadow image of the converter but was unable to image the thick, high Z material in the electrode area. The CT method removed the superposition of X-ray images and produced through body planes but lacked the resolution to image the interelectrode gap. The short circuit must be caused by a connection within the converter. The nonconductive, ceramic seal separating the portions of the converter may have failed. The converter may have been physical damaged causing components to touch and create the short. A large flake of CVD-Re may have broken off from the collector and contacted the emitter. The inability of LEOS to successfully bond CVD-Re to the emitter during the construction of this diode makes collector breakage a most likely candidate for further investigation. When nondestructive means have been exhausted, a destructive evaluation will be performed. The results will be correlated with the data gathered in the NDE investigations.

SECTION V
TESTING AND CHARACTERIZATION OF A RE-RE CONVERTER

The second LEOS thermionic converter uses CVD-Re on molybdenum for both electrode surfaces. The design and materials of this converter are identical to the Mo-Re diode described previously, except for the emitter surface. LEOS apparently overcame earlier problems bonding the rhenium to the molybdenum emitter substrate.

5.1 **Experimentation**

The testing of the Re-Re converter followed the same procedures and used the same test station as the Mo-Re diode. After degassing the diode and evacuating the bell jar, the temperatures of the emitter and cesium reservoir were set on their respective controllers. The sweep controller biased the collector, and the oscilloscope displayed and collected the output data.

The first set of tests varied the emitter temperature from 1450 to 1750°C. The reservoir temperature was set at 327°C but never reached its set point. The reservoir attained its highest value of 323°C, at T_E = 1500°C, with the cesium heater receiving its maximum rated current of eight amps. A typical output curve is shown in Figure 5.1, with the complete set of output curves in Appendix B.

The heat pipe, in these tests, was not surrounded by a radiation shield. The purpose of the shielding is to reduce thermal radiation exchange between the heat pipe and its surroundings. When radiation heat transfer is the only means to remove heat from the converter, such as in space applications, the size of the radiator is reduced as its temperature increases. The effect of increasing the radiator temperature is considerable due to the nature of thermal radiation as embodied in the Stefan-Boltzmann law for radiation heat transfer,

$$q_{rad} = A_i F_{ij} \sigma \left(T_i^4 - T_j^4 \right) \quad . \tag{5.1}$$

For a fixed heat load, shape factor, and space temperature near zero Kelvin, as the radiator temperature increases, its area decreases proportional to the inverse fourth power of its temperature. Elevated heat rejection temperatures make thermionic conversion a very competitive, low to medium power conversion system for space borne platforms.

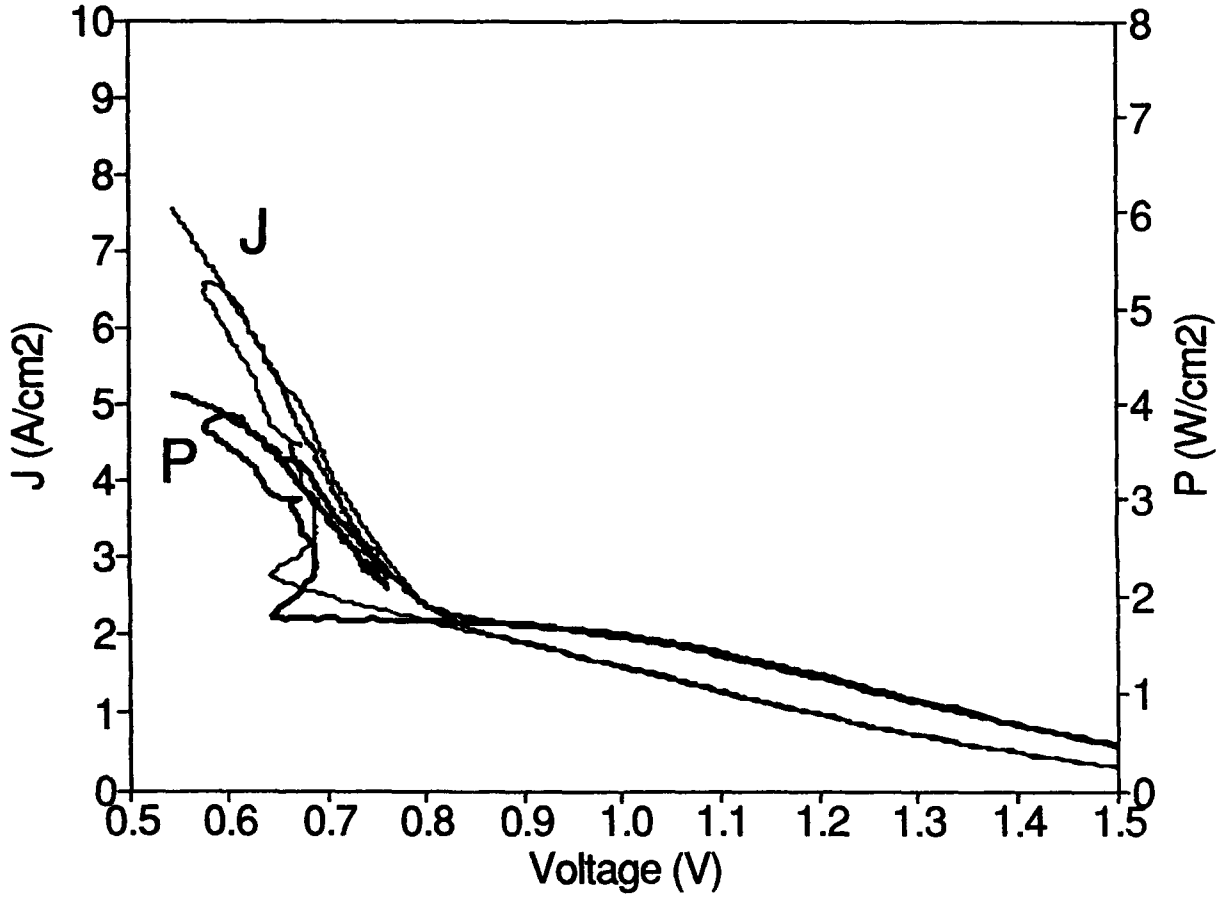

Figure 5.1. Re-Re converter output without a heat shield. T_E = 1600°C, T_C = 562°C, T_R = 324°C.

A second set of output data was gathered after a radiation shield was wrapped around the heat pipe. This shield is a tantalum foil cylinder. The shiny, metallic shield has a low emissivity of ≈0.1 [44]. As shown in Appendix C, the shield reduced the heat transfer from the heat pipe enough to return its isothermal operation.

Figure 5.2 shows the effect of the radiation shielding upon the heat pipe temperature drop. The nonshielded heat pipe had temperature drops of 30 to 40°C whereas the shielded heat pipe experienced only 1 to 3°C losses. For a heat pipe to operate properly, the region between the evaporator and the condenser should be adiabatic. The adiabatic region will act as an additional heat sink if it is allowed to radiate large amounts of heat.

Using the temperature data from the two Re-Re tests, temperature calibration curves were created. These calibration curves, Figure 5.3, allow one to determine the collector temperature knowing the emitter temperature. The effect of the radiation shielding can also be seen from these curves. At a fixed emitter temperature, the collector temperature for the nonshielded case is 65 to 83°C lower than for the tests with shielding. The radiation to the surroundings increased the heat transfer from the collector. For space applications where maneuverability, survivability, and radiator mass are to be minimized, the thermal radiation between the heat pipes and their surroundings must be reduced.

5.2 Characterization of Output Data

The output from the Re-Re diode has the classic high-pressure characteristics described in reference [4]. The output voltage, or current, is deficient in comparison to ideal vacuum characteristics due to collisions. Collisions, though resulting in beneficial electron and ion production, also alter the momentum and energy of the colliding electrons. High pressure, cesiated diodes with refractory metal electrodes have achieved the highest TEC performance in spite of the voltage, or current, drop compared to the ideal. The beneficial effects of high cesium pressure outweigh its detrimental effects.

Collector temperature affects the performance of the converter by altering the collector work function and the back emission. A typical cesiated collector work function plotted against the ratio of collector to reservoir temperature, Figure 5.4, is minimum near $T_C/T_R \approx 1.8$. The output of a thermionic converter decreases as T_C is increased beyond the optimum because higher collector temperatures increase back emission and the collector work function. Below the minimum, as T_C decreases and ϕ_C increases, output voltage is reduced.

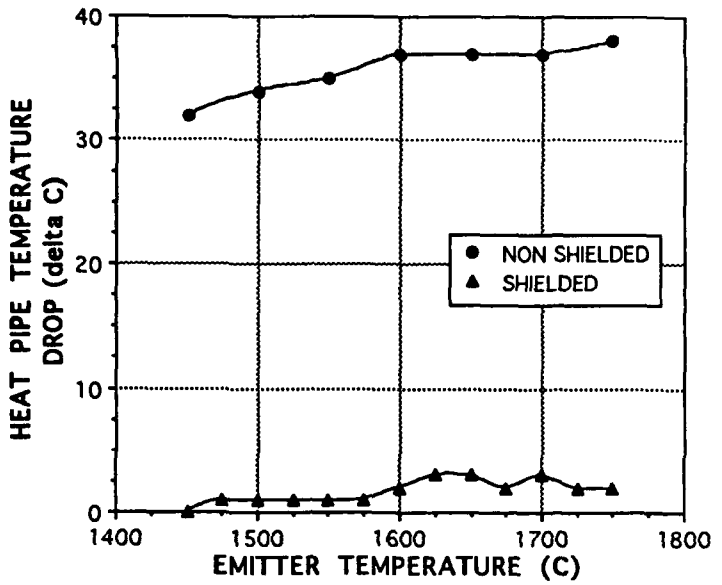

Figure 5.2. Effect of radiation shielding upon heat pipe temperature drop.

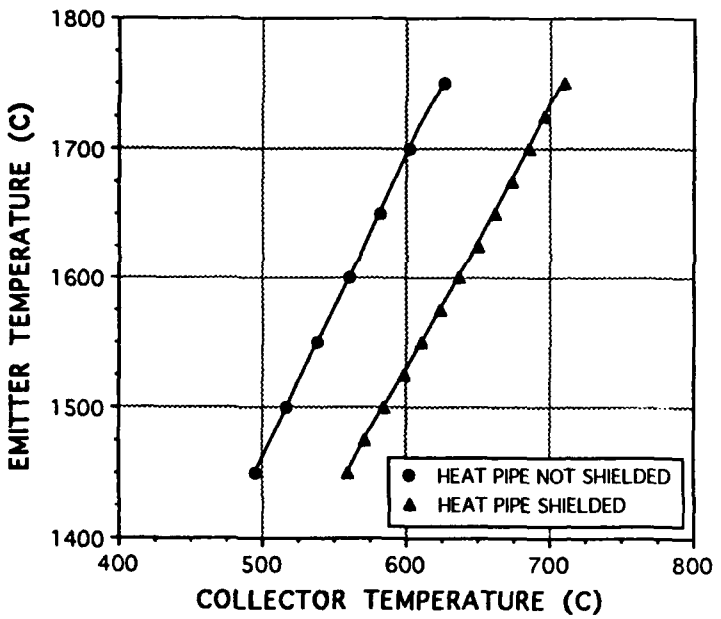

Figure 5.3. Re-Re diode temperature calibration curves with and without heat pipe shielding.

From Figure 2.2 the output voltage of a thermionic converter is the difference in Fermi levels, $eV = \varepsilon_{fC} - \varepsilon_{fE}$. If the Fermi levels are substituted by electron motives and work functions, the output voltage becomes

$$eV = (\psi_C - \psi_E) + (\phi_E - \phi_C) \tag{5.2}$$

If the collector work function is changed to $\phi_C+\Delta\phi_C$, the output voltage will change to $V+\Delta V$. If these changes are introduced into equation 5.2, the following is obtained.

$$e(V + \Delta V) = (\psi_C - \psi_E) + (\phi_E - [\phi_C + \Delta\phi_C]) \tag{5.3}$$

If equation 5.2 is subtracted from equation 5.3, the difference

$$e|\Delta V| = -\Delta\phi_C \tag{5.4}$$

is the change in output voltage due to a change in collector work function. The shift in J-V output predicted by equation 5.4 has been experimentally verified from collector temperature optimized J-V characteristics. The lack of independent collector temperature control on the LEOS diode prevents a direct comparison using equation 5.4 since T_E and T_R must be maintained at constant values while T_C is varied.

The second set of data, with the shielded heat pipe, was collected for emitter temperatures of 1450 to 1750°C at 25°C intervals. These output curves are in Appendix D. The cesium reservoir was again set at 327°C. The reservoir temperature did not attain its maximum of 323°C until the emitter reached 1625°C during these tests. The radiation shield surrounding the heat pipe reduced the energy flow from the heat pipe to the reservoir. In the nonshielded tests, the reservoir attained 323°C at an emitter temperature 125 degrees less than the tests with shielding.

A cross plot from the two sets of J-V output, Figure 5.5, shows the dependence of output voltage on collector temperature at a current density of 8 A/cm^2. The voltage change, $\Delta V \equiv 0\text{-}V(J=8)$, is plotted versus the ratio of collector to cesium reservoir temperature. As the collector temperature increases the voltage change also increases in magnitude and the J-V characteristic moves to the right. From equation 5.4 the shape of the ΔV curve should be similar to the shape of the ϕ_C versus T_C/T_R curve if back emission is negligible. The diode was not operated at high

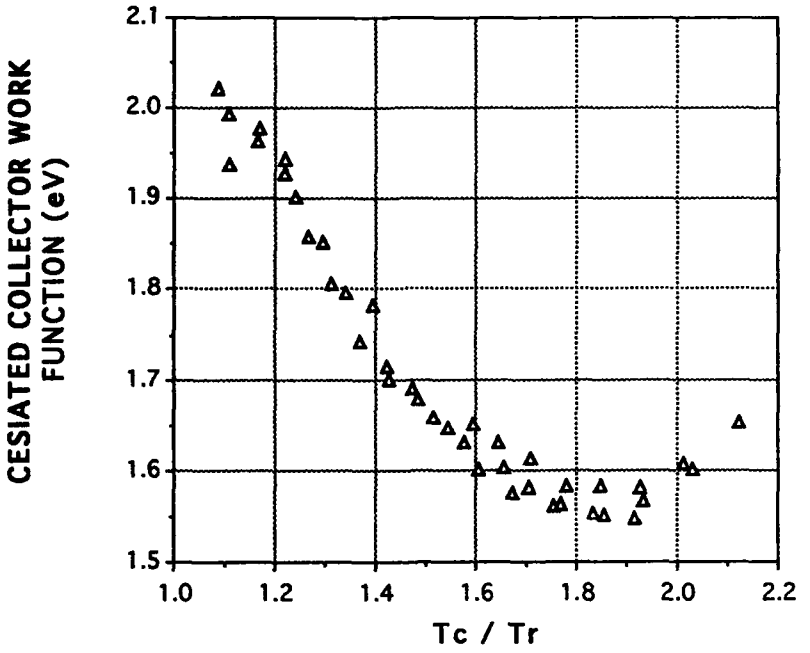

Figure 5.4. Experimentally measured work function of a cesiated Mo collector. Source: Hatsopoulos, G.N. and E.P. Gyftopoulos. *Thermionic Energy Conversion Vol. II.*

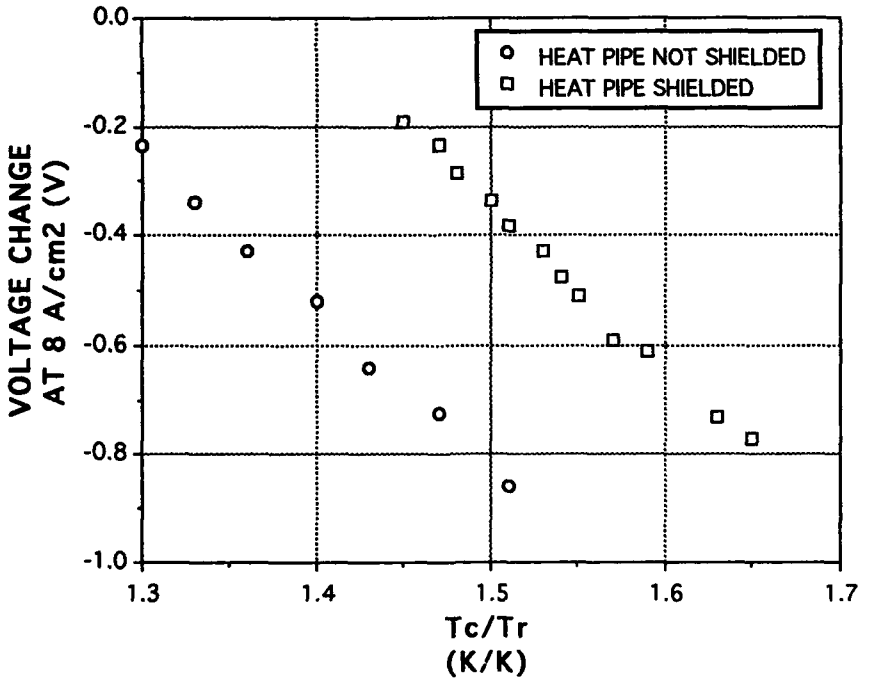

Figure 5.5. Cross plot from J-V output showing the dependence of output voltage on collector temperature at J = 8 A/cm^2.

enough temperatures to cause $|\Delta V|$ to decrease as T_C/T_R increased. The two curves can be directly compared if the value of ϕ_C/e at low collector temperatures, where back emission is negligible, is added to ΔV.

The maximum current density, J_{max}, and the peak power density, P_{max}, are both of interest in the characterization of thermionic output. The maximum current is indicative of the saturation level of operation while the peak power is a primary characteristic of any power producing device. In Figure 5.6, both J_{max} and P_{max} are plotted versus emitter temperature for the shielded and nonshielded cases.

The J_{max} curves are nearly constant at 9.5 A/cm^2 as T_E increases, except for a decrease at high T_E for the shielded case. As T_E increased the output voltage also increased, shifting the J-V curves to the right. This can be seen in the output from the appendices or from the voltage change in Figure 5.5, where as T_E increases, T_C/T_R increases and $|\Delta V|$ increases.

The radiation shield affected the J_{max} and P_{max} curves through changes in collector and reservoir temperatures. The collector temperatures were lower for the nonshielded tests, reducing back electron emission. The reservoir temperatures were higher without the shielding due to radiant energy exchange. Higher reservoir temperatures increase the J-V output by reducing the emitter work function. An increase in heat transfer from the collector improved the performance of the nonshielded tests.

A graph of ignition current density and ignition voltage versus emitter temperature for both shielded and nonshielded cases is shown in Figure 5.7. The ignition points are those values of J and V immediately prior to ignition from the unignited mode. The dependence of ignition current on emitter temperature is nearly linear. This is in accordance with other experimental work [45], but contrasts with the exponential dependence found from theory [46]. The pseudosaturation current of the unignited mode and not the ignition current is related to emitter temperature in the theory. The pseudosaturation current is not seen in the J-V curves at high emitter temperatures (T_E => 1600°C in the appendices). This may account for the discrepancy between theory and experiment.

The ignition voltage also increases with emitter temperature. This trend can be noted from the experimental output or from Figure 5.5. The trend can also be verified by the Richardson-Dushmann equation where J as a function of V and T_E is given by

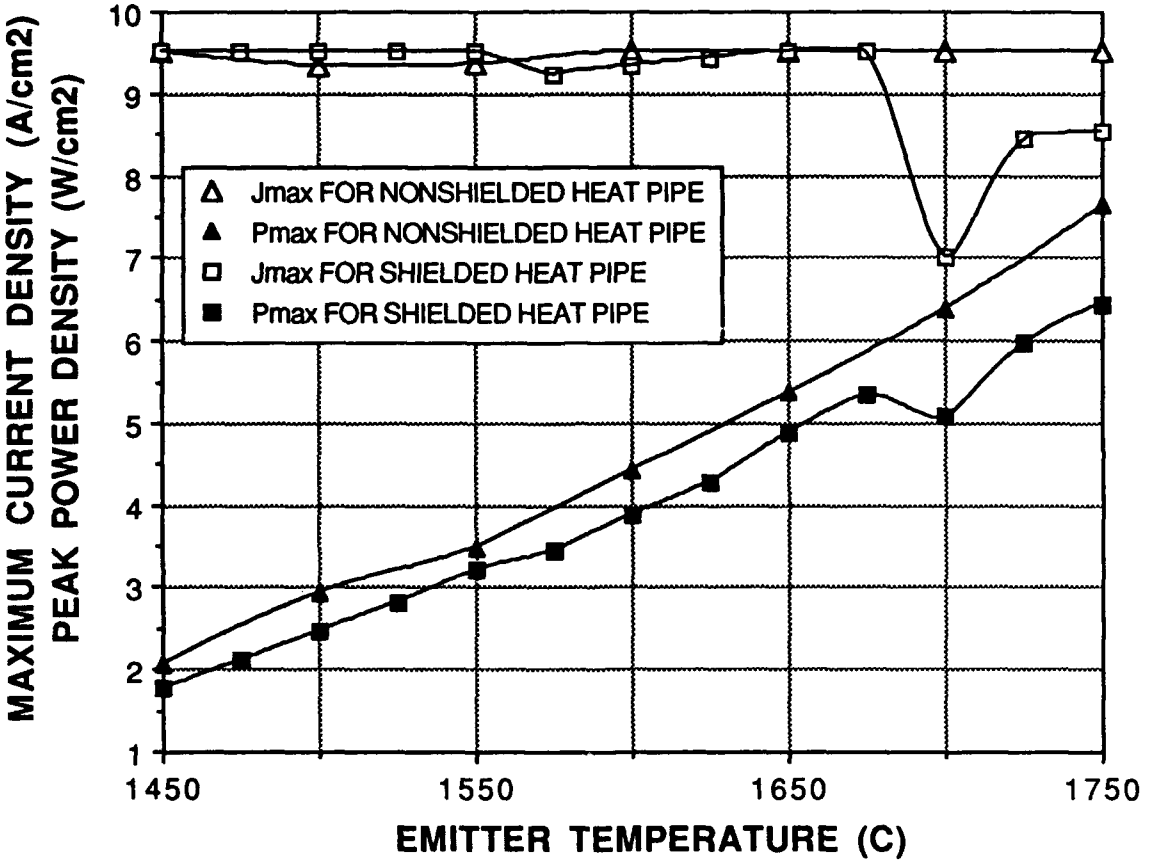

Figure 5.6. Maximum current and power densities versus emitter temperature.

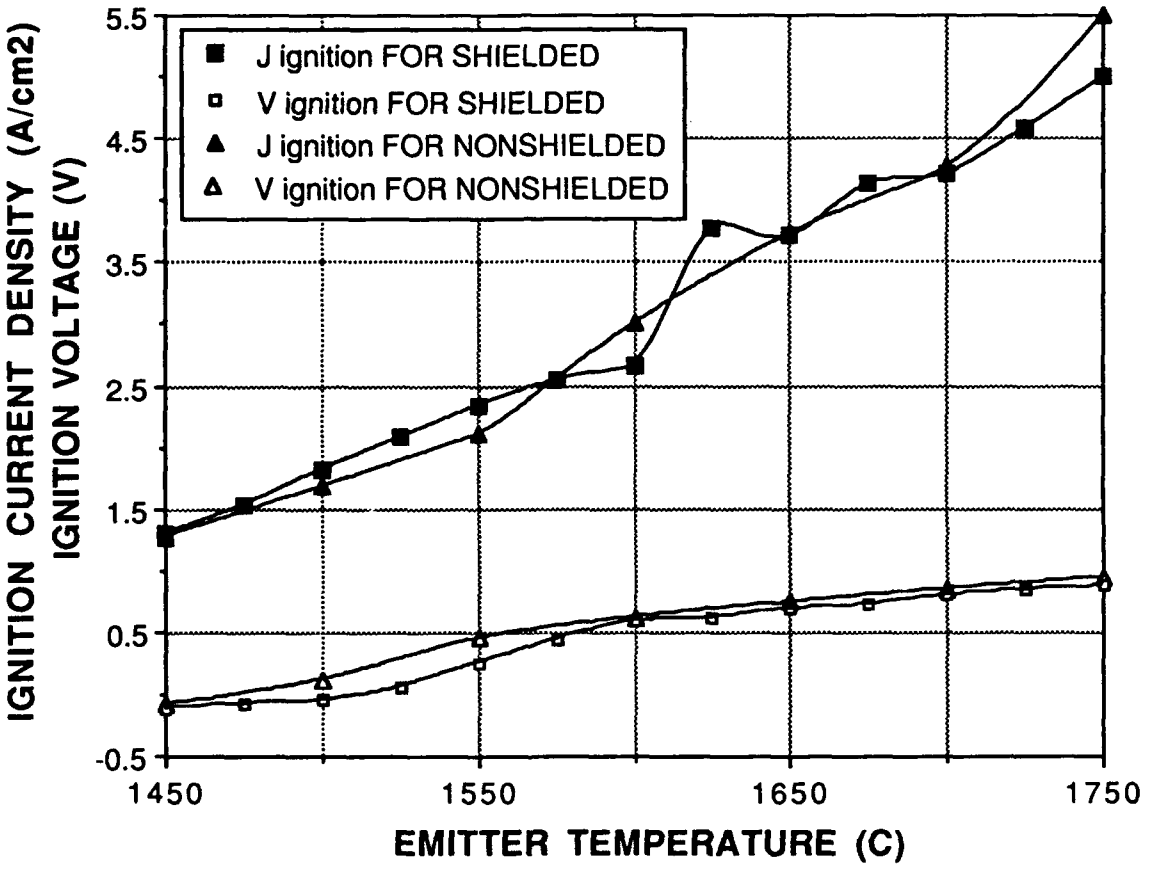

Figure 5.7. Ignition current densities and voltages for the Re-Re diode versus emitter temperature.

$$J = AT_E^2 \exp\left(-\frac{eV}{kT_E}\right) \tag{5.5}$$

with V, the voltage measured across the electrodes, related to the Fermi levels and work functions. If this equation is solved for V as a function of J and T_E,

$$V = \frac{kT_E}{e} \ln\left(\frac{AT_E^2}{J}\right) , \tag{5.6}$$

and the derivative taken with respect to T_E, the following equation results.

$$\frac{dV}{dT_E} = \frac{k}{e}\left[2 + \ln\left(\frac{AT_E^2}{J}\right)\right] \tag{5.7}$$

Since $AT_E^2 \gg J$, the logarithmic term is greater than zero. With $dV/dT_E > 0$ the output voltage will increase as emitter temperature increases. The dynamic parameters of both the external load and the converter control the exact shape of the J-V characteristic near the ignition and deignition regions.

The ignited mode of operation occurs when positive ions in the plasma are primarily produced with energy from inelastic collisions. Peak power is generated within the ignited region, making it a primary region of interest. The ignited region is characterized by large currents as the voltage is decreased. In the experimental output curves the ignited region is a nearly linear region. Figure 5.8 shows the linear, ignited J-V curves for the shielded heat pipe tests. The maximum current densities correspond to J_{max}. The curves show greater output voltages as the emitter temperature increases.

The nearly linear ignited region has been found in much experimental output. This characteristic shape allows algebraic correlations to be developed that take advantage of the linearity of this region. In the design of TEC systems, empirical relations would allow the prediction of J-V and P-V output without relying upon complex analytical forms based upon detailed theory. An empirical correlation for a rhenium-niobium thermionic converter that predicts the output voltage as a function of the temperatures and current is given in [47]. An algebraic

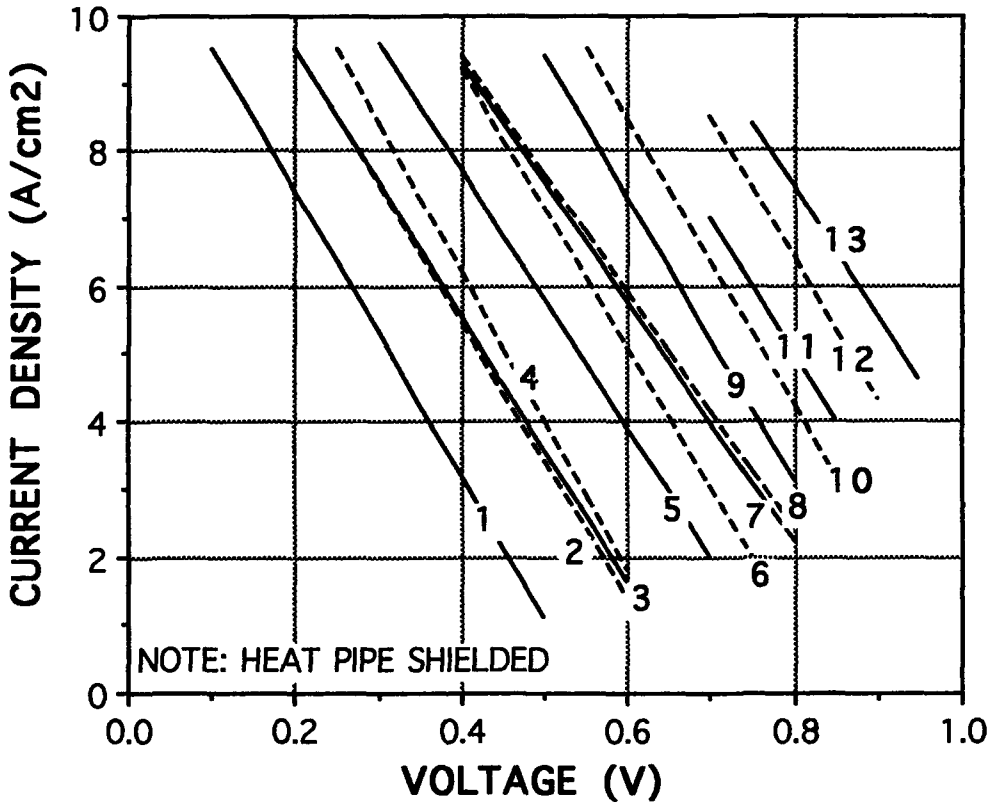

Figure 5.8. Linear nature of output characteristics in the ignited mode. The numbers refer to figures in Appendix D where T_E ranged from 1450 to 1750°C.

equation was developed for a lanthanum hexaboride diode and compared to experimental data to facilitate the design of terrestrial thermionic power topping systems. This work was presented at the Florence World Energy Research Symposium (FLOWERS) '92 conference. The abstract is provided in Appendix E. It was found that empirical relations of the ignited region could provide power system designers with thermionic output characteristics that have been verified by comparisons with experimental data.

The optimal performance of a thermionic converter is achieved at a certain combination of T_E, T_C, T_R, and d. The emitter and reservoir are the only independent temperatures since the collector is radiantly coupled to the emitter. The gap spacing is fixed at 0.1016 mm. To determine the optimized operational envelopes, the output is obtained while varying only one parameter. The emitter temperature, and consequently T_C, was varied while holding the reservoir at a constant temperature.

The reservoir had not achieved its set point of 327°C in previous tests. The copper block that attaches the cooling system was removed from the reservoir tube to reduce heat loss. The reservoir was then able to attain the set point even at an emitter temperature of 1450°C. As the emitter reached 1700 and 1750°C, the reservoir increased to 329 and 338°C, respectively. With the current setup, the reservoir temperature is either too low or can increase without control.

The output from the emitter temperature optimization is given in Appendix F. The curves follow the trend of increased output with increasing emitter temperature. The test at T_E = 1750°C and T_R = 338°C produced the highest output current density of any test performed, over 10 A/cm^2. The high cesium temperature (pressure) reduced the emitter work function. The reduced ϕ_E improved electron emission while the elevated pressure increased the number of collisions. The energy lost to collisions was more than compensated by increased electron emission.

The output performance of the LEOS diode employing CVD-Re on molybdenum electrodes was investigated. The maximum output current (current density) obtained was 43.4 A (10.1 A/cm^2). The power (power density) peaked at 32.7 W (7.6 W/cm^2). The effects of temperature and electrode properties upon the output characteristics compared well with those predicted by theory. This diode performed better at high emitter temperatures, low collector temperatures, and high cesium temperatures. A radiation shield surrounding the heat pipe decreased radiant heat transfer, increased the collector temperature, and reduced conversion performance. An emitter temperature performance mapping confirmed that increased emitter temperatures increase converter output, a basic postulate of the Richardson-Dushmann equation.

SECTION VI

COMPARISON OF THERMIONIC CONVERSION COMPUTER SIMULATIONS

Thermionic conversion simulation models are used to validate experimental data, provide thermionic parameter estimates for nuclear-thermionic system studies, evaluate promising TEC materials and operating conditions, and assess the importance of physical parameters upon TEC performance. The computer simulation must accurately calculate the J-V characteristics of the specified converter configuration. The program must also be able to reproduce experimental trends due to changes in electrode and cesium reservoir temperatures, gap distance, and electrode materials. Thermionic simulations follow either a fundamental model based upon first principles or an elementary model utilizing insight from experimental and measurable phenomena.

6.1 First Principles TEC Analyses

For given converter conditions, a first principles analysis of thermionic performance involves the simultaneous considerations of emission and transport phenomena. The electrostatic field created by the electric charges in motion within the gap influences the emission properties of each electrode. This Schottky effect couples the emission from the electrodes to the transport of charged particles in the gap.

A first principles description of a thermionic plasma diode would include the macroscopic transport equations and plasma states resulting from multistep nonequilibrium ionization. This technique identifies the transport, ionization, and recombination coefficients derived from microscopic collision physics. Various different approximations are made to numerically solve the equations.

Numerical analysis of a high pressure thermionic converter is a formidable task. The theoretical complexities of thermionic and ion emission and the coupling of emission and transport phenomena require lengthy calculations. The highly nonlinear nature of local processes, such as ionization and recombination, contribute to the difficulty of solution. Simplifications to the fundamental equations are generally made to assist solution.

A plasma-ideal thermionic discharge is defined and classified in [48]. This model uses mass and transport equations for ions and electrons to describe an ignited mode thermionic converter. It was found that the plasma-ideal discharge has more losses than the vacuum ideal diode due to the role of the plasma in backscattering electrons. Exact collisionless sheath theory

was coupled to an isothermal electron model of a thermionic converter in [49]. Ion reflection at the emitter and trapped ions in the emitter sheath were found to reduce ignited mode performance. This model suggests little improvement can be made to the ignited mode due to ion reflection and trapping. In addition, it was shown that when the emitter returns too many ions, the plasma arc is extinguished due to insufficient resistive heating. Ionization cannot be maintained below a minimum electron temperature. The time dependent behavior of a thermionic converter was analyzed using a program that models the neutral plasma region and the plasma sheath-electrode boundaries in [50,51]. When the loss of ions to the collector is large, it was found that output voltage, plasma density, and electron temperature will oscillate, reducing power. An increase in the output voltage may be realized by connecting the oscillating thermionic converter to a pulsing circuit.

The thermionics simulation program GT-TEC is a time dependent program that models the electron temperature and plasma density across the interelectrode gap. This first principles model was developed to compute plasma conditions at discrete time intervals. The program calculates the plasma densities, electron temperatures, sheath heights, and other relevant thermionic parameters as time increases. If the iterations are continued for a sufficient time, convergence may occur. The plasma will then ignite and steady-state converter operation is reached. The fundamental equations necessary for analysis of the transport of charged particles in the interelectrode gap under the influence of both electrostatic forces and interparticle collisions are described in [45].

GT-TEC couples collisionless sheath theory with an isothermal electron model of a thermionic converter. The plasma conditions of a thermionic device were investigated using this program in references [51,52]. The program was used to characterize the experimental output from a lanthanum hexaboride thermionic diode in [53]. The simulation was able to reproduce the experimental variations in output due to changes in emitter and collector temperatures. Areas of the program found to need improvement were modelling at low cesium pressures, the ignition-deignition region, and the elimination of a "hump" between the ignited and saturation regions. Reference [49] recommends that the "hump" should not be taken as an expected experimental result and is a result of the lack of knowledge in matching the collisionless sheath to the neutral plasma.

An updated version of this program was evaluated in [54]. The program simulations were compared to experimental output from single crystalline tungsten (110) and rhenium (0001)

thermionic diminiodes. It was found that the recommended values of the bare emitter work functions did not allow the program to effectively simulate the characteristics of the experimental data. Revised work functions compared well with experimental work function data reviewed in [55] and allowed improved simulations.

The research from [54] was presented at the American Society of Metals Advanced Aerospace Materials/Processes (AeroMat) '91 Conference. The abstract is provided in Appendix E. The discrepancies in work functions were explained from a materials deterioration point of view. Oxygen could have lowered the cesiated emitter work function if cesium oxide was formed on the emitter surface [56]. The collector work function could approach that of the emitter as a result of emitter material deposition on the collector surface. Also, the capacity to ionize the plasma is reduced if cesium adsorption coverage is diminished by surface contamination. This effect would increase with time as the adsorbed surface area is reduced. These circumstances would reduce the output of a thermionic converter compared to the simulation output. The simulation was found to be deficient in matching the different regimes of operation. The program also had particular problems simulating the space-charge limited region. Other noted areas of improvements involved error checking, the elimination of the "hump" between the saturation and ignited regions, the incorporation of satellite programs into the main program, and reducing the lengthy time required for a simulation run.

6.2 Phenomenological TEC Analyses

The phenomenological TEC theories are based upon analytical models which may include the continuity of electron current, ion current, and energy flux at the plasma-electrode interfaces and across the plasma [57]. Detailed collisional effects on plasma transport and maintenance are not included. The elementary model of references [58,59] identifies the overall effect of macroscopic plasma properties on converter performance. A comparison with experimental data permits plasma characterization by physically meaningful parameters. An analysis of experimental output was performed on the basis of current and charge carrier energy balances in [60]. It was possible to establish some general regularities and to formulate an empirical model of the ignited mode of operation. Plasma parameters near the electrodes and the emission current were determined from physical parameters. A hydrodynamic plasma theory, considering coulombic scattering, volume ionization, and the assumption of constant electron temperature, is used in reference [61] to generate J-V characteristics.

The program TECMDL is an implementation of the phenomenological model of a thermionic plasma diode described in [57]. This model has been used to evaluate very high temperature (2400-3000 K) burst power applications where the simulated output compared well with experimental data generated in the USSR [62]. Reference [63] incorporated this model into a coupled thermal-nuclear-thermionics program to investigate the effects of cesium pressure upon electric power delivered to a load. TECMDL has also been included in the analysis of a semi-two-dimensional TFE cell in [64]. The approximate treatment of radiation energy loss by resonance lines from the cesium plasma requires the incorporation of a separate model for the unignited mode. This model also has been used to perform diagnostics of experimental, in-core thermionic converters.

This phenomenological model considers the continuity of electron and ion currents and the energy flux across the plasma and at the electrode-plasma boundaries. The energy loss from the plasma by photons is considered from 6S-6P cesium resonance lines only. The plasma is assumed to be collisionless with no voltage drop in the plasma itself. Electric fields are also assumed negligible within the plasma.

The ignited mode is divided into two major regions, the obstructed region ($V > V'$) and the saturation region ($V < V'$). The transition point (J',V') is the point of maximum slope on the J-V curve. This point occurs when the positive ions generated in the plasma are just sufficient to neutralize the space-charge of the saturation current, J_{sat}, with no electric field influence. From Figure 2.5B, it can be seen that the transition voltage is

$$V' = \phi_E - \phi_C - V'_d \tag{6.1}$$

where V'_d is the minimum arc drop required to maintain the plasma in the ignited mode. The program assesses the validity of the simulation by comparing the output to the transition values. The model is not valid for current densities in the deep saturation or obstructed regions.

Common to both simulation programs is the use of the NEDSPHI work function model. This module computes the cesiated emitter work function given the emitter and cesium reservoir temperatures and the bare surface work function. The physics is derived from reference [65] in which a hypothetical adsorption/emission cycle defines the change in surface work function due to ion adsorption. The value of the cesiated work function is related to the bare work function through transition energies which control the adsorption and emission of a single particle. Figure

6.1 illustrates the relationship of the energy difference between ionic and atomic states, E, the ionization potential, I, and the work functions associated with atom and ion adsorption, ϕ_a and ϕ_i. The layer of adsorbed ions and their negative images create a dipole layer. This layer imparts an energy $\Delta\phi$ to the electrons as they traverse the electric field of the dipole layer. This energy is not present on a bare surface and accounts for the difference in work functions, $\Delta\phi = \phi_O - \phi$.

6.3 TEC Simulation Comparison

The output from both GT-TEC and TECMDL was compared to Re-Re diode experimental data. The emitter temperature was varied from 1450 to 1750°C, the collector ranged from 560 to 709°C, and the cesium reservoir temperature, though set at 327°C, only reached 310 to 323°C. The heat pipe was shielded in these tests. Maximum experimental curves for both the ignited and unignited modes were chosen from the output data in Appendix D.

Both simulation programs prompt the user for the temperatures of the emitter, collector, and reservoir. The gap distance was 0.1016 mm. The collector work function is calculated from a polynomial curve fit to experimental data. The simple correlation is appropriate for cesiated collector work functions (Figure 5.4). The emitter work function, calculated by NEDSPHI, requires the bare emitter work function. The bare work function is used to singularly characterize the material surface being adsorbed by cesium. Two values have been recommended for CVD-Re emitters, 5.16 and 5.28 eV. These values are both greater than the recommended value of 5.0 eV found in reference [55]. The bare work function of a CVD surface should be higher than the polycrystalline value because thermodynamic equilibrium forces a stable state to be formed. High stability means reduced electron emission and a higher work function.

The high bare work function of the materials used for thermionic emitters have been experimentally found to have low cesiated work functions [4,45,65]. If the Richardson-Dushmann equation is differentiated with respect to ϕ, the result can be expressed as

$$\frac{dJ}{J} = -\frac{d\phi}{kT} \quad . \tag{6.2}$$

A low emitter work function is desirable because electron emission, and therefore the output current density, increases.

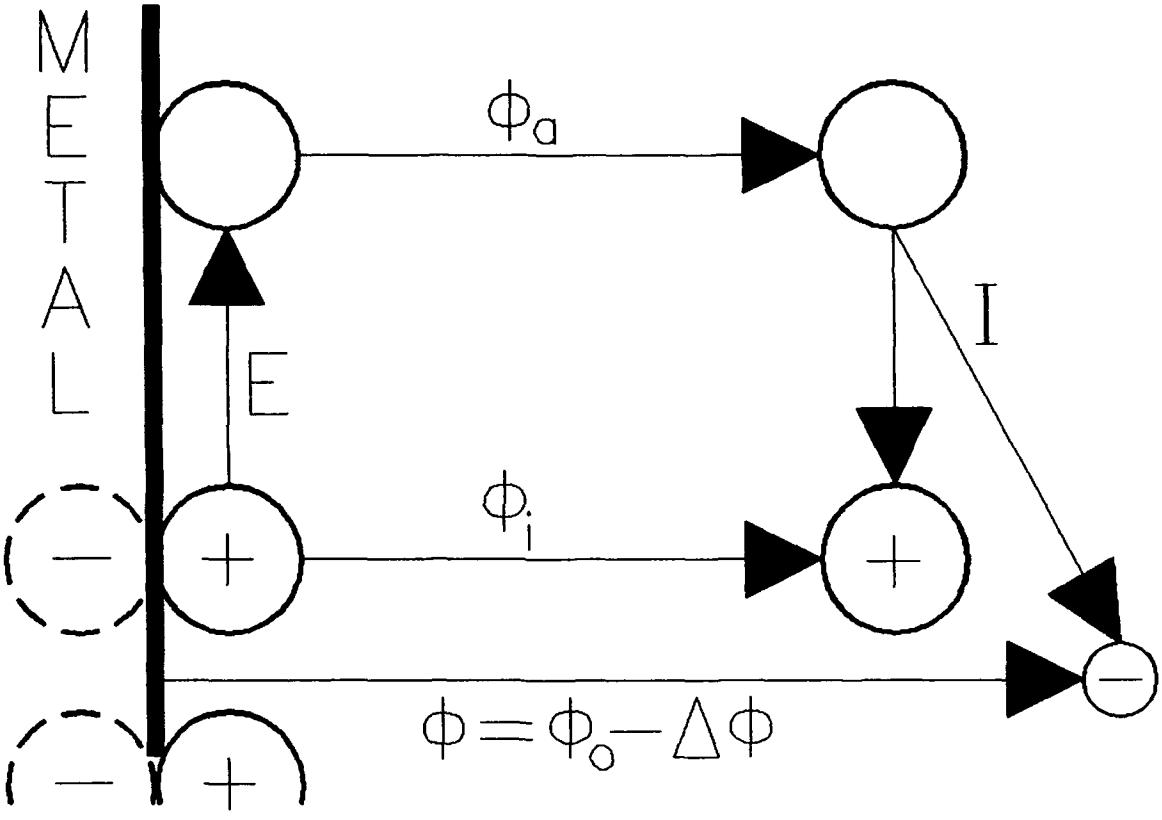

Figure 6.1. Diagram of a hypothetical cycle relating the various emission and transition energies. Source: Rasor, N.S. and C. Warner. "Correlation of Emission Processes for Adsorbed Alkali Films on Metal Surfaces."

The comparisons of the experimental output and the simulations from TECMDL and GT-TEC are shown in Appendix G. Two simulations were performed by each program and compared with the corresponding experimental data. Figure 6.2 shows the comparison for T_E = 1500°C. The experimental data shows both the pseudosaturation and ignited modes. If extrapolated, the ignited region would indicate a short circuit current density of ≈13 A/cm^2.

Both simulation programs were used with the recommended values of ϕ_o for CVD-Re. The effect on both programs was to increase the output current as ϕ_o increased. GT-TEC predicted that the current increased at the greatest rate, followed by TECMDL with ϕ_o = 5.28 and 5.16 eV, and the experimental data.

There are other problems associated with GT-TEC that reduce the confidence in its simulations. The transient nature of this program requires a characteristic end time to determine whether the output has converged to steady-state. At end times less than ≈500, saturation, ignited, and space-charge limited regions are calculated, but at current orders of magnitude too high. At end times greater than ≈500, the program will not calculate in the space-charge limited regime and still overestimates the output.

The program is very sensitive to the cesium reservoir temperature. The limited range of reservoir temperatures in the experimental testing of the LEOS diode allowed its simulation by GT-TEC. In reference [54], an attempt to simulate a thermionic diode with reservoir temperatures in the range of 177 to 577°C was only successful for T_R = 277 or 327°C and locked up the computer otherwise. Error checking is needed to eliminate frequent computer lock up. During the simulations of the Re-Re diode, the program locked up between 25-30 A/cm^2, before the saturation region had been attained.

The characteristics predicted by GT-TEC do not match those obtained experimentally. The voltages at low currents are much greater than found experimentally. The mismatch between the ignited regions is even greater. GT-TEC predicts saturation currents on the order of 80 A/cm^2 where, experimentally, saturation can be extrapolated to be between 10 to 20 A/cm^2.

A third simulation was performed using TECMDL in an attempt to obtain simulations that matched the experimental output characteristics. In this simulation the short circuit currents predicted by the program were matched to those extrapolated from the experimental output. This was accomplished by changing the value of the bare work function used by NEDSPHI. Figure 6.3 compares the experimental output to the revised TECMDL simulations. The bare work functions used in these simulations had a mean and sample standard deviation of 5.07 and 0.06

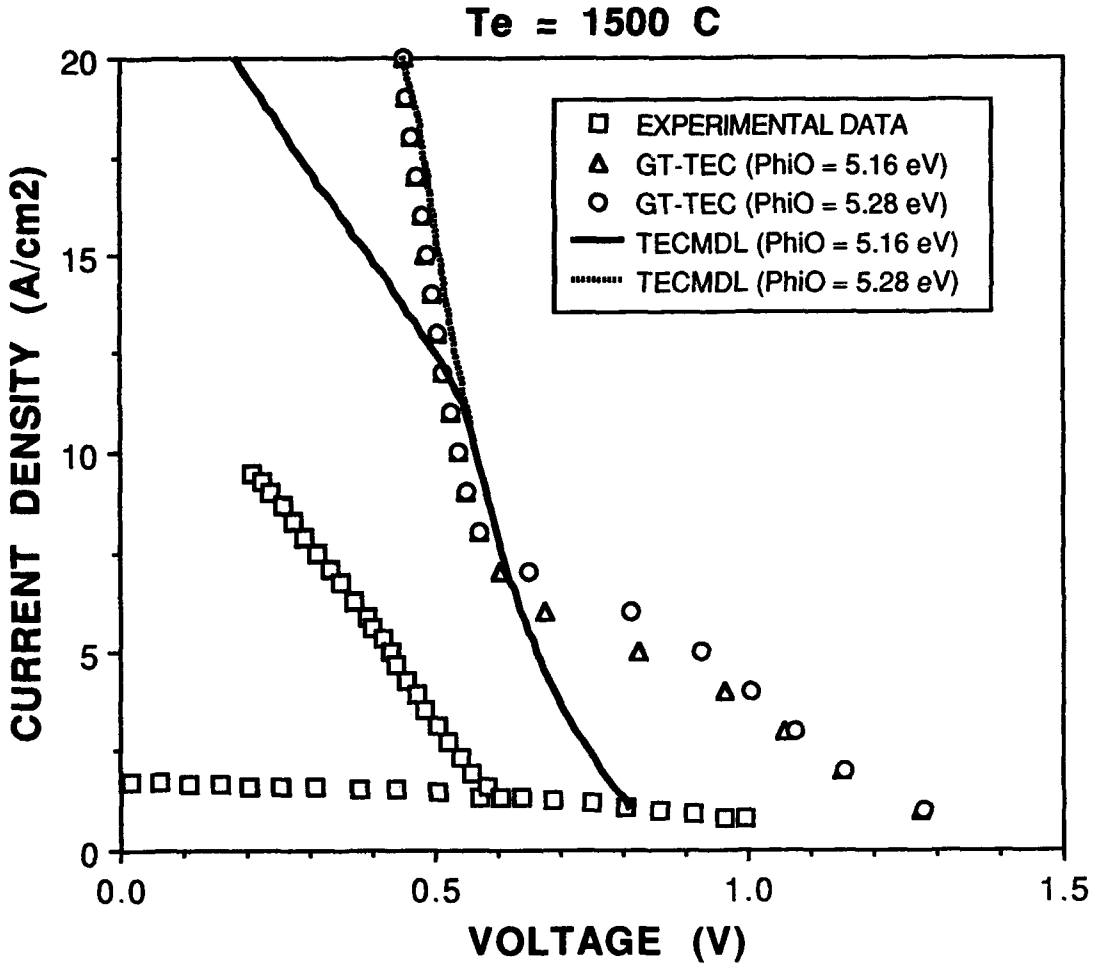

Figure 6.2. Comparison of TECMDL, GT-TEC, and experimental data for T_E = 1500°C, ϕ_O = 5.16 eV and 5.28 eV.

(A)

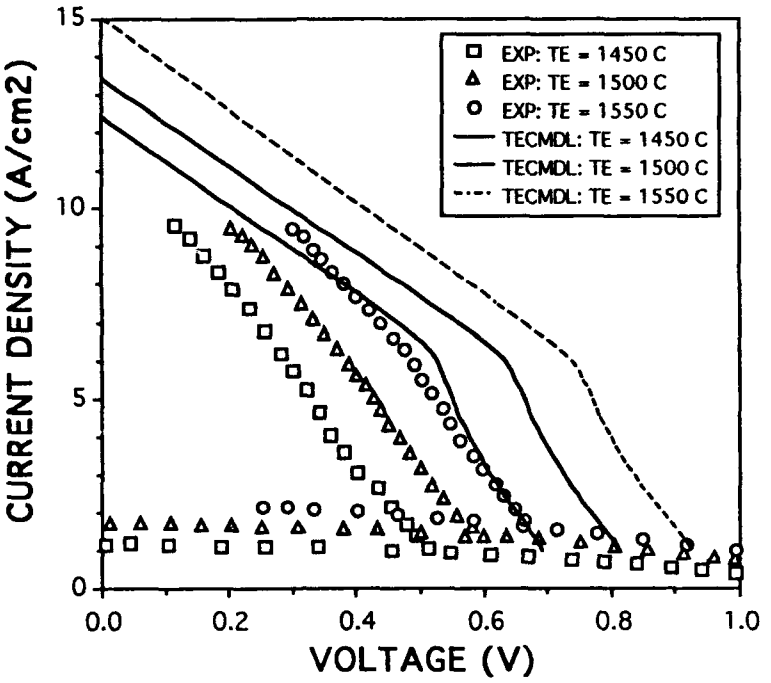

(B)

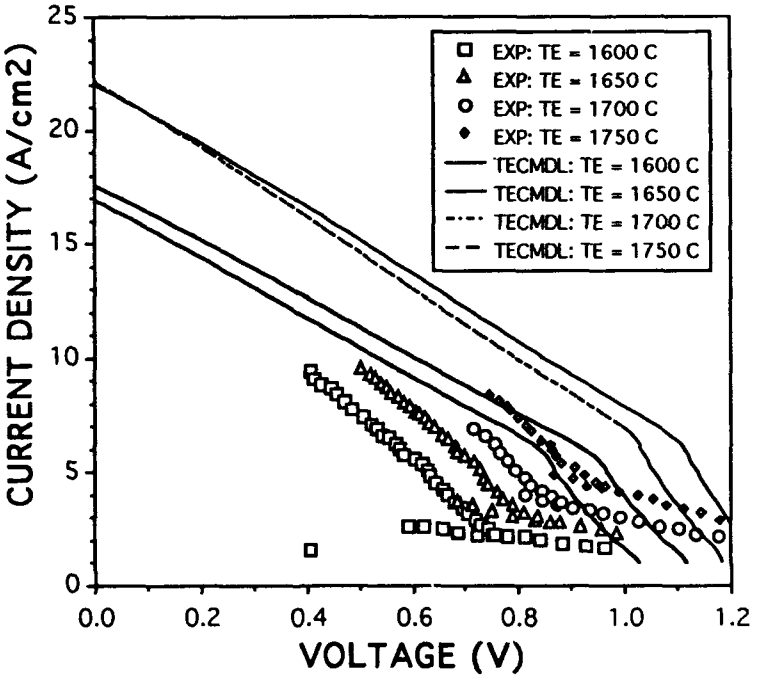

Figure 6.3. The revised TECMDL simulations compared to experimental results. (A) 1450 ≤ T_E ≤ 1550°C, (B) 1600 ≤ T_E ≤ 1750°C.

eV. This compares well with the mean, 4.90 eV, and standard deviation, 0.21 eV, for polycrystalline rhenium from reference [55]. The reduction of bare work function necessary to match short circuit currents may indicate that the CVD-Re may not have the (0001) preferred orientation LEOS measured in similarly prepared samples.

The presence of oxygen in the converter can be considered an impurity or an additive depending upon the amount introduced into the converter and whether it can be controlled. If enough oxygen is present to form cesium oxide and cover the emitter surface, the work function will be reduced further than possible with cesium alone. If the amount of oxygen is low, the work function will not be reduced to the extent capable with cesium oxide. The oxygen molecules will preferentially collect on the grain boundaries, since the state of order of the boundaries is low and the surface energy is high. The oxygen will cause the grain boundaries to weaken, which may increase the creep rate of the high temperature electrodes. The positive aspects of oxygen as an additive have not been realized due to the inability to control the oxygen within the converter [4].

The revised TECMDL simulations follow the trends found in the experimental data better than previous TECMDL or GT-TEC simulations. Both the experimental data and TECMDL simulations increase with an increase in emitter temperature. Figure 6.4 compares the voltage change, at a current density of 8 A/cm^2, found in the experiments and calculated by TECMDL. The revised TECMDL simulations calculated voltage changes nearly 0.2 volt greater, in magnitude, than measured experimentally. If this value was subtracted from the simulated J-V curves, the obstructed region would match well with the experimental data whereas the saturation region would underestimate the experimental output. The assumption of no voltage drop across the plasma may explain the higher voltages in the TECMDL simulations. A plasma voltage drop, dependant upon the charged particle number density within the plasma, should be deducted from the output voltage. The plasma drop, found from the electron transport equation [59], neglecting thermal diffusion, is

$$\frac{V_{pd}}{kT_E} = \frac{3J_E}{e u_{av} \lambda} \int_0^d \frac{dx}{n(x)} - \ln\left(\frac{n_E}{n_C}\right) . \qquad (6.3)$$

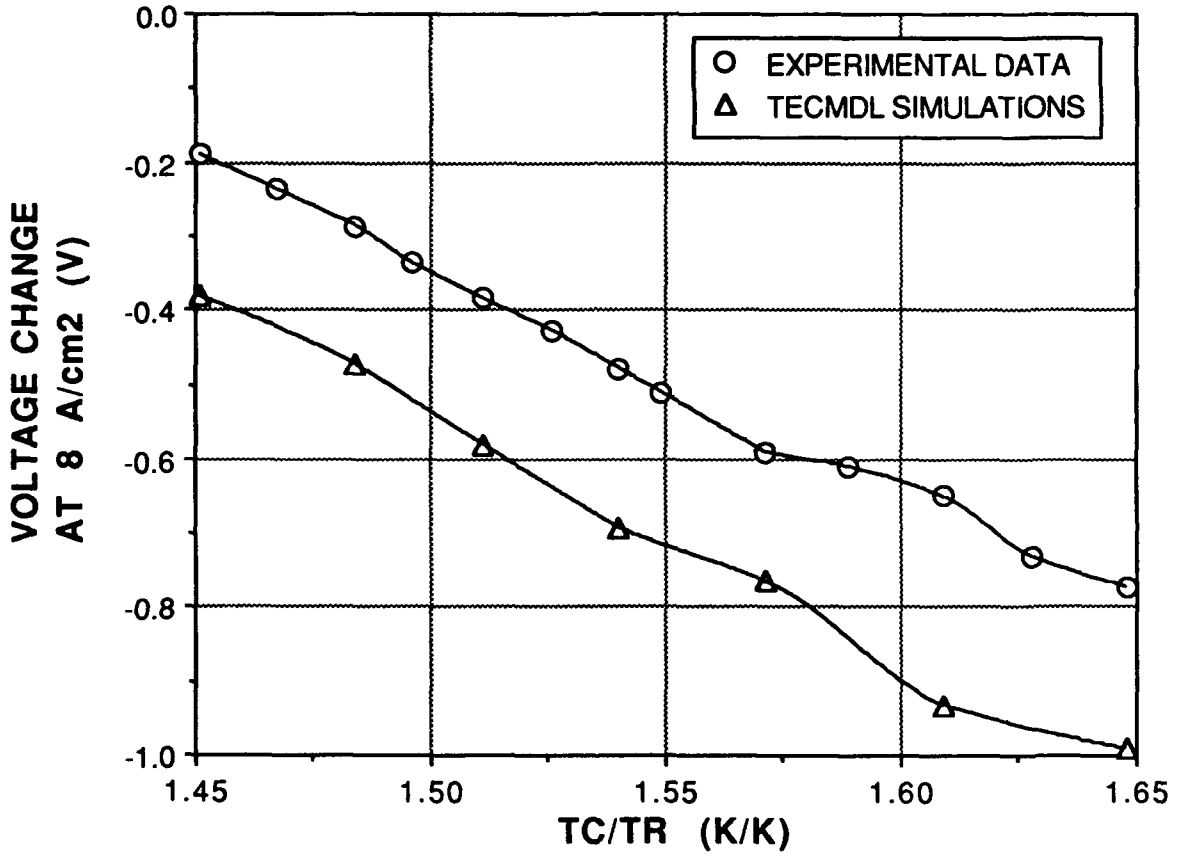

Figure 6.4. Voltage change, at J = 8 A/cm^2, for Re-Re diode experimental data and revised TECMDL simulations.

The phenomenological model avoids an explicit calculation of the charged particle density necessary to solve the electron transport equation. Ways must be developed to incorporate the effects of the plasma voltage drop in the TECMDL formulation.

Two thermionic conversion simulation programs were evaluated and compared to experimental data from a Re-Re diode. The characteristics predicted by the first principles program, GT-TEC version 1.1, did not match those of the experimental data. The short circuit currents predicted were over an order of magnitude too large. The slope of the ignited region was too great, as were the voltages predicted at low current densities. This program has not been updated since its release in May 1990. Other problems associated with this program are lengthy calculation times, a "hump" resulting from the matching of the sheaths to the plasma, and the tendency to lock up the computer at high or low values of the reservoir temperature.

The phenomenological program, TECMDL revision F, was found to better characterize the experimental output. Improved simulations were obtained with revised values of the bare work function for the CVD-Re emitter. The range of revised bare work functions compares well with experimental data from reference [55]. The matching of the simulation obstructed regions to the experimental data suggests this mode of operation for the Re-Re diode. The increased voltages predicted by TECMDL may result from neglecting electric fields within the plasma. A plasma voltage drop, due to charged particles in the plasma, would reduce the voltage difference between the experimental data and the simulations. Further enhancements to this program, necessary to improve its simulation capabilities, include modelling ion trapping in the collector sheath, improving the radiation loss formulation to eliminate a negative resistance at low currents, and calculating the charge carrier distribution in the plasma.

Both programs revealed that changes on the order of 0.01 eV in the emitter work function have a significant effect on output characteristics. The recommended values of bare work functions used in NEDSPHI do not necessarily characterize the emitter surfaces of experimental diodes. Changes in the emitter surface could result from grain boundary migration, recrystallization, or contamination of the cesium vapor. These surface changes may explain the discrepancy between recommended bare work functions and those necessary to produce better simulations. The experimental determination and computer modelling of surface work functions must maintain a high degree of accuracy in order to allow the accurate characterization of thermionic converters.

SECTION VII
CONCLUSIONS AND RECOMMENDATIONS

Two conduction heated, heat pipe cooled thermionic energy converters were experimentally evaluated. The J-V and P-V outputs from both a Mo-Re and Re-Re diode were obtained at emitter temperatures between 1450 and 1750°C. The maximum current density produced was 10.1 A/cm^2 while the power density peaked at 7.6 W/cm^2. The trends due to changes in the emitter, collector, and cesium reservoir temperatures and the electrode work functions qualitatively compare well with the theories of Hatsopoulos and Gyftopoulos [4,45] and the Richardson-Dushmann equation.

Nondestructive failure analysis was performed on the Mo-Re diode to determine the reason for its short circuit. The low vapor pressures of the refractory metal electrodes makes their evaporation negligible. Thermally induced electrode expansion into the gap was also found to be small. Attempts to image the interelectrode gap using X-rays were limited by either the source energy or detector resolution. Further investigations will be made to find high powered NDE equipment with the necessary spacial resolution to image the diode. The cause of the short remains unknown, but separation of the CVD coating from the collector substrate is the most likely reason for an emitter to collector connection. The results from destructive examinations will be correlated with information found after exhausting all NDE possibilities.

The output from two simulation programs was compared to experimental thermionic data. The characteristics predicted by GT-TEC did not compare well with the output from the Re-Re diode. The simulations performed by TECMDL were made to more closely match the experimental data by changing the bare work function used to characterize the emitter surface. The emission properties of electrode surfaces are not constant and are affected by cesium vapor impurities. Small changes in surface properties will have large effects upon emission processes.

The trends found in the experimental data and those predicted by TECMDL show excellent correlation, but direct comparison of the outputs reveal deficiencies. The coupled emission and transport processes within the plasma create difficulties in the formulation and solution of the necessary equations, as evidenced by the failure of the first principles-based program to predict experimental output characteristics. The elementary model is hampered by neglecting processes of limited physical understanding or complex formulation. This, too, limits the capability to simulate experimental data.

To increase the understanding of and confidence in thermionic conversion, further experimental testing is required. The LEOS diodes must be fully characterized and evaluated before space qualified hardware can be produced. The ability to independently control the collector temperature must be established. This may be accomplished with a liquid cooling system attached to the radiator. Controlling the temperature of the cesium reservoir is also a problem. Two resistance heaters, instead of one, can be coiled around the reservoir tube and used in conjunction with the cooling system. This would allow the effects of varying cesium temperature to be investigated.

Once the conditions controlling the output of the diode can be controlled, a sensitivity analysis should be performed. Important parameters, such as the electrode work functions and the conditions for optimum performance, can be determined after performance mapping. With this information, output characteristics, such as the linear, ignited region, can be correlated and provided to systems designers.

SECTION VIII

REFERENCES

[1] Morris, J.F. "Optimize Out-of-Core Thermionic Energy Conversion for Nuclear Electric Propulsion," *International Conference on Plasma Science*, IEEE, May 1978 (NASA TM-73892).

[2] Kennel, E.B. and M.S. Perry. "Advanced Thermionic Nuclear Electric Propulsion for LEO to GEO Transfer in 14 Days," *Proc. 23rd Intersociety Energy Conversion Engineering Conference*, Vol. 1, 1988, 597.

[3] Wilson, V.C. "Thermionic Power Generation," *IEEE Spectrum*, May 1964, 75.

[4] Hatsopoulos, G.N. and E.P. Gyftopoulos. *Thermionic Energy Conversion Vol. I: Processes and Devices*, Cambridge, Mass.: MIT Press, 1973.

[5] Fitzpatrick, G.O. and E.J. Britt. "Thermionic Power Plant Design Point Selection: The Economic Impact," *Proc. 13th Intersociety Energy Conversion Engineering Conference*, 1978.

[6] Fitzpatrick, G.O., E.J. Britt, and R.S. Dick, Jr. "Thermionic-Combustor Combined-Cycle Systems," DOE report 11293-T4-V.3, May 1981.

[7] Breitwieser, R., E.J. Manista, and A.L. Smith. "Computerized Performance Mapping of a Thermionic Converter With Oriented Tungsten Electrodes," *Proc. Thermionic Conversion Specialist Conference*, IEEE, Oct 1969 (NASA TM-52714).

[8] Manista, E.J., J.F. Morris, A.L.Smith, and R.B. Lancashire. "Computer Acquired Performance Data From a Chemically Vapor Deposited Rhenium, Niobium Planar Diode," NASA TM X-2924, Nov 1973. Also available: Re-Mo (NASA TM X-2481), PVD W-Nb (NASA TM X-2330), CVD W-Nb (NASA TM X-2373).

[9] Rasor, N.S., et al. "Thermionic Reactor Based on Radiant Heat Transfer and Demonstrated Components," *Proc. Thermionic Conversion Specialists Conference*, 1967.

[10] Snyder, H.J., T.A. Sagammato, and M.J. Woodring. "STAR-C: A Thermionic Reactor for Low Power Space Applications," *Proc. 22nd Intersociety Energy Conversion Engineering Conference*, 1987.

[11] Anderson, E.A., P. Jalichandra, and R.W. Hamerdinger. "Thermionic Critical Technology Investigation: Report-Task 1," Wright Laboratory Report, USAF contract F33615-87-C-2706, Jan 1989.

[12] Gontar, A.S., M.V. Nelidov, and Yu.V. Nikolaev. "Deformation Behavior of a Thermionic Fuel Element Under Conditions of Thermal Cycling With a Small Temperature Change," *Proc. 25th Intersociety Energy Conversion Engineering Conference*, Vol. 2, 1990, 290.

[13] Bohl, R.J., R.C. Dahlberg, D.S. Dutt, and J.T. Wood. "Thermionic Fuel Element Verification Program - Overview," *Proc. 26th Intersociety Energy Conversion Engineering Conference*, Vol. 3, 1991, 121.

[14] Pawlowski, R.A., A.C. Klein, and J.B. McVey. "Coupled Thermionic and Thermalhydraulic Analyses of Thermionic Fuel Elements," *Proc. 26th Intersociety Energy Conversion Engineering Conference*, Vol. 3, 1991, 99.

[15] Edison, T.A. "A Phenomenon of the Edison Lamp," *Engineering*, Dec 1884, 553.

[16] Fleming, J.A. "Rectification of Electric Oscillations by Means of a Vacuum Valve," *Proceedings of the Royal Society (London)*, Vol. 74, 1905, 476.

[17] Schlichter, W. *Die Spontane Electronemission von Gluhender Metalle und das Gluhelektrische Element*, Ph.D. dissertation, Göttingen University, Germany, 1915.

[18] Morgulis, N.D. "Conversion of Thermal into Electrical Energy by Thermionic Emission," *Advanced Physical Sciences (Moscow, USSR)*, Vol. 70, 1960, 679 (in Russian).

[19] Champeix, M.R. "Transformation of Heat into Electrical Energy in Thermionic Phenomena," *Le Vide*, Vol. 6, 1951, 936 (in French).

[20] Hatsopoulos, G.N. *The Thermo Electron Engine*, Sc.D. dissertation, Massachusetts Institute of Technology, 1956.

[21] Lewis, H.W. and J.R. Reitz. "Thermoelectric Properties of the Plasma Diode," *Journal of Applied Physics*, Vol. 30, No. 9, Sep 1959, 1439.

[22] Lewis, H.W. and J.R. Reitz. "'Open Circuit' Voltages in the Plasma Thermocouple," *Journal of Applied Physics*, Vol. 30, No. 11, Nov 1959, 1838.

[23] Lewis, H.W. and J.R. Reitz. "Efficiency of the Plasma Thermocouple," *Journal of Applied Physics*, Vol. 31, No. 4, Apr 1960, 723.

[24] Hatsopoulos, G.N. "Transport Effects in Cesium Thermionic Converters," *Proc. of the IEEE*, May 1963, 725.

[25] Rasor, N.S. "Emission Physics of the Thermionic Energy Converter," *Proc. of the IEEE*, May 1963, 733.

[26] Lancashire, R.B., E.J. Manista, J.F. Morris, and A.L. Smith. "Emitter Surface Temperature Distribution for a Miniature Thermionic Diode," NASA TM X-2588, Aug 1972.

[27] Morris, J.F. "Energy Conversion Research and Development With Diminiodes," NASA TM X-71533, May 1974.

[28] Morris, J.F., A.L. Smith, and E.J. Manista. "Thermionic Performance of a Variable-Gap Cesium Diminiode With a 110-Single-Crystal-Tungsten Emitter and a Polycrystalline-Niobium Collector," NASA TM X-2953, Mar 1974.

[29] Tsao, B.H. *High Temperature Thermionics*, Ph.D. dissertation, Arizona State University, 1989.

[30] Tsao, B.H., M.L. Ramalingam, B.D. Donovan, and J.S. Cloyd. "Thermionic Energy Conversion With A Preferentially Oriented Tungsten Emitter," *Proc. Eighth Symposium on Space Nuclear Power Systems*, American Institute of Physics, Jan 1991, 787.

[31] Dvornikov, V.D., S.T. Latushkin, V.A. Krestov, L.M. Tikhomirov, and L.I. Yudin. "Powerful Tacitrons and Certain of Their Characteristics in the Nanosecond Range," Trans. from *Pribory i Tekhnika Éksperimenta*, No. 4, Aug 1972, 108.

[32] Dvornikov, V.D., S.T. Latushkin, L.I. Yudin, and V.M. Komarov. "A Tacitron Oscillator for Shaping Rectangular Voltage Pulses Across a Capacitive Load. Trans. from *Pribory i Tekhnika Éksperimenta*, No. 6, Dec 1973, 87.

[33] Gryaznov, G.M., A.B. Novikov, N.N. Sveshnikov, V.I. Serbin, V.B. Kaplan, and A.M. Martsinovsky. "Thermionic Plasma Switching Elements," *Proc. 25th Intersociety Energy Conversion Engineering Conference*, Vol. 2, 1990, 300.

[34] Henderson, B.W. "U.S. Buying Soviet Topaz 2 to Boost Space Nuclear Power Program," *Aviation Week and Space Technology*, 14 Jan 1991, 54.

[35] Gubbels, G.H.M., R. Metselaar, E. Penders, and L.R. Wolff. "Combustion Heated Thermionic Energy Converter," *Proc. 21st Intersociety Energy Conversion Engineering Conference*, Vol. 2, 1986, 1343.

[36] Gubbels, G.H.M., and R. Metselaar. "A Thermionic Energy Converter With an Electrolytically Etched Tungsten Emitter," *Journal of Applied Physics*, Vol. 68, No. 4, Aug 1990, 1883.

[37] Lewis, B.R., R.A. Pawlowski, and A.C. Klein. "Advanced Thermionic Reactor Systems Design Code," *Proc. 25th Intersociety Energy Conversion Engineering Conference*, Vol. 2, 1990, 305.

[38] Nassersharif, B., M.J. Gaeta, K. Berge, L. Guffee, and K. Williams. "Extension of the CENTAR System Simulation Code to Thermionic Space Nuclear Reactors," *Proc. 26th Intersociety Energy Conversion Engineering Conference*, Vol. 3, 1991, 166.

[39] Angrist, S.W. *Direct Energy Conversion*, 4th ed., Boston: Allyn and Bacon, Inc., 1982.

[40] Dunn, P.D. and D.A. Reay. *Heat Pipes*, 3rd ed., Oxford: Pergamon Press, 1982.

[41] Nesmeyanov, A.N. *Vapor Pressure of the Chemical Elements*, ed. R. Gray, Amsterdam: Elsevier Publishing Co., 1963.

[42] *CRC Handbook of Chemistry and Physics*, 65th ed., ed. R.C. Weast, Boca Raton, Fl.: CRC Press, Inc., 1984.

[43] Perel'man, F.M. *Rubidium and Caesium*, 2nd ed., trans. R.G.P. Towndrow, New York: John Wiley and Sons, Inc., 1985.

[44] Incropera, F.P. and D.P. DeWitt. *Fundamentals of Heat and Mass Transfer*, 2nd ed., New York: John Wiley and Sons, Inc., 1985.

[45] Hatsopoulos, G.N. and E.P Gyftopoulos. *Thermionic Energy Conversion Vol.II: Theory, Technology, and Application*, Cambridge, Mass.: MIT Press, 1979.

[46] Wilkins, D.R. and E.P. Gyftopoulos. "Theory of Thermionic Converter Extinguished-Mode Operation With Applications to Converter Diagnostics," *Proc. 26th Annual Conference on Physical Electronics*, Mar 1966, 40.

[47] Breitwieser, R. "Correlation Expression for the Performance of an Etched-Rhenium Emitter, Niobium Collector Thermionic Converter," NASA TM X-2380, Sep 1971.

[48] Lawless, J.L. and S.H. Lam. "An Analytical Model of Thermionic Discharges," *Journal of Applied Physics*, Vol. 58, No. 6, Mar 1986, 1875.

[49] Main, G.L. and S.H. Lam. "Effects of Emitter Sheath Ion Reflection and Trapped Ions on Thermionic Converter Performance Using an Isothermal Electron Model," *IEEE Trans. on Plasma Science*, Vol. 15, No. 3, June 1987, 309.

[50] Main, G.L., R. Bouwmans, G.L. Riddersbusch, D. Hamm, J.P. Dansereau, and W.P. Coleman. "A Time Dependent Model of a Thermionic Energy Converter Using a Three Scale Asymptotic Analysis of the Electrode Plasma Boundaries," *Proc. 22nd Intersociety Energy Conversion Engineering Conference*, Vol. 4, 1987, 1935.

[51] Main, G.L. *Emitter Sheath Effects in Thermionic Converter Performance*, Ph.D. dissertation, Princeton University, 1984.

[52] Lawless, J.L. and S.H. Lam. "The Plasmadynamics and Ionization Kinetics of Thermionic Energy Conversion," Dept. of Mechanical and Aerospace Engineering, Princeton University, New Jersey, 1982.

[53] VanDam, S.A. and M.L. Ramalingam. "Application of a One-Dimensional TEC Code to the Characterization of a Lanthanum-Hexaboride Diode," *Proc. 25th Intersociety Energy Conversion Engineering Conference*, Vol. 2, 1990, 346.

[54] Young, T.J. "A Computer Simulation of Thermionic Converter Performance of Tungsten(110) and Rhenium(0001) Cesium Diminiodes," USAF Graduate Student Research Program, Wright Research and Development Center, contract F49620-88-C-0053, Sep 1990.

[55] Fomenko, V.S. *Handbook of Thermionic Properties*, ed. G.V. Samsomov, New York: Plenum Press Data Division, 1966.

[56] Langmuir, I. and K.H. Kingdon, "Thermionic Effects Caused by Vapors of Alkali Metals," *Proceedings of the Royal Society (London) A*, Vol. 107, 1925, 61.

[57] Rasor, N.S. "Thermionic Energy Conversion," Chap. 5 in *Applied Atomic Collision Physics*, Massey, McDaniel, and Bederson, eds. New York: Academic Press, 1982.

[58] McVey, J.B. "TECMDL Ignited Mode Planar Thermionic Converter Computer Model," Software users' manual, Rasor Associates, Inc., Jan 1991.

[59] "TECMDL Converter Physics," Rasor Associates, Inc., Jun 1987.

[60] Karbyshev, V.Z. "A Phenomenological Model of the Arc Mode of a Thermionic Energy Converter," *Proc. 24th Intersociety Energy Conversion Engineering Conference*, Vol. 2, 1989, 1149.

[61] Lundgren, L. "Ion Trapping in the Emitter Sheath in Thermionic Converters," *Journal of Applied Physics*, Vol. 58, No. 11, Dec 1985, 4032.

[62] Rasor, N.S., J.B. McVey, and R.C. Cooper. "Evaluation of Thermionic Converter Performance at Very High Temperatures for Burst Power Applications," *Proc. 22nd Intersociety Energy Conversion Engineering Conference*, Vol. 4, 1987, 1997.

[63] El-Genk, M.S., C.S. Murray, and S. Chaudhuri. "Effects of Cs Vapor Pressure on Steady-State and Transport Operation of Thermionic Converters," *Proc. 26th Intersociety Energy Conversion Engineering Conference*, Vol. 3, 1991, 179.

[64] McVey, J.B. "CYCLON Semi-2D Cylindrical Converter Model," Rasor Associates, Inc., Sep 1990.

[65] Rasor, N.S. and C. Warner. "Correlation of Emission Processes for Adsorbed Alkali Films on Metal Surfaces," *Journal of Applied Physics*, Vol. 35, No. 9, Sep 1964, 2589.

APPENDIX A

EXPERIMENTAL DATA FROM THE MO-RE CONVERTER

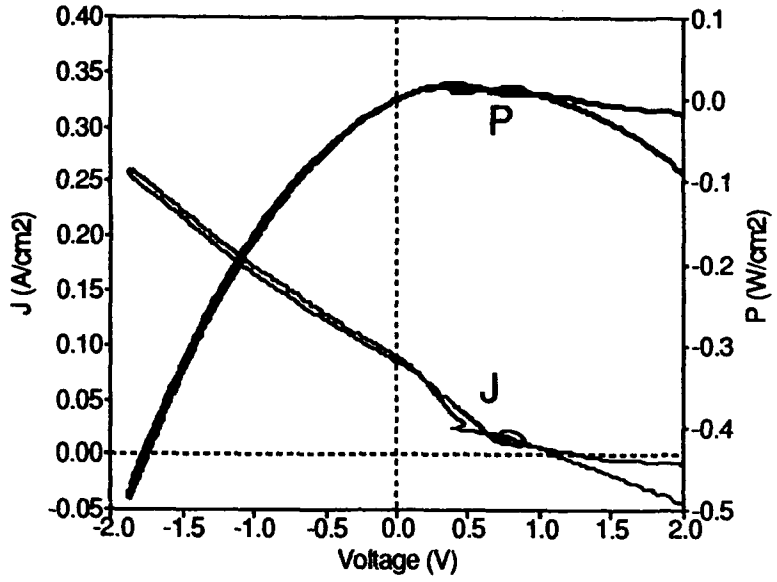

Figure A1. Mo-Re converter output.
T_C = 717°C, T_R = 227°C.

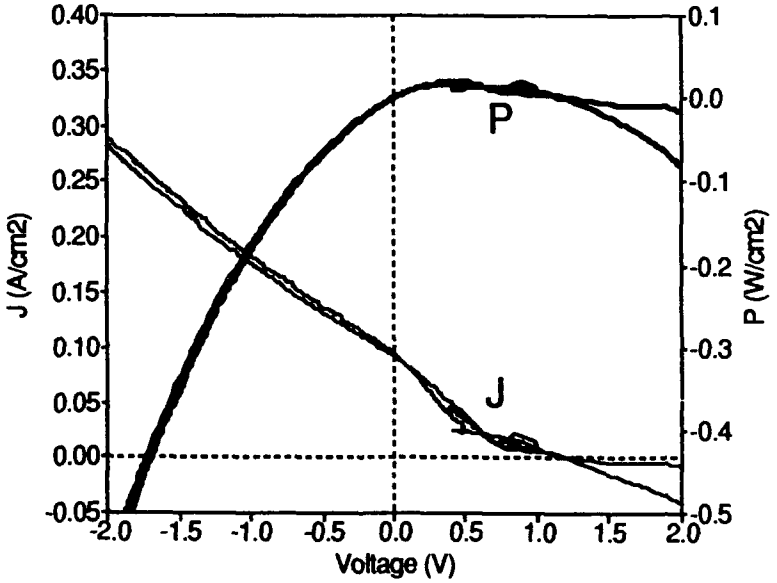

Figure A2. Mo-Re converter output.
T_C = 717°C, T_R = 252°C.

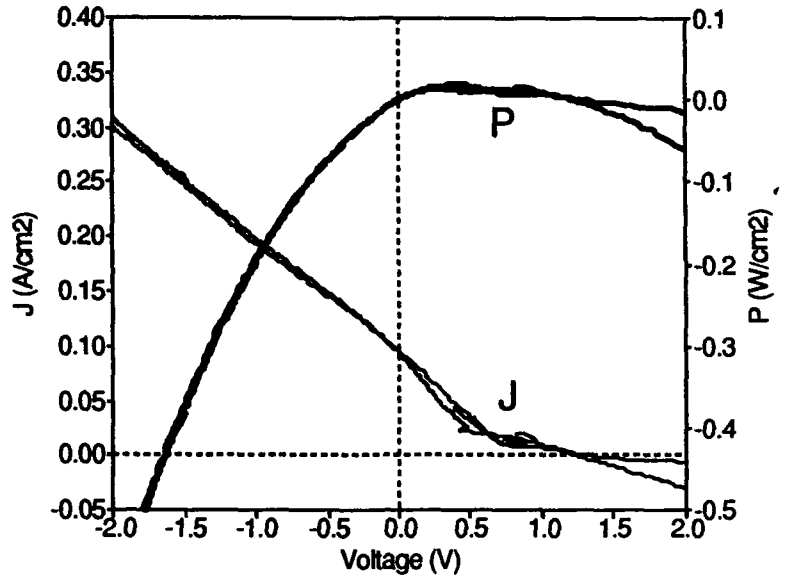

Figure A3. Mo-Re converter output.
T_C = 717°C, T_R = 277°C.

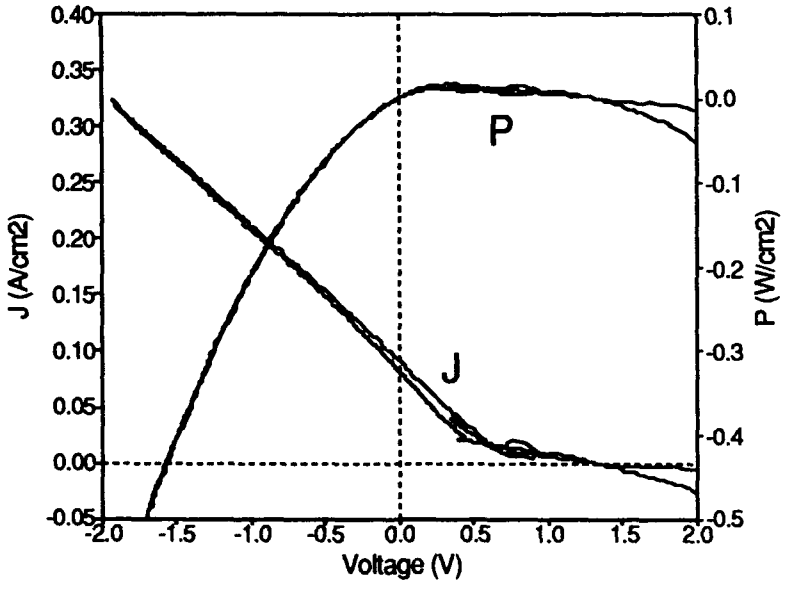

Figure A4. Mo-Re converter output.
T_C = 717°C, T_R = 302°C.

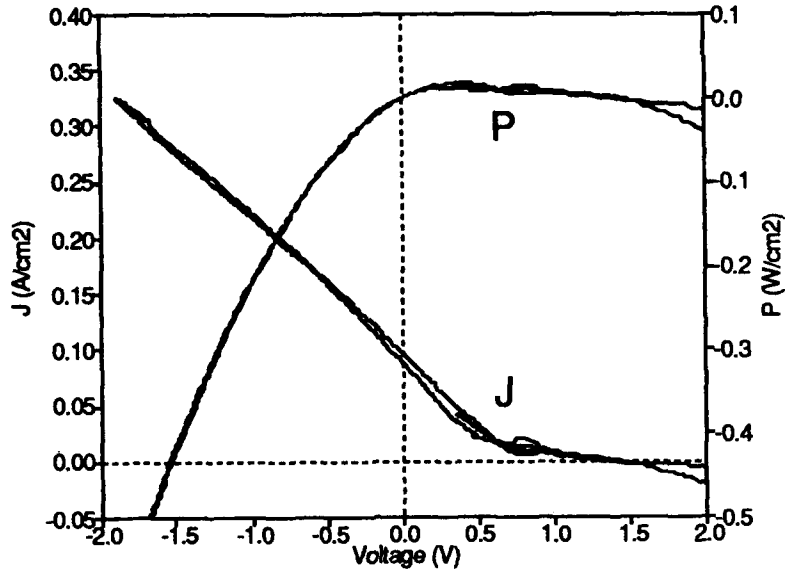

Figure A5. Mo-Re converter output.
T_C = 717°C, T_R = 327°C.

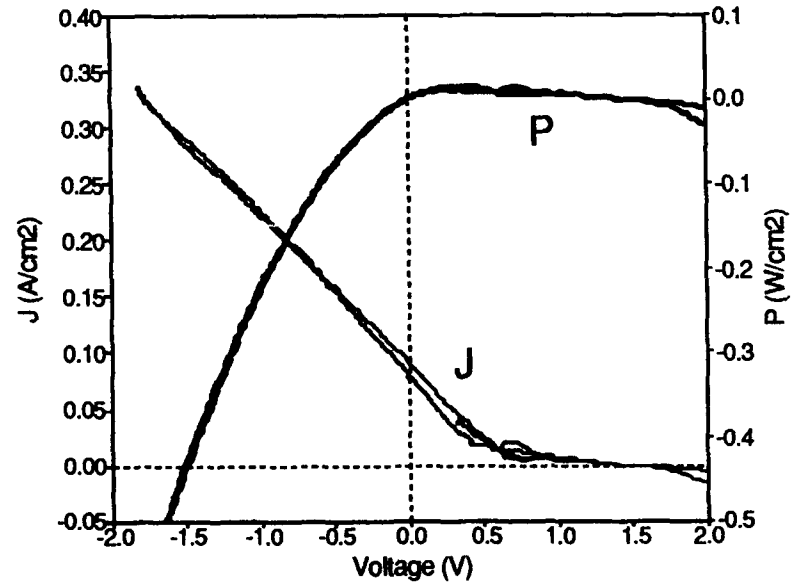

Figure A6. Mo-Re converter output.
T_C = 717°C, T_R = 352°C.

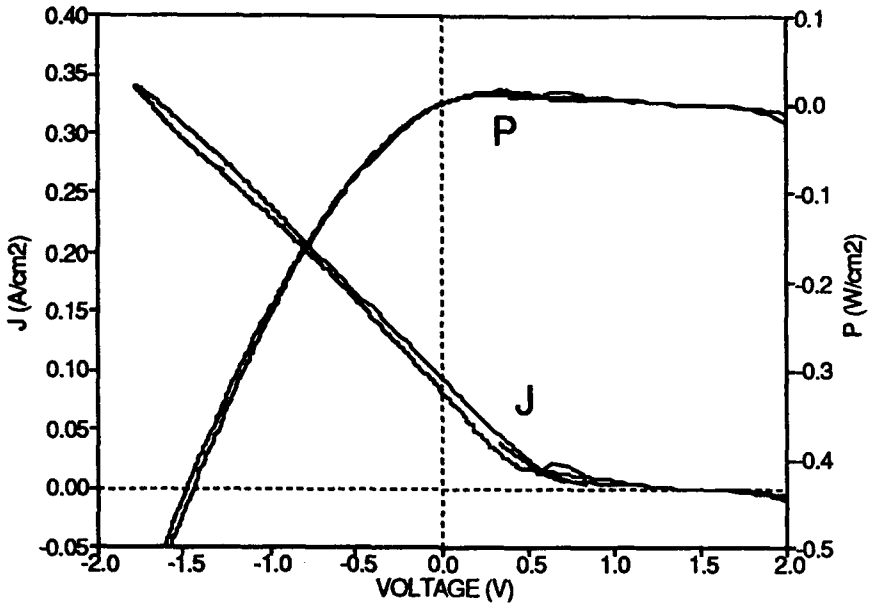

Figure A7. Mo-Re converter output.
T_C = 717°C, T_R = 377°C.

APPENDIX B

EXPERIMENTAL DATA FROM THE RE-RE CONVERTER

(HEAT PIPE NOT SHIELDED)

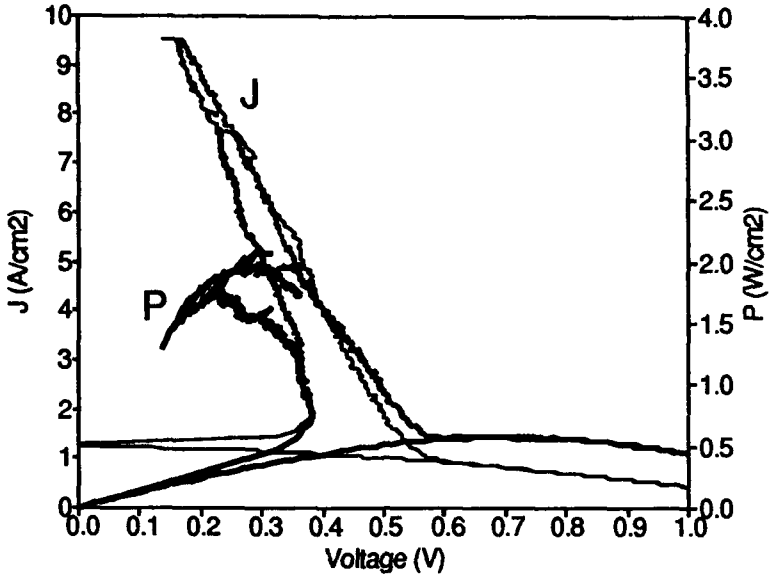

Figure B1. Re-Re converter output without heat pipe shielding.
T_E = 1450°C, T_C = 495°C, T_R = 316°C.

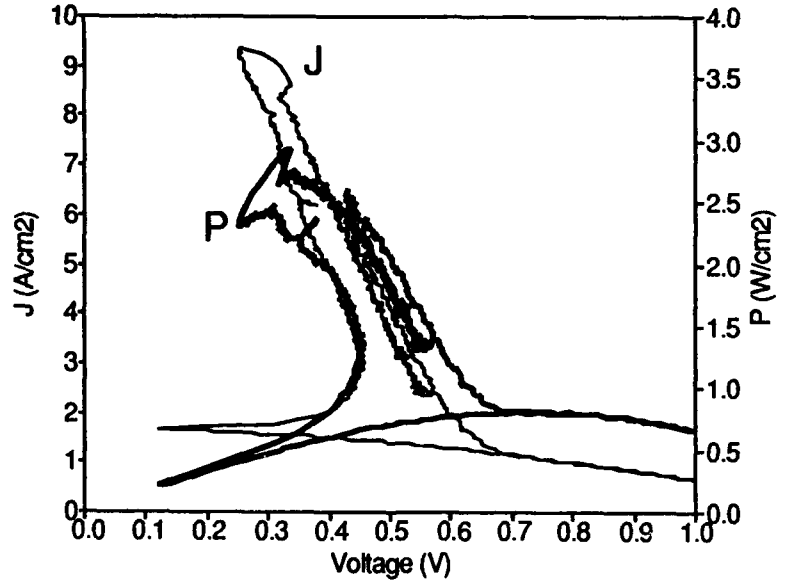

Figure B2. Re-Re converter output without heat pipe shielding.
T_E = 1500°C, T_C = 517°C, T_R = 323°C.

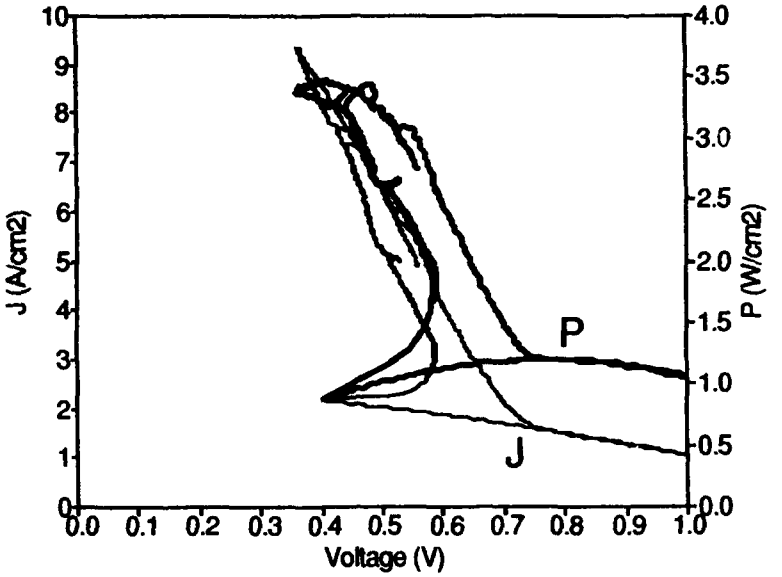

Figure B3. Re-Re converter output without heat pipe shielding.
T_E = 1550°C, T_C = 538°C, T_R = 323°C.

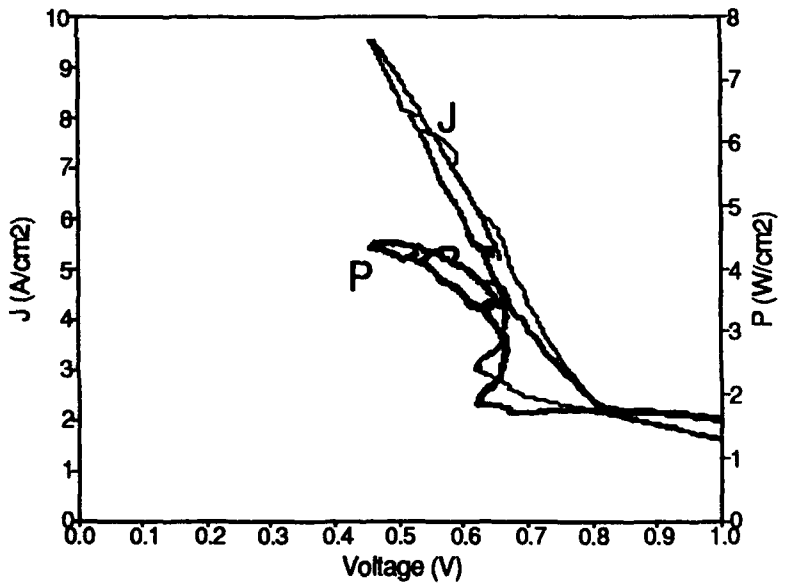

Figure B4. Re-Re converter output without heat pipe shielding.
T_E = 1600°C, T_C = 561°C, T_R = 323°C.

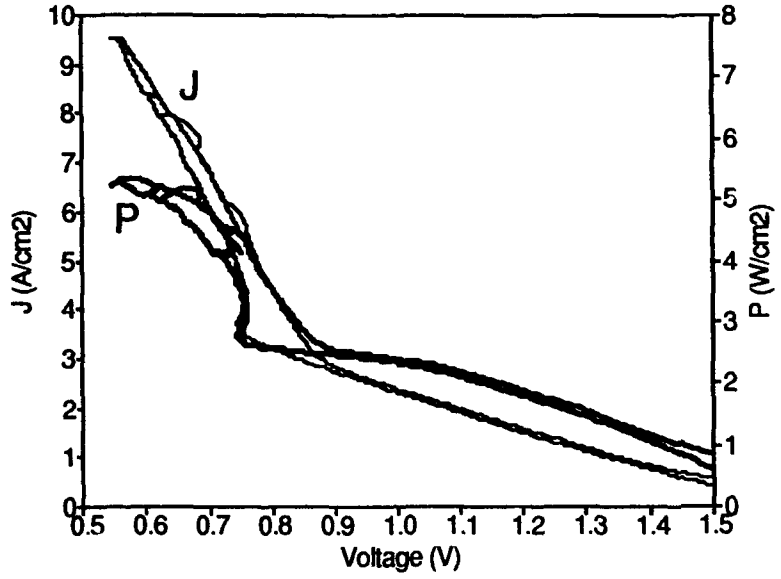

Figure B5. Re-Re converter output without heat pipe shielding.
T_E = 1650°C, T_C = 582°C, T_R = 323°C.

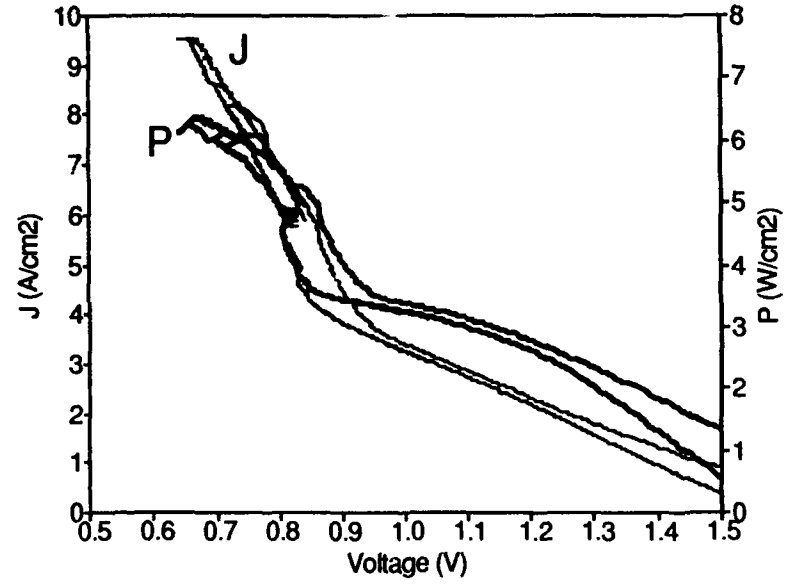

Figure B6. Re-Re converter output without heat pipe shielding.
T_E = 1700°C, T_C = 602°C, T_R = 323°C.

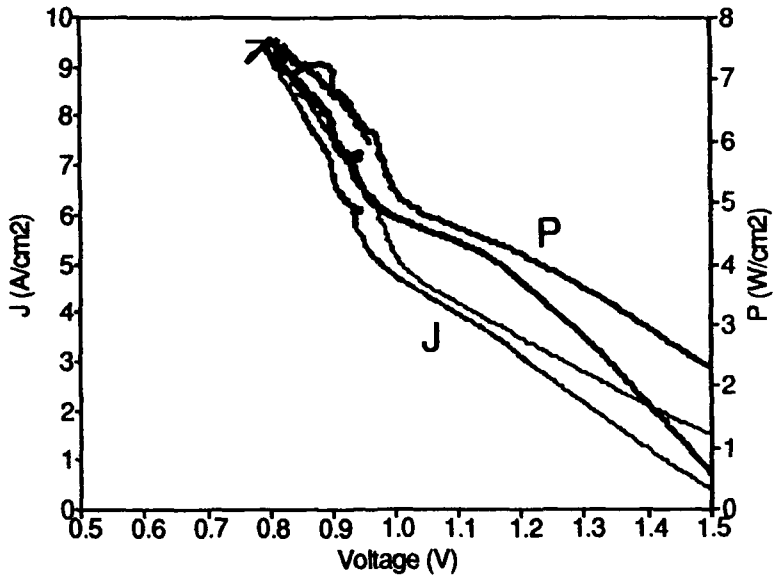

Figure B7. Re-Re converter output without heat pipe shielding.
T_E = 1750°C, T_C = 626°C, T_R = 323°C.

APPENDIX C

DERIVATION OF RADIANT ENERGY EXCHANGE RELATION

DERIVATION OF RADIANT HEAT TRANSFER RELATION FOR A SHIELDED HEAT PIPE

The derivation of the change in radiant heat transfer from the heat pipe begins with the selection of a proper control volume. The heat pipe, thermal radiation shield, and the radiator fin are completely enclosed within the bell jar. The ultrahigh vacuum maintained within the bell jar eliminates convection. Figure C1 defines the heat flows within the control volume.

Assuming no radiation shield and no change in heat transfer ($\Delta q = \Delta q_{43} = 0$), an energy balance around bodies 1 and 4 gives

$$q = q_{13} + q_{43} \quad . \tag{C1}$$

This analysis will assume all energy generation and storage terms are zero. An energy balance considering a control volume only around the heat pipe gives

$$q = q_{43} + q_{14} \quad . \tag{C2}$$

Equating the heats entering the heat pipe gives

$$q_{43} = q_{14} \, , \tag{C3}$$

or any energy not radiated by the heat pipe is transferred to the radiator fin.

Assuming that the shield is in place, a change in heat transfer term, $\Delta q \neq 0$, is allowed to exist between the heat pipe and radiator fin. A corresponding term, Δq_{13}, accounts for any change in heat transfer between the radiator fin and the bell jar. Performing an energy balance around bodies 1, 2, and 4 gives

$$q = q_{12} + q_{43} + \Delta q_{43} \tag{C4}$$

while an energy balance around bodies 1 and 2 gives

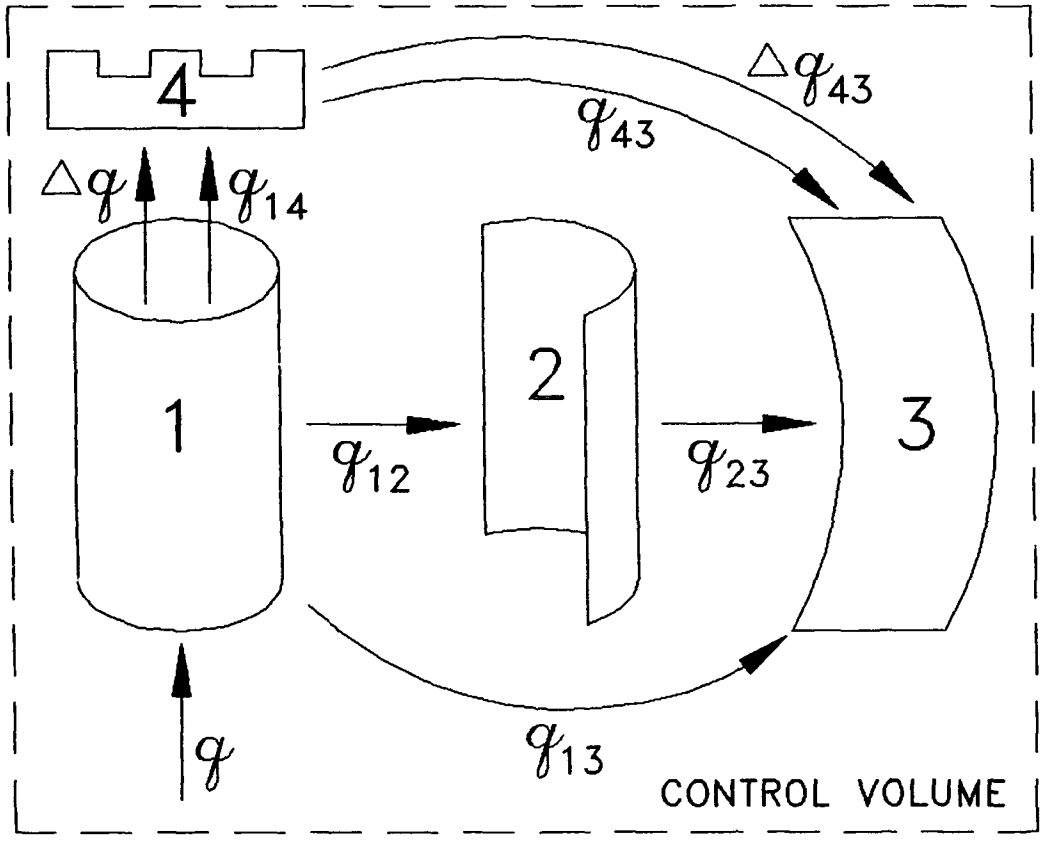

Figure C1. Control volume for radiant energy analysis.

$$q = q_{12} + q_{14} + \Delta q \quad . \tag{C5}$$

Equating (C1) to (C5), and incorporating (C3), gives the following for the change in heat transfer due to the insertion of the shield

$$\Delta q = q_{13} - q_{12} \quad . \tag{C6}$$

If $\Delta q = 0$ then the amount of heat lost to the shield and the bell jar is equal and the shield has no effect. If $0 < \Delta q < q_{13}$ then the shield has reduced the radiant heat transfer from the heat pipe. If $\Delta q = q_{13}$ then the heat pipe has ceased to radiate, which can only be true if the temperature of the heat pipe is absolute zero.

Radiation heat transfer is given by the Stefan-Boltzmann law as

$$q_{13} = \frac{\sigma}{R_{13}}\left(T_1^4 - T_3^4\right) \tag{C7}$$

where

$$R_{13} = \frac{1-\epsilon_1}{\epsilon_1 A_1} + \frac{1}{A_1 F_{13}} + \frac{1-\epsilon_3}{\epsilon_3 A_3} \tag{C8}$$

is the total resistance to radiation exchange between two diffuse, gray, isothermal surfaces. The radiant energy exchange for q_{12} is determined from (C7) and (C8) by replacing subscript 3 replaced by 2. The change in heat transfer is given by

$$\Delta q = \frac{\sigma}{R_{13}}\left(T_1^4 - T_3^4\right) - \frac{\sigma}{R_{12}}\left(T_1^4 - T_2^4\right) \quad . \tag{C9}$$

This equation can be manipulated to the following form,

$$\Delta q = \sigma \left[\frac{T_1^4 (F-C) + (A+B)\left(T_2^4 - T_3^4\right) + C T_2^4 - F T_3^4}{(A+B+C)(D+E+F)} \right] \qquad \text{(C10)}$$

where the view factors are unity, A, B, and C are the three terms of R_{13}, and D, E, and F are the corresponding terms in R_{12}. From (C8), A=D and B=E when $F_{13}=F_{12}$.

To determine whether $\Delta q > 0$, the signs of the terms on the right hand side of (C10) must be found. The $(F-C) >? 0$ term can be shown as

$$\frac{1-\epsilon_2}{1-\epsilon_3} >? \frac{\epsilon_2}{\epsilon_3}\frac{A_2}{A_3} \quad . \qquad \text{(C11)}$$

If the area of the bell jar is much greater than the area of the shield, $A_3 > A_2$, and the emissivity of the bell jar is greater than that of the shiny, foil shield, $\epsilon_3 > \epsilon_2$, then $(\epsilon_2/\epsilon_3)(A_2/A_3) < 1$ and the sign of $(F-C)$ is positive. Similarly, the sign of $(A+B)(T_2^4-T_3^4)$ is positive if $T_2 > T_3$. It follows that $CT_2^4 > 0$ and $-FT_3^4 < 0$. The sum of these three terms is greater than zero, as is the product (A+B+C)(D+E+F). Since both the numerator and denominator of (C10) is positive, Δq must be positive. The radiation shield does reduce the radiant heat transfer from the heat pipe.

If the physically reasonable values shown in Table C1 are used in (C10), the heat transfer change, Δq, is 64 watts. This value may be small compared to the input heat of ≈500 watts (50A•10V), but was enough to return the heat pipe to nearly isothermal operation.

Table C4
Physically Reasonable Parameters to Estimate
Heat Transfer Change

	HEAT PIPE	SHIELD	BELL JAR
Area, (cm^2)	23.6	28.3	1650
Temperature, (K)	982	700	300
Emissivity	0.6	0.1	0.8
View Factors:	$F_{12} = 0.8$ $F_{13} = 1$		

APPENDIX D

EXPERIMENTAL DATA FROM THE RE-RE CONVERTER

(HEAT PIPE SHIELDED)

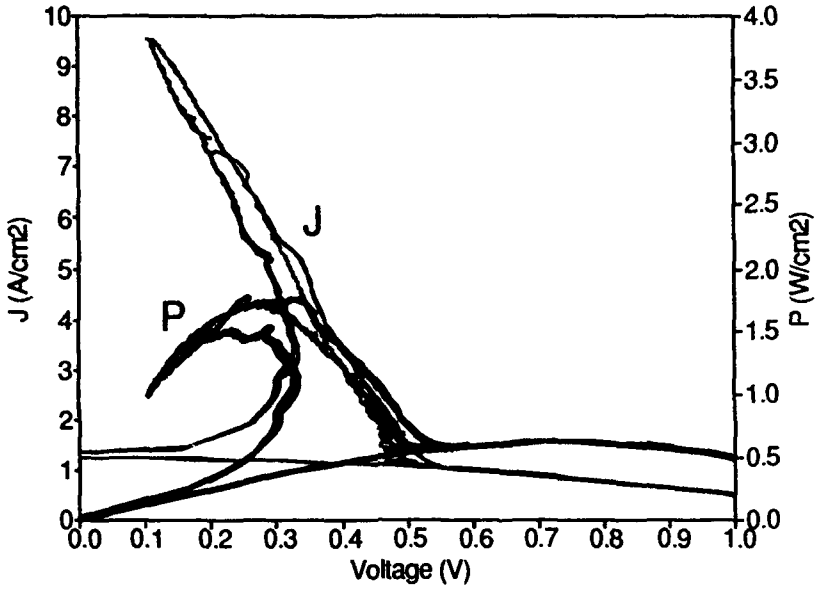

Figure D1. Re-Re converter output with heat pipe shielding.
T_E = 1450°C, T_C = 560°C, T_R = 301°C.

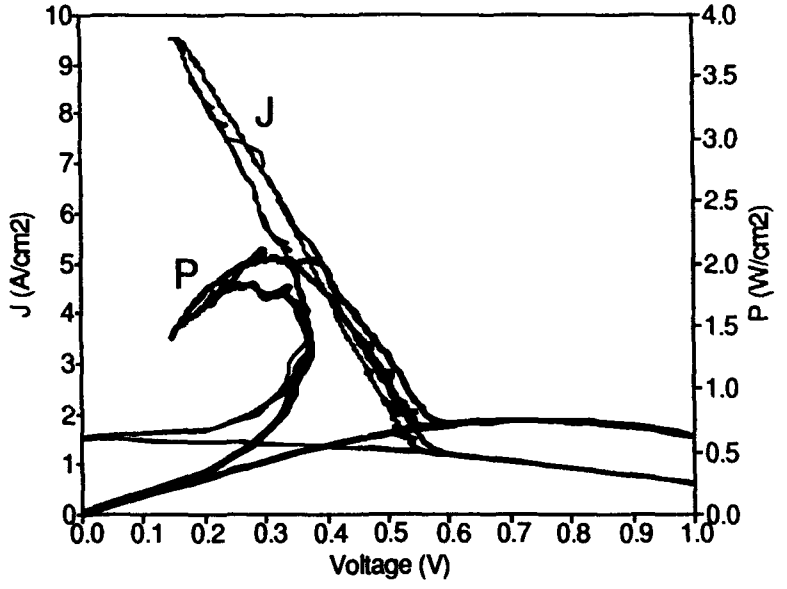

Figure D2. Re-Re converter output with heat pipe shielding.
T_E = 1475°C, T_C = 572°C, T_R = 303°C.

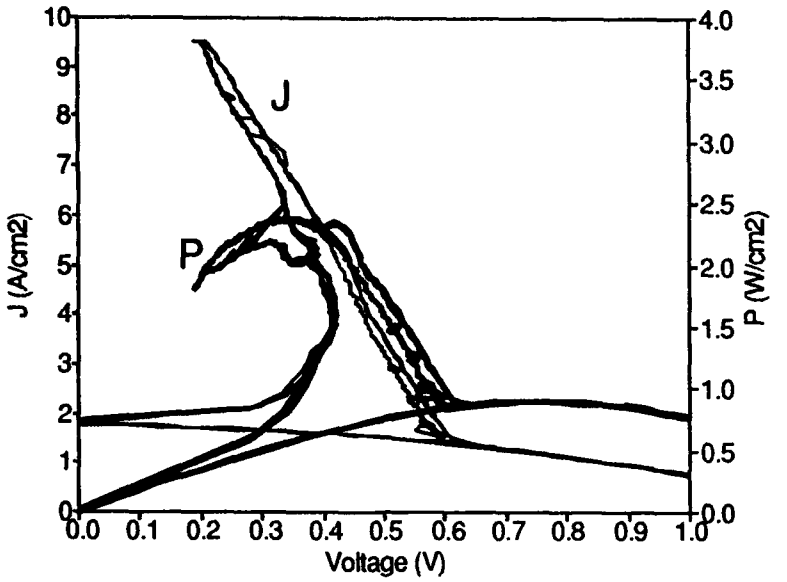

Figure D3. Re-Re converter output with heat pipe shielding.
T_E = 1500°C, T_C = 585°C, T_R = 305°C.

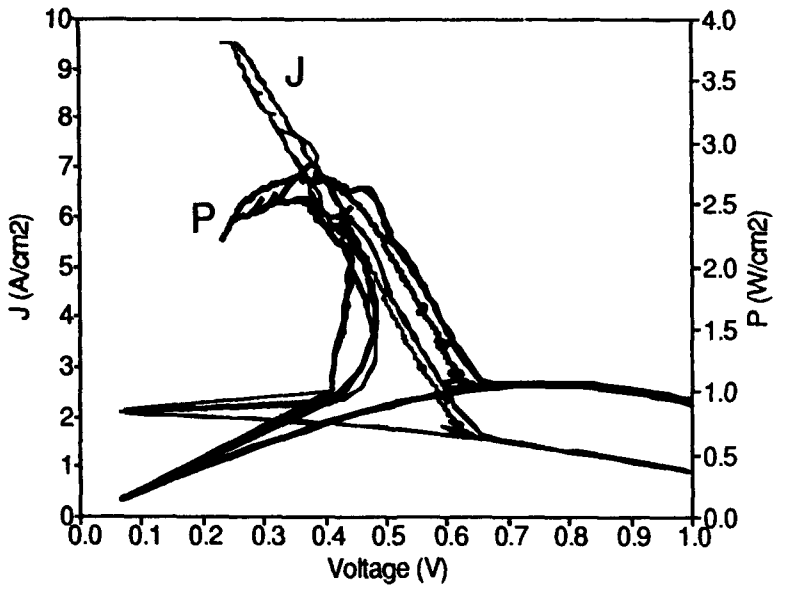

Figure D4. Re-Re converter output with heat pipe shielding.
T_E = 1525°C, T_C = 599°C, T_R = 310°C.

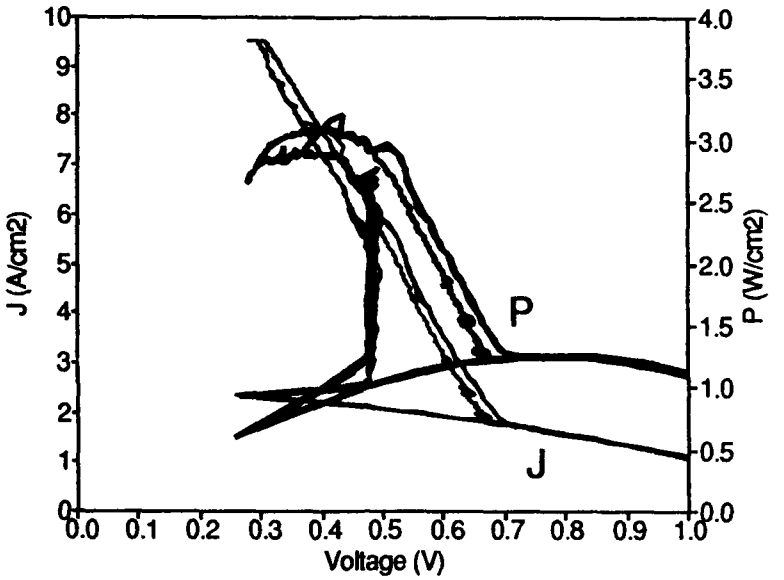

Figure D5. Re-Re converter output with heat pipe shielding.
T_E = 1550°C, T_C = 611°C, T_R = 312°C.

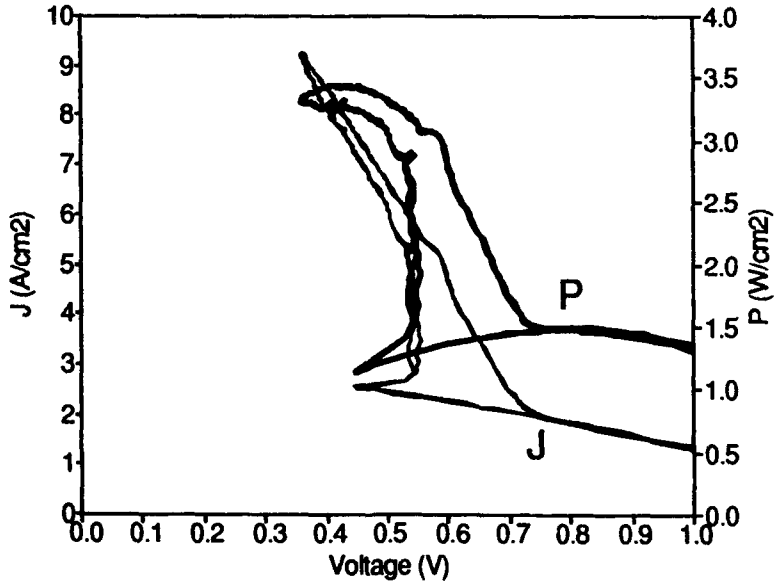

Figure D6. Re-Re converter output with heat pipe shielding.
T_E = 1575°C, T_C = 624°C, T_R = 315°C.

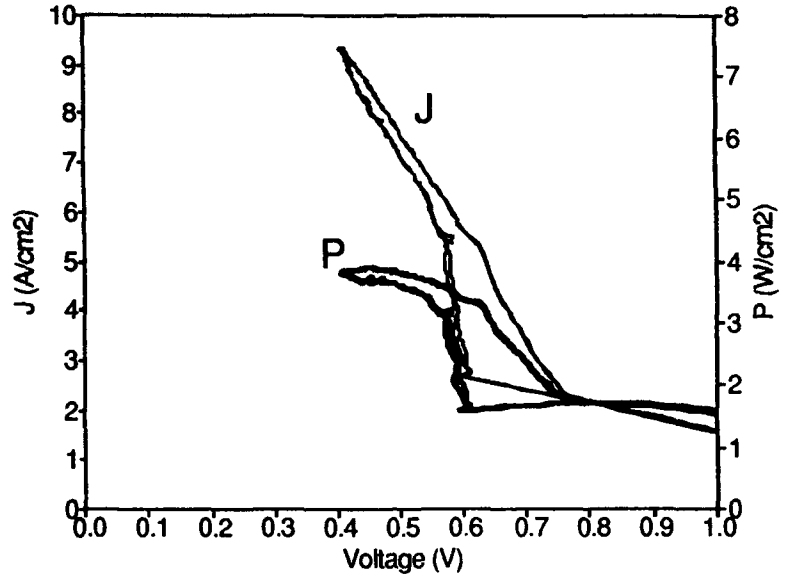

Figure D7. Re-Re converter output with heat pipe shielding.
T_E = 1600°C, T_C = 637°C, T_R = 318°C.

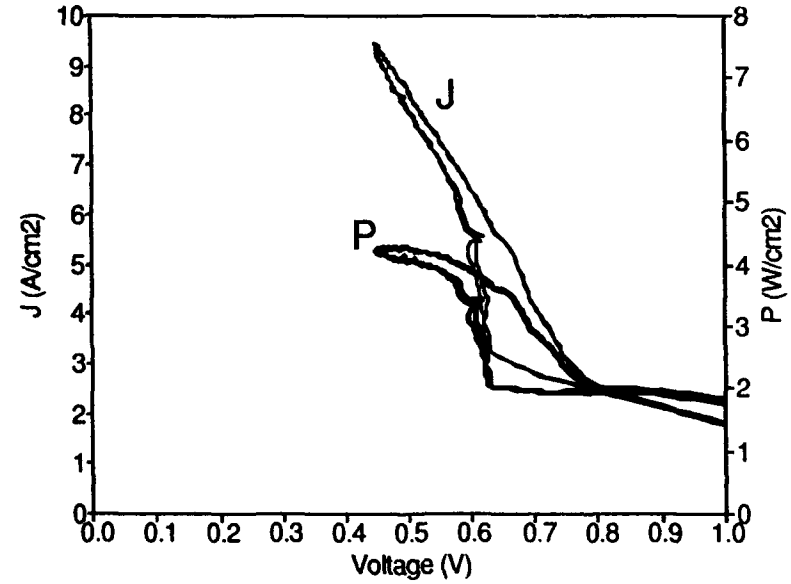

Figure D8. Re-Re converter output with heat pipe shielding.
T_E = 1625°C, T_C = 650°C, T_R = 323°C.

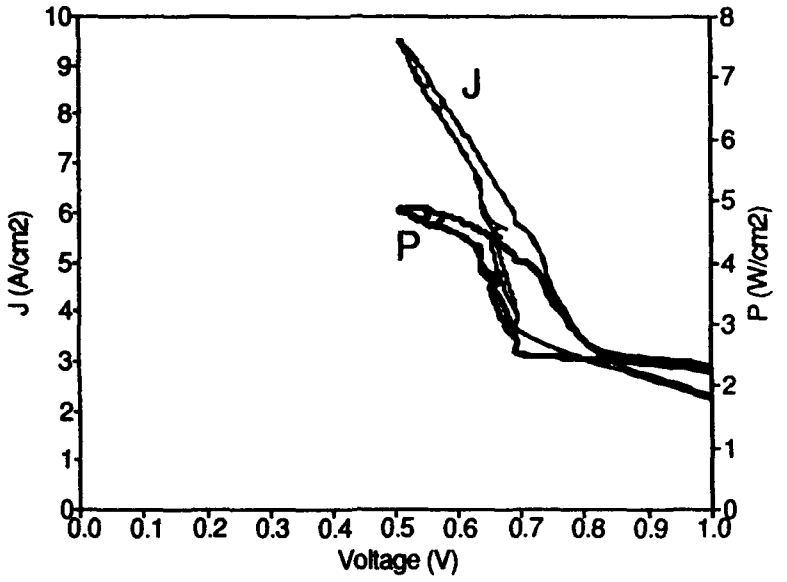

Figure D9. Re-Re converter output with heat pipe shielding.
T_E = 1650°C, T_C = 662°C, T_R = 322°C.

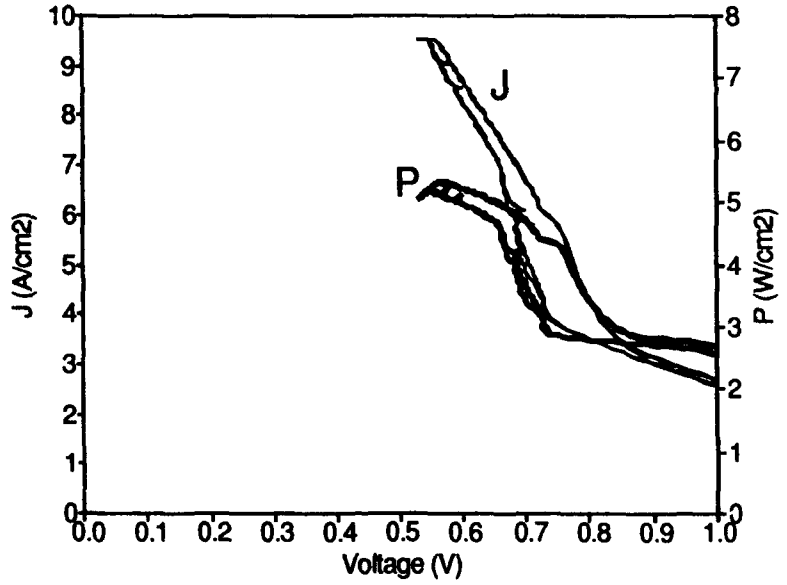

Figure D10. Re-Re converter output with heat pipe shielding.
T_E = 1675°C, T_C = 674°C, T_R = 323°C.

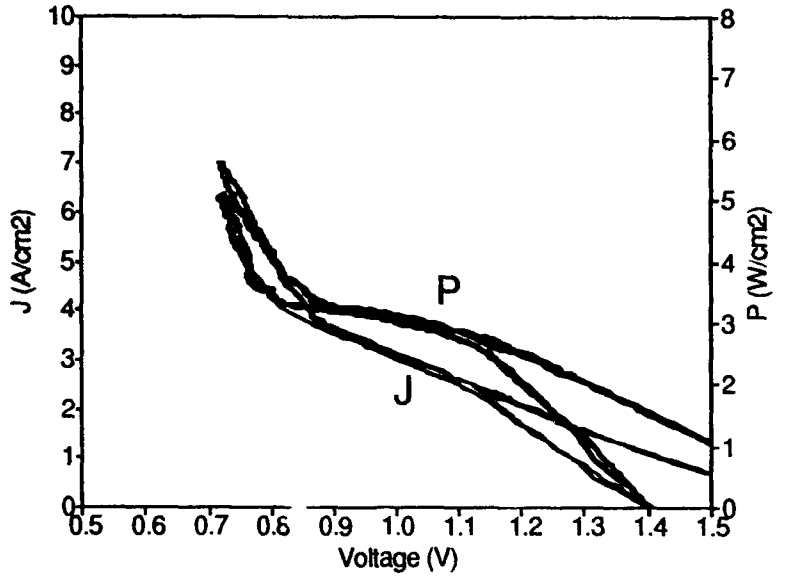

Figure D11. Re-Re converter output with heat pipe shielding.
T_E = 1700°C, T_C = 686°C, T_R = 323°C.

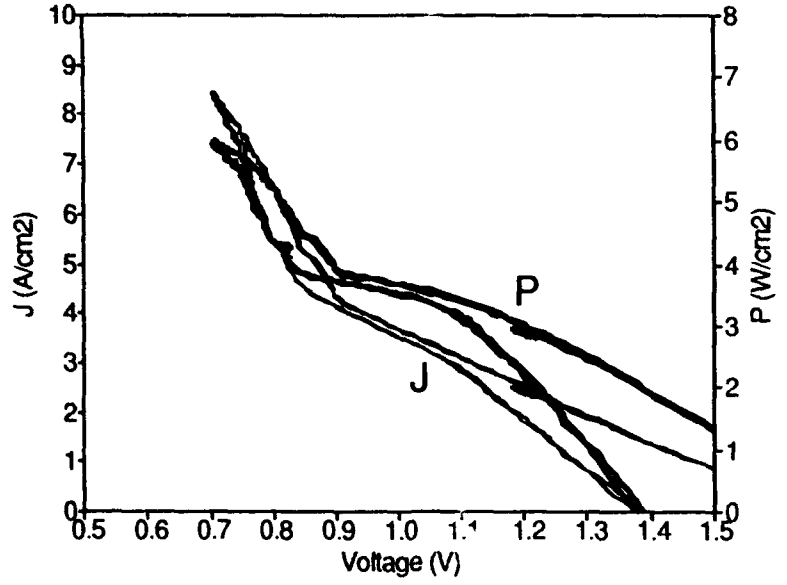

Figure D12. Re-Re converter output with heat pipe shielding.
T_E = 1725°C, T_C = 697°C, T_R = 323°C.

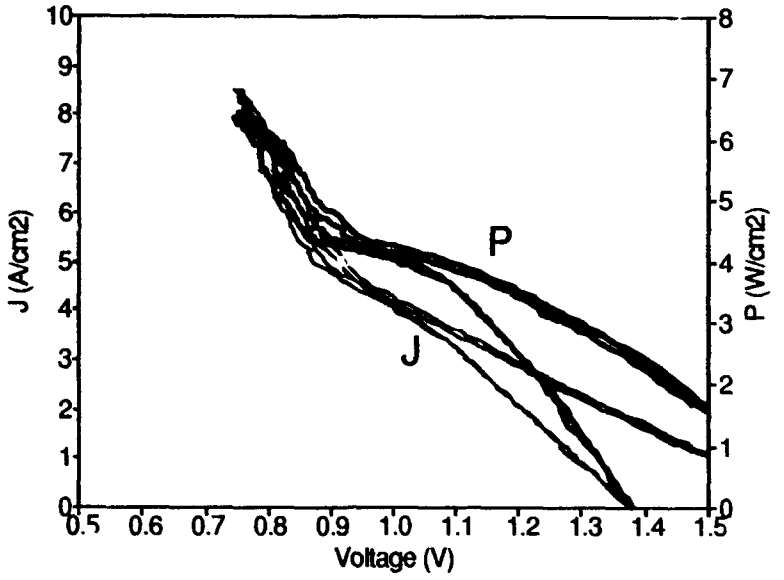

Figure D13. Re-Re converter output with heat pipe shielding.
T_E = 1750°C, T_C = 709°C, T_R = 323°C.

APPENDIX E

ASM AEROMAT '91 CONFERENCE ABSTRACT

AND

FLOWERS '92 CONFERENCE ABSTRACT

ASM AeroMat '91: Space Power System Materials

Session I: Refractory Metals

Thermionic Emission Characterization of Preferentially Oriented Tungsten and Rhenium Emitters

T.J. Young and S.J. Cloyd
Aerospace Power Division
Wright Laboratory / POOC
Wright-Patterson AFB, OH 45433-6563

B.H. Tsao and M.L. Ramalingam
UES, Inc.
4401 Dayton-Xenia Road
Dayton, OH 45432-1894

Thermionic Energy Conversion is a method of converting heat energy directly into electrical energy through electron emission. Fixed gap cesiated diodes with tungsten(110) and rhenium(0001) emitters accompanied by niobium collectors were experimentally tested in order to generate output current density versus voltage curves. The experimental output was generated for an emitter temperature range of 1700 to 1900 K, a collector temperature range of 800 to 1000 K, and a cesium reservoir temperature range of 550 to 650 K. A parallel effort on the recrystallization studies indicated that the preferentially oriented refractory metals had high creep strength and resistance to recrystallization. The experimental output was then compared with analytically obtained output characteristics.

A time dependent one dimensional thermionic energy conversion code was used to characterize the experimental output from the diodes. Converter conditions change often and as electrode materials yield better performance, the range of operating conditions for thermionic systems becomes broader. Computer simulations would allow untested combinations of thermionic parameters to be evaluated with promising models catalogued for further examination. Computer simulations were performed to model cesium vapor filled diodes with W(110) and Re(0001) emitters in the temperature ranges mentioned above. The code was found to be very sensitive to the cesium reservoir temperature and the interelectrode spacing as s result of which several discrepancies in thermophysical properties (work functions) of the refractory metals were observed. An attempt has been made to explain these discrepancies from a materials deterioration point of view.

Florence World Energy Research Symposium (FLOWERS) '92
Conventional Energy Conversion Systems

"Conventional Energy Conversion And Thermionic Emission With Lanthanum Hexaboride Electrodes"

Timothy J. Young
Aerospace Power Division
Wright Laboratory / POOC-2
Wright-Patterson AFB, OH 45433-6563

Mysore L. Ramalingam
UES, Inc.
4401 Dayton-Xenia Road
Dayton, OH 45432-1894

and

Loren A. Anderson
Mechanical and Aerospace Engineering
University of Central Florida
Orlando, FL 32816-0093

An experimental technique is demonstrated for determining the optimum operating characteristics of a thermionic power topping system for terrestrial applications. A lanthanum hexaboride thermionic diode was tested with the emitter and cesium reservoir temperatures held at 1700 K and 485 K, respectively. The collector temperature was varied from 750 K to 1020 K to allow performance mapping of the diode. The maximum output power density and short circuit current density obtained were 5.4 Watts/cm^2 and 27.7 Amps/cm^2 at a collector temperature of 900 K. An algebraic correlation for the current density in the ignited mode of operation as a function of the output voltage and emitter, collector, and cesium reservoir temperatures is developed and compared with experiment.

Acknowledgments

This work was performed at the Thermionics Lab of the USAF Wright Laboratory, Wright-Patterson AFB, Ohio and at the University of Central Florida, Orlando, Florida. The hardware was provided by the Strategic Defense Initiative Office and work was performed in compliance with the USAF Palace Knight program through the mentorship of Dr. Thomas Mahefkey, WL/POO.

APPENDIX F

EXPERIMENTAL DATA FROM THE RE-RE CONVERTER

(EMITTER TEMPERATURE PERFORMANCE MAPPING)

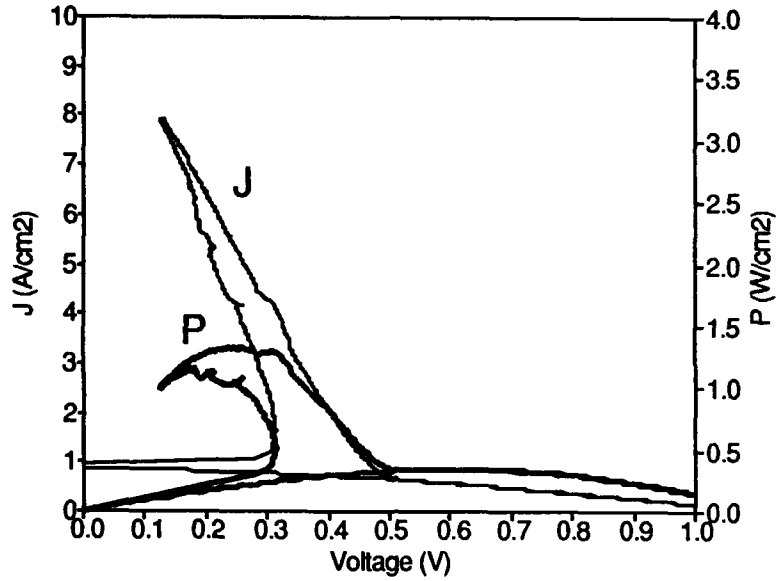

Figure F1. Re-Re converter output, emitter temperature optimization.
T_E = 1450°C, T_C = 556°C, T_R = 327°C.

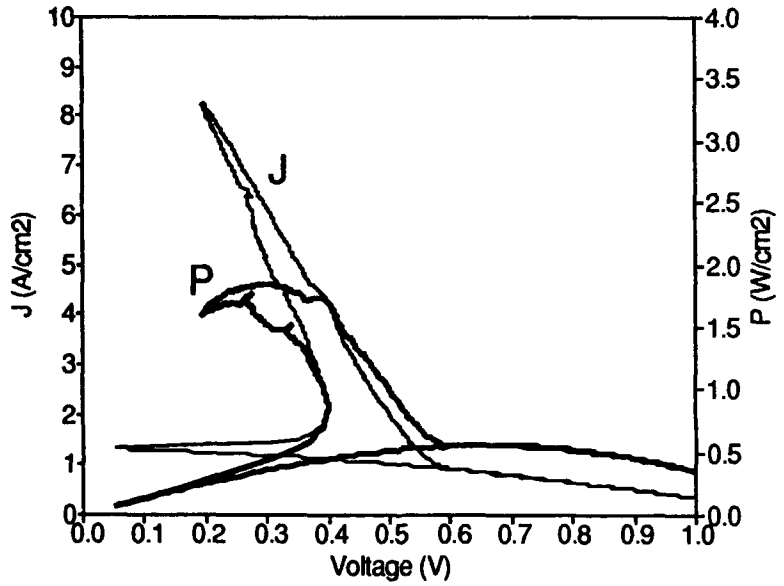

Figure F2. Re-Re converter output, emitter temperature optimization.
T_E = 1500°C, T_C = 582°C, T_R = 327°C.

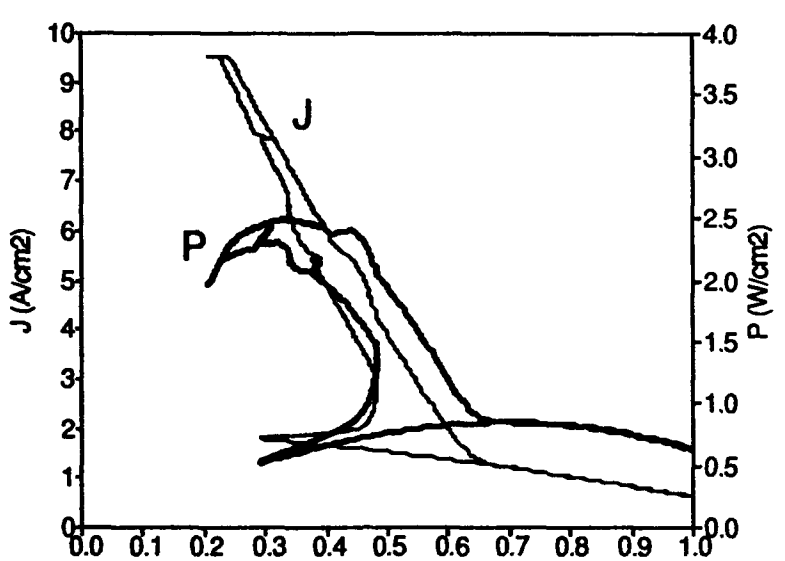

Figure F3. Re-Re converter output, emitter temperature optimization.
T_E = 1550°C, T_C = 609°C, T_R = 327°C.

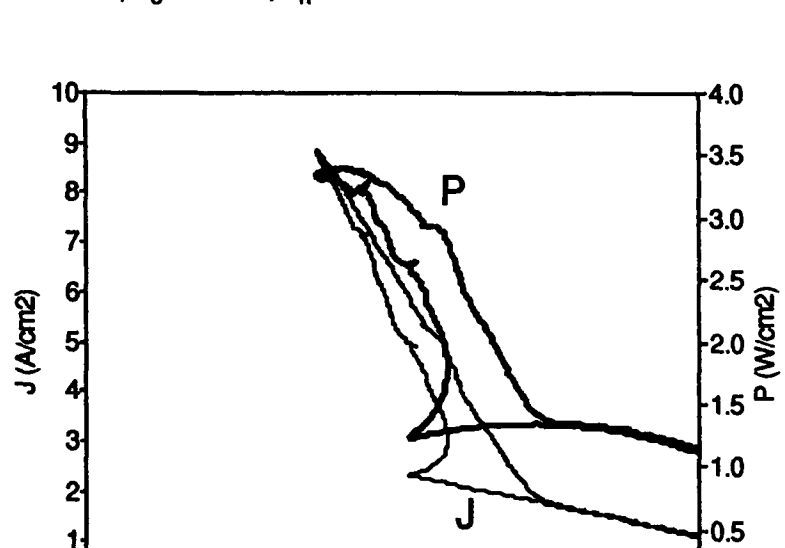

Figure F4. Re-Re converter output, emitter temperature optimization.
T_E = 1600°C, T_C = 634°C, T_R = 327°C.

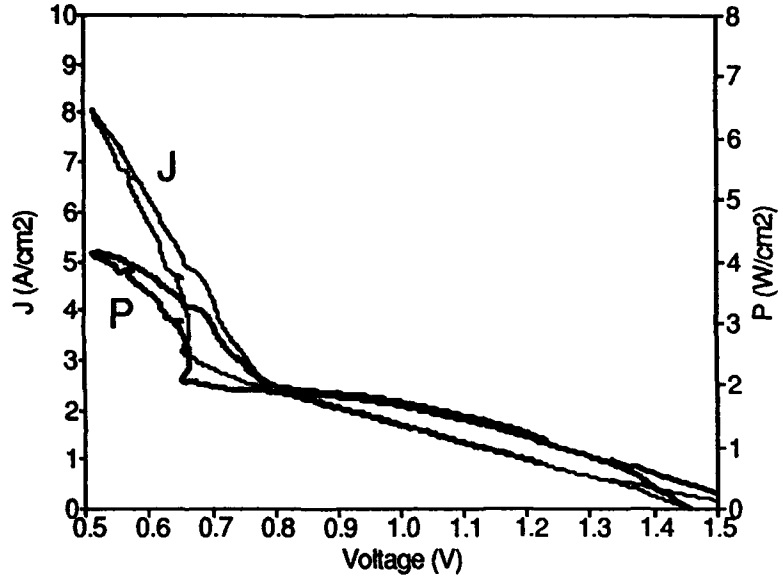

Figure F5. Re-Re converter output, emitter temperature optimization.
T_E = 1650°C, T_C = 659°C, T_R = 327°C.

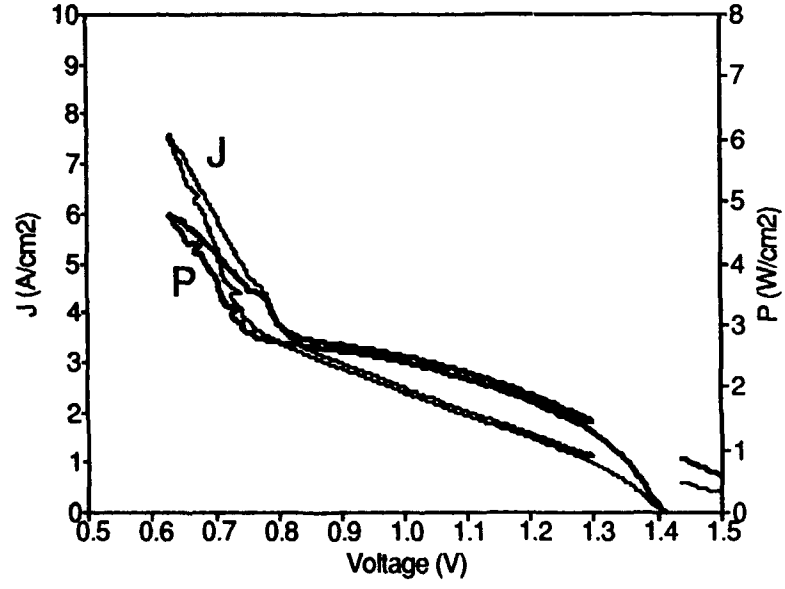

Figure F6. Re-Re converter output, emitter temperature optimization.
T_E = 1700°C, T_C = 684°C, T_R = 329°C.

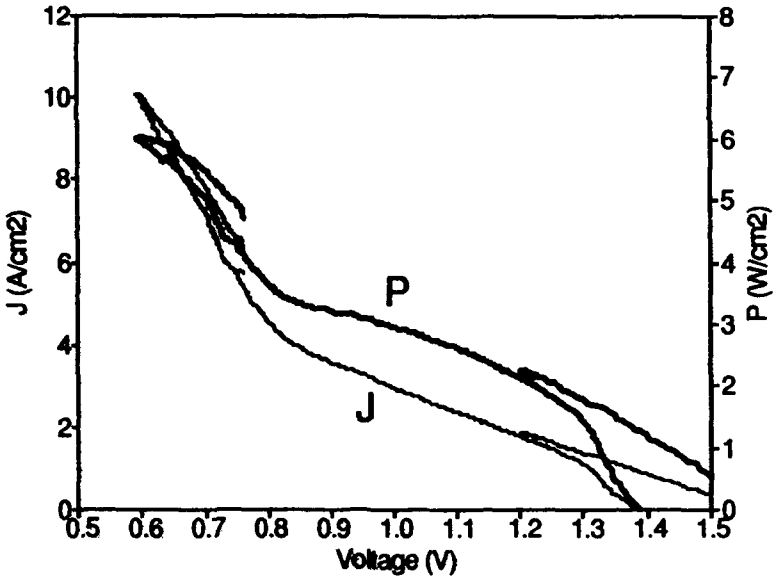

Figure F7. Re-Re converter output, emitter temperature optimization. T_E = 1750°C, T_C = 709°C, T_R = 338°C.

APPENDIX G

COMPARISONS OF EXPERIMENTAL DATA WITH THERMIONIC COMPUTER SIMULATION PROGRAMS GT-TEC AND TECMDL

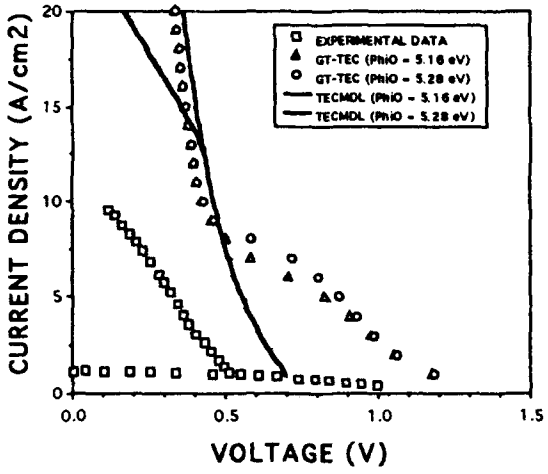

Figure G1. Comparison between GT-TEC, TECMDL, and experiment. T_E = 1450°C.

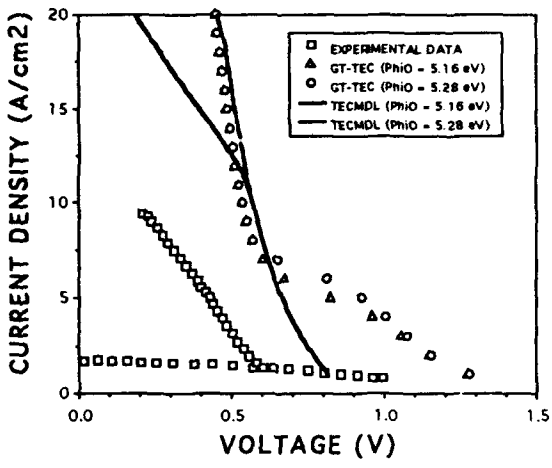

Figure G2. Comparison between GT-TEC, TECMDL, and experiment. T_E = 1500°C.

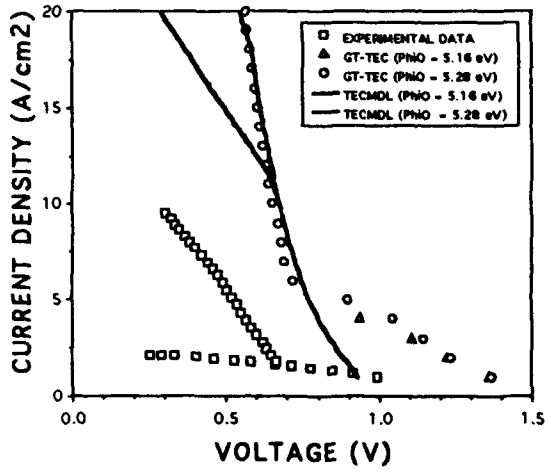

Figure G3. Comparison between GT-TEC, TECMDL, and experiment. T_E = 1550°C.

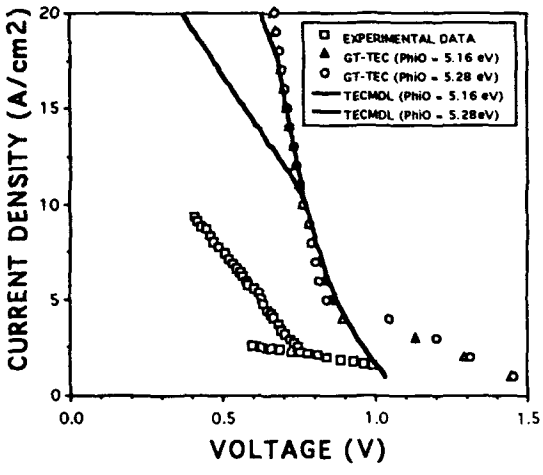

Figure G4. Comparison between GT-TEC, TECMDL, and experiment. T_E = 1600°C.

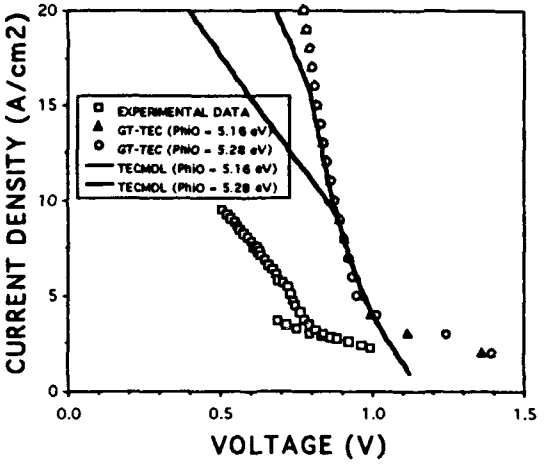

Figure G5. Comparison between GT-TEC, TECMDL, and experiment. T_E = 1650°C.

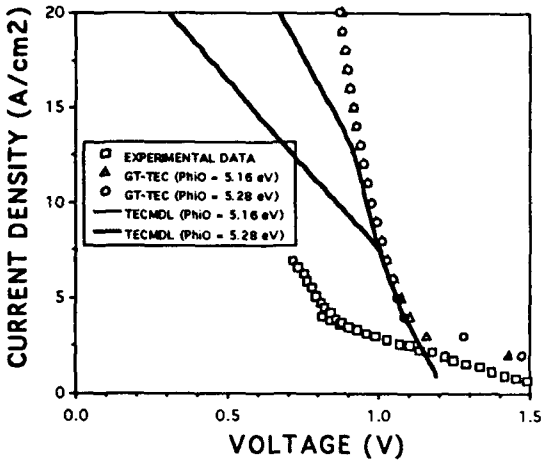

Figure G6. Comparison between GT-TEC, TECMDL, and experiment. T_E = 1700°C.

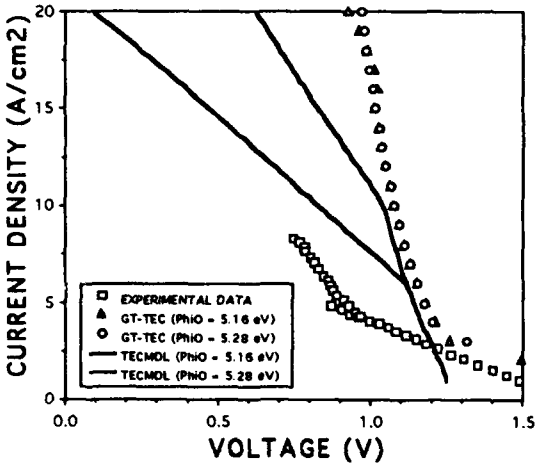

Figure G7.Comparison between GT-TEC, TECMDL, and experiment. T_E = 1750°C.

U.S. GOVERNMENT PRINTING OFFICE: 1992 - 648-127/62550